

ABSTRACT

Title of Dissertation: THE INTEGRATION OF REMOTELY SENSED DATA INTO A WATERSHED MODELING APPROACH TO CHARACTERIZE WINTER COVER CROP NITRATE UPTAKE FUNCTION AND WETLAND INUNDATION AT THE LANDSCAPE SCALE

Sangchul Lee, Doctor of Philosophy, 2017

Dissertation directed by: Dr. In-Young Yeo
Department of Geographical Sciences

The Chesapeake Bay (CB) is the largest and most productive estuary in the United States (US), supporting more than 3,600 species of plants and animals (CEC, 2000). Degrading water quality of the CB estuaries requires implementing conservation practices to reduce excessive nutrients loads from agricultural lands. The role of both winter cover crops (WCCs) and wetland restoration and enhancement in reducing agricultural nutrient loads on the Coastal Plain of the Chesapeake Bay Watershed (CBW) has been widely recognized. In order to effectively reduce nutrient loads using two conservation practices, it is important to understand their long-term, cumulative impacts at the watershed scale. A watershed

modeling approach has been recommended to simulate the cumulative effects of conservation practices on nutrient loads at the watershed scale. When using a watershed modeling approach, accurate characterization of physical processes of conservation practices within a modeling context and consideration of multiple stressors (e.g., climate change and human activities) are critical for obtaining reliable information. This dissertation has sought to characterize and evaluate the long-term impacts of WCCs and wetlands on hydrology and water quality at the watershed scale, using a watershed modeling approach in conjunction with remotely sensed data.

The WCCs are planted during winter fallow seasons to absorb residual soil nitrate. The WCC nitrate uptake capacity is dependent on its biomass as soil nitrate is being converted to WCC biomass. The WCC growth was first estimated using landscape-level biomass observations derived from remotely sensed data and field measurements to accurately represent WCC nitrate uptake efficiency. Then, the long-term effect of WCC on nitrate loads was evaluated at the watershed scale by considering WCC planting methods, soil properties, and crop rotations. The simulation results represent the typical growth pattern of WCCs observed in this region, and demonstrate the most effective WCC implementation method for enhanced WCC water quality benefits, regarding local characteristics.

Inundation is a key abiotic factor characterizing wetland ecosystem functions including water purification. Thus, the accurate prediction of the spatial distribution of inundation can indicate the capacity of wetlands to remove nutrient loads at the local landscape scale. An integrated wetland-watershed modeling approach is

presented to show how remotely sensed data can be used to improve spatial prediction of wetland inundation while reducing prediction uncertainty. The simulation results demonstrate that the model prediction with wetland parameters derived from remotely sensed data accurately replicates the observed spatial inundation pattern. These findings provide useful information for identifying the locations in need of wetland restoration and enhancement.

A watershed modeling approach that incorporated remotely sensed data accurately demonstrates the effective way to implement WCCs and wetland restoration and enhancement for reducing agricultural nutrient loads. Therefore, this dissertation would contribute to achieving nutrient reduction goals of the CB.

THE INTEGRATION OF REMOTELY SENSED DATA INTO A WATERSHED
MODELING APPROACH TO CHARACTERIZE WINTER COVER CROP
NITRATE UPTAKE FUNCTION AND WETLAND INUNDATION AT THE
LANDSCAPE SCALE

by

Sangchul Lee

Dissertation submitted to the Faculty of the Graduate School of the
University of Maryland, College Park, in partial fulfillment
of the requirements for the degree of
Doctor of Philosophy
2017

Advisory Committee:

Dr. In-Young Yeo, Chair

Dr. Ralph Dubayah

Dr. Chengquan Huang

Dr. Megan W. Lang

Dr. Ali M. Sadeghi

Dr. Adel Shirmohammadi (Dean's Representative)

© Copyright by
Sangchul Lee
2017

Foreword

The materials discussed in Chapters 2 – 4 are derived from peer-reviewed journals that I have participated in. My research outcomes during my Ph. D. have been represented as peer-reviewed articles listed below.

- Yeo, I.-Y., Lee, S., Sadeghi, A. M., Beeson, P. C., Hively, W. D., McCarty, G. W., & Lang, M. W. (2014). Assessing winter cover crop nutrient uptake efficiency using a water quality simulation model. *Hydrology and Earth System Sciences*, 18(12), 5239-5253. **(Chapter 2)**
- Lee, S., Yeo, I.Y., Sadeghi, A.M., McCarty, G.W. & Hively, W.D. (2015). Prediction of climate change impacts on agricultural watersheds and the performance of winter cover crops: Case study of the upper region of the Choptank River Watershed, Proceedings of the ASABE 1st Climate Change Symposium: Adaptation and Mitigation, Chicago, IL.
- Lee, S., Yeo, I.-Y., Sadeghi, A. M., McCarty, G. W., Hively, W. D., & Lang, M. W. (2016). Impacts of watershed characteristics and crop rotations on winter cover crop nitrate-nitrogen uptake capacity within agricultural watersheds in the Chesapeake Bay region. *PLoS One*, 11(6), e0157637. **(Chapter 3)**
- Sharifi, A., Lang, M. W., McCarty, G. W., Sadeghi, A. M., Lee, S., Yen, H., Rabenhorst, M.C., Jeong, J. & Yeo, I.Y. (2016). Improving model prediction reliability through enhanced representation of wetland soil processes and constrained model auto calibration—A paired watershed study. *Journal of Hydrology*.
- Lee, S., Yeo, I.-Y, Lang, M. W., McCarty, G. W., Sadeghi, A. M., Sharifi, A., Jin, H. & Liu, Y. (2016). Reducing uncertainty of an integrated wetland-watershed hydrologic model using remotely sensed data *Environmental Modelling & Software* (under review, **Chapter 4**)

Acknowledgements

I would like to thank my adviser, Dr. In-Young Yeo, for her guidance and support. I am grateful to my committee members, Drs. Ralph Dubayah, Chengquan Huang, Megan W. Lang, Ali M. Sadeghi, and Adel Shirmohammadi, for being serve as academic mentors. I would like to thank Drs. Greg McCarty and W. Dean Hively for their advices.

I deeply appreciate all people who are in Korea and U.S. for their concern and assist. My people in Korean warmly greeted me during my travel. My people in U.S. shared their time and life with me to celebrate my achievements and help me to get over my frustrations.

Lastly, I would like express my gratitude to my parents, brother, sister-in-law and adorable niece. Without their unconditional love, I would not have completed this long journey.

My research was supported by National Aeronautics and Space Administration (NASA) Land Cover and Land Use Change (LCLUC) Program and the U.S. Department of Agriculture (USDA) Conservation Effects Assessment Project (CEAP).

Table of Contents

Foreword.....	ii
Acknowledgements.....	iii
Table of Contents.....	iv
List of Tables.....	vi
List of Figures.....	vii
List of Abbreviations.....	ix
Chapter 1 Introduction.....	1
1.1 Background.....	1
1.1.1 Conservation practices for coastal ecosystems.....	2
1.1.2 Deterioration in the Chesapeake Bay region and conservation efforts.....	2
1.1.3 Agricultural best management practices.....	3
1.1.4 Necessity of a watershed modeling approach.....	6
1.1.5 Important considerations to assess conservation practices using a watershed modeling approach.....	8
1.1.6 Application of remotely sensed data within a watershed modeling approach.....	10
1.2 Research Objectives.....	12
1.3 Outline of dissertation.....	13
Chapter 2 Assessing winter cover crop nutrient uptake efficiency using a water quality simulation model.....	15
2.1 Introduction.....	15
2.2 Data and Methods.....	18
2.2.1 Description of the study site.....	18
2.2.2 SWAT model: model description, data, calibration and validation.....	21
2.3 Results and Discussions.....	33
2.3.1 SWAT calibration and validation.....	33
2.3.2 Multiple scenario analysis.....	37
2.3.3 Geospatial analysis to identify high nitrate load areas.....	43
2.4 Conclusions.....	45
Chapter 3 Impacts of Watershed Characteristics and Crop Rotations on Winter Cover Crop Nitrate-Nitrogen Uptake Capacity within Agricultural Watersheds in the Chesapeake Bay region.....	47
3.1 Introduction.....	47
3.2 Data and Methods.....	51
3.2.1 Study area.....	51
3.2.2 SWAT watershed process model.....	55
3.2.3 Input data.....	57
3.2.4 Calibration and validation of the SWAT model.....	64
3.2.5 Statistical analysis of WCC impacts.....	68
3.3 Results.....	69
3.3.1 SWAT calibration and validation.....	69

3.3.2 Watershed-scale assessment of winter cover crop effects on water budget and nitrate loads	74
3.3.3 Site characteristic impacts on nitrate fate and winter cover crop performance	77
3.3.4 Crop rotation impacts on winter cover crop performance over winter seasons	81
3.4 Conclusions.....	85
Chapter 4 Reducing uncertainty of an integrated wetland-watershed hydrologic model using remotely sensed data	87
4.1 Introduction.....	87
4.2 Data and Methods	93
4.2.1 Study area.....	93
4.2.2 Soil and Water Assessment Tool (SWAT) model: an overall approach to watershed simulation	97
4.2.3 Representation of wetland processes	99
4.2.4 Parameterization of wetlands.....	104
4.2.5 Model calibration and validation	109
4.2.6 Evaluation of inundated area prediction uncertainty: spatial pattern analysis	112
4.2.7 Evaluation of inter-annual variability of wetland water storage.....	116
4.3 Results and Discussions.....	117
4.3.1 Model calibration and validation	117
4.3.2 Effects of wetland parameterization on simulated inundated area	119
4.3.3 Spatial parameterization to improve understanding on wetland function	126
4.4 Summary and conclusion.....	128
Chapter 5 Summary and conclusions.....	131
5.1 Summary and major findings.....	131
5.2 Policy-related contribution of this dissertation	134
5.3 Scientific contribution of this dissertation	136
5.4 Future research.....	137
5.5 Concluding remarks	140
Bibliography	141

List of Tables

Table 2.1. List of data used in this study	26
Table 2.2. List of calibrated parameters.....	27
Table 2.3. List of winter cover crop scenarios.....	30
Table 2.4. Agricultural practices and management scheduling for the baseline and winter cover crop scenarios.	32
Table 2.5. Model performance measures for streamflow and nitrate.	35
Table 3.1. Soil properties and land use distribution of TCW and GW	55
Table 3.2. List of data used in this study	58
Table 3.3. Representative crop rotation information and distribution of corn and soybean fields.....	60
Table 3.4. The management schedules for baseline and winter cover crop scenarios	61
Table 3.5. The list of calibrated parameters.....	67
Table 3.6. Model performance measures for streamflow and nitrate loads.....	71
Table 3.7. Analysis of variance for the reduction of annual nitrate loads by watershed, WCC planting species and timing.....	77
Table 3.8. The reduction amount and rate of water and nitrate fluxes by winter cover crops.....	81
Table 4.1. List of input data	98
Table 4.2. List of calibrated parameters.....	112
Table 4.3. Wetland parameters and normal depth of RW estimated by three parameterizations	114
Table 4.4. Model performance measures for streamflow	118

List of Figures

Figure 2.1. Geographical location of the study area (German Branch watershed, with the size of 50 km ²)	20
Figure 2.2. Characteristics of the study site: land cover, elevation, and hydrologic soil map group.	21
Figure 2.3. Schematic diagram of modeling procedure	22
Figure 2.4. Observed and simulated streamflow and nitrate loads during the monitoring period (1992-1995) at the watershed scale.....	34
Figure 2.5. Estimation of winter cover crop biomass during the winter fallow period	37
Figure 2.6. The 9-year average streamflow, annual actual evapotranspiration (ET), and annual nitrate loads at watershed scale under multiple cover crop scenarios	38
Figure 2.7. Nitrate reduction rates by varying degree of winter cover crop implementation evaluated at the watershed scale.	41
Figure 2.8. The 8-year average nitrate leaching and delivery to waterways during winter fallow assessed at the field scale under multiple winter cover crop scenarios.	42
Figure 2.9. The spatial distribution of nitrate export potential from agricultural fields	44
Figure 3.1. The location of the Tuckahoe Creek Watershed and Greensboro Watershed near Chesapeake Bay.	52
Figure 3.2. The physical characteristics of the Tuckahoe Creek Watershed (left) and Greensboro Watershed (right); (a) land use, (b) hydrologic soil groups, and (c) elevation.	54
Figure 3.3. The spatial distribution of crop rotations in agricultural fields over the simulation period.	59
Figure 3.4. The temporal sequence of crop rotations under baseline and winter cover crop scenarios.....	62
Figure 3.5. Comparison of observed and simulated monthly streamflow and nitrate loads for the (a) Tuckahoe Creek Watershed and (b) Greensboro Watershed	71
Figure 3.6. 7-year average of early-planted winter cover crop biomass over winter seasons (October – March) calibrated to the field observation collected from 2005-2006.....	73
Figure 3.7. 8-year average of annual hydrologic variables under winter cover crop scenarios at the watershed scale: (a) streamflow and evapotranspiration (ET) and (b) nitrate loads normalized by the total watershed area.	76
Figure 3.8. 7-year average of annual (a) water and (b) nitrate fluxes at the cropland scale under winter cover crop scenarios over winter seasons (October-March) normalized by the total cropland area.	80
Figure 3.9. 7-year average of annual (a) nitrate fluxes (delivered to streams and leached into groundwater), and (b) nitrate from mineralization of N in residue in two crop rotations at the cropland scale under the baseline and rye early scenarios over winter seasons (October-March).....	84
Figure 3.10. Temporal distribution of 7-year average of (a & b) nitrate from mineralization of N in residue and (c & d) nitrate fluxes (delivered to streams and	

leached into groundwater) in two crop rotations at the cropland scale under early-planted rye scenario over winter seasons (October-March).	85
Figure 4.1. The location of the Tuckahoe Creek Watershed and Greensboro Watershed near Chesapeake Bay.	95
Figure 4.2. The physical characteristics of the TCW: (a) elevation, (b) soil properties, (c) land use, and (d) wetlands identified by the NWI map (adapted from Lee et al. 2016)	96
Figure 4.3. The representation of riparian wetlands and non-riparian wetlands, and wetland drainage zones delineated by the ArcGIS geo-processing tools.	102
Figure 4.4. The conceptual model that illustrates lateral surface flow exchange between riparian wetlands and streams (adapted from Liu et al. (2008)).	103
Figure 4.5. Estimation of the proportion of the inundated area at the normal and maximum water level using NWI and the 2007 inundation map: (a) the sub-watershed including the extremely small portion (“slivers”) of the NWI polygon after partitioning (# 54), (b) gaps inside inundation polygon created after vectorizing inundation pixels, (c) spatially aggregated NWI polygons and inundation pixels, and (d) the aggregated NWI polygon (in C) ungrouped into original NWI polygons to estimate the relative inundated areas for the NWI (# 22 and 23).	108
Figure 4.6. Flow diagram illustrating SWAT wetland module calibration procedures.	111
Figure 4.7. The normal volume and area of RWs by stream orders; (a & b) Set A, (c & d) Set B, and (e & f) Set C.	115
Figure 4.8. Observed and simulated daily streamflow without and with wetland modules	118
Figure 4.9. Comparison of simulated daily streamflow ($m^3 \cdot s^{-1}$) from three sets of wetland parameters	120
Figure 4.10. Statistical comparison of simulated and observed inundation within riparian wetlands: (a) Spearman’s rank-order correlation coefficient (r_s) and (b) MSE value between inundation maps and simulated inundation with three parameterizations.	121
Figure 4.11. The spatial distribution of inundated areas (ha) within riparian wetlands derived from inundation maps and simulated inundation (A-C) under different weather conditions (Normal: 2003, Wet: 2005, and Dry: 2006).	123
Figure 4.12. The relationship between inundation maps and simulated inundation areas within riparian wetlands from (a) Set A, (b) Set B, and (c) Set C, assessed at the sub-watershed scale under different weather conditions (\times : Dry, $+$: Normal, and Δ : Wet condition).	125
Figure 4.13. Seasonal variations in water volume stored in RWs by stream orders estimated using an 8-year monthly simulation.	128

List of Abbreviations

ANOVA	Analysis Of Variance
ARS	Agricultural Research Service
BE	Early-planted Barley
BL	Late-planted Barley
BMP	Best Management Practice
CB	Chesapeake Bay
CBP	Chesapeake Bay Program
CBW	Chesapeake Bay Watershed
C-CAP	Coastal Change Analysis Program
CDL	Cropland Data Layer
CEAP	Conservation Effectiveness Assessment Project
Db WW/Soybean	Double crops of winter wheat and soybean
DEM	Digital Elevation Model
EO	Executive Order
ET	Evapotranspiration
Flow_W	Simulated streamflow with wetland modules
Flow_WO	Simulated streamflow without wetland modules
GB	German Branch
GW	Greensboro Watershed
GWQ	Water flux delivered to streams by groundwater flow
HEC	Hydrologic Engineering Center
HLZ	High Loading Zones
HRU	Hydrologic Response Unit
HSG	Hydrologic Soil Group
LAI	Leaf Area Index
LATQ	Water flux delivered to streams by lateral flow
LEA	Nitrate leached into groundwater
LiDAR	Light Detection and Ranging
LOADEST	LOAD Estimator
MACS	Maryland Agricultural Water Quality Cost-Share
MANOVA	Multivariate Analysis Of Variance
MDA	Maryland Department of Agriculture
MD-DNR	Maryland Department of Natural Resources
MRLC	Multi-Resolution Land Characteristics
N	Nitrogen
NALTQ	Nitrate flux delivered to streams by lateral flow
NAPP	National Aerial Photography Program
NASS	National Agriculture Statistics Service
NCDC	National Climate Data Center
NGWQ	Nitrate flux delivered to streams by groundwater flow
NHD	National Hydrography Dataset
NOAA	National Oceanic Atmospheric Administration

NRCS	Natural Resources Conservation Service
NRW	Non-Riparian Wetland
NSE	Nash-Sutcliffe efficiency coefficient
NSURQ	Nitrate flux delivered to streams by surface runoff
NWI	National Wetland Inventory
P	Phosphorus
PDSI	Palmer Drought Severity Index
PERC	Water percolation entering to groundwater
Percent-bias	P-bias
PHU	Potential Heat Unit
PPU	Percent Prediction Uncertainty
RE	Early-planted Rye
RL	Late-planted Rye
RMSE	Root Mean Squared Error
RSR	RMSE-standard deviation ratio
RW	Riparian Wetland
RWM	Riparian Wetland Module
SCS CN	Soil Conservation Service Curve Number
SSURGO	Soil Survey Geographical Database
SURQ	Water flux delivered to streams by surface runoff
SWAT	Soil and Water Assessment Tool
SWF	Subpixel Water Fraction
SWIM	Soil and Water Integrated Model
TCW	Tuckahoe Creek Watershed
TIGER	Bureau Topologically Integrated Geographic Encoding and Referencing
TMDL	Total Maximum Daily Load
USDA	US Department of Agriculture
USDA-FSA- APFO	USDA-Farm Service Agency-Aerial Photography Field Office
USEPA	US Environmental Protection Agency
USFWS	US Fish and Wildlife Service
USGS	U.S. Geological Survey
VACS	Virginia Agricultural Best Management Practices Cost-Share Program
WCC	Winter Cover Crop
WE	Early-planted Wheat
WIP	Watershed Implementation Plan
WL	Late-planted Wheat
WXGEN	Weather generator embedded in SWAT

Chapter 1 Introduction

1.1 Background

The Chesapeake Bay (CB) is the largest and most productive estuary in the United States (US), supporting more than 3,600 species of plants and animals (CEC, 2000). Degrading water quality of the river basins of the Chesapeake Bay Watershed (CBW) requires implementing conservation practices to reduce excessive nutrients loads from agricultural lands. Both winter cover crops (WCCs) and wetland restoration and enhancement have been recommended as effective conservation practices to reduce agricultural nutrient loads from the Coastal Plain of the CBW, where agricultural lands are most abundant within the CBW. To accomplish the nutrient reduction goals using the these conservation practices, their long-term cumulative impacts on reducing nutrient loads should be understood at the management scale specified in current conservation strategies and plans to effectively implement conservation practices.

A watershed modeling approach has been emphasized as it is capable of predicting the long-term cumulative impacts of conservation practices on water and nutrient budgets at the management scale (Di Luzio et al., 2004; Van Liew et al., 2007; USEPA, 2010b). Accurate assessment of conservation practices using a watershed modeling approach requires accurate representation of model parameters or structures associated with conservation practices. However, our understanding of the impacts of WCCs and wetland restoration and enhancement at the watershed scale are currently limited.

1.1.1 Conservation practices for coastal ecosystems

The implementation of conservation practices is increasingly necessary for coastal ecosystems (i.e., estuaries) to maintain biodiversity, productivity, and a wide range of ecosystem services being provided by them (UNEP, 2011). Over the past several decades, overfishing, development, destruction, and pollutant loads have deteriorated the overall health of coastal ecosystems (Smith, 2003). Nutrient loads are identified as one of main contributing factors (Smith, 2003). Rapid population increases have also led to land transformation (e.g., forest to urban or agricultural lands) in order to meet the demand for residential areas and food (Smith et al., 2006), resulting in excessive nutrient loads to estuaries. Increased nitrogen (N) and phosphorus (P) loads to coastal ecosystems resulted in over-reproduction of phytoplankton biomass and eutrophication (Smith et al., 2006). As a result, submerged aquatic vegetation, and population of fish and shellfish dramatically decreased in estuaries (Smith, 2003 and Smith et al., 2006). Accordingly, the control of nutrient loads has become an urgent environmental problem for mitigating deterioration of the health of coastal ecosystems.

1.1.2 Deterioration in the Chesapeake Bay region and conservation efforts

Water quality degradation of the CB has been known as the single most critical problem within the CB and mainly attributed to agricultural nutrient loads from its drainage area, the CBW. Agricultural lands that cover only 25 % of the CBW have been reported to be responsible for 42 % of the total N loads to the Bay (CBP, 2016). Atmospheric deposition (24 %), septic (3 %), wastewater flow (15%), and

urban runoff (16 %) are also identified as N sources (CBP, 2016). The Coastal Plain of the CBW is known to be a critical source of nutrient loads due to abundant agricultural lands (Fisher et al., 2010; Ator and Denver, 2012).

In response to continuous degradation of the CB and its watershed, numerous efforts have been made to improve the Bay's ecosystem. The Chesapeake Bay Agreement was first made in 1983 in order to facilitate cooperative conservation efforts involving multiple jurisdictions within CBW (Maryland, Virginia, Pennsylvania and the District of Columbia) and the US Environmental Protection Agency (EPA). This agreement was reaffirmed in 1987, 2000, and 2014 with more rigorous conservation goals and participation of three additional jurisdictions across the CBW (New York, West Virginia, and Delaware) (CBP, 1983 and 2014). The CB Executive Order (EO) 13508 of 2009 was put forth to direct collaborative efforts towards the protection and restoration of the Bay's ecosystem (Federal Leadership Committee for the Chesapeake Bay, 2010). In 2010, the USEPA established the CB Total Maximum Daily Load (TMDL) due to insufficient progress in water quality improvement despite long-term conservation efforts. This regulation limits the allowable amount of N, P, and sediment loads to meet target water quality goals (USEPA, 2010a).

1.1.3 Agricultural best management practices

Agricultural best management practices (BMPs) have been emphasized throughout the CBW for the sake of achieving conservation goals. Traditional agricultural BMPs were focused on reducing sediment loads, but their focus has lately

turned to alleviating nutrient loads (Camacho, 1990). Cost-share programs have been launched to promote the adoption rate of agricultural BMPs on local croplands by providing a subsidy for BMP implementation. For example, the Maryland Agricultural Water Quality Cost-Share (MACS) program offered \$ 31.2 million to local farmers for installation of eligible agricultural BMPs in 2015 (MDA, 2015). The Virginia Agricultural Best Management Practices Cost-Share Program (VACS) established in 1984 has provided economical assistant for BMP implementation and educational support for management and conservation methods (VDCR, 2016). Two agricultural BMPs (e.g., winter cover crop and wetland restoration and enhancement) are strongly recommended on the Coastal Plain where agricultural nutrient loads are most prominent within the CBW.

1.1.3.1 Winter cover crop

Planting winter cover crop (WCC) is an effective BMP, especially to reduce nitrate leached into the groundwater during winter seasons. Besides water quality benefits, WCCs contribute to protecting soil erosion, impeding weed growth, increasing water infiltration into soil, and improving soil physical properties (Dabney et al., 2001). Due to the high effectiveness of WCC at reducing nitrate loads during winter seasons, the use of WCCs has been emphasized, and federal and state cost-share programs are available to farmers to subsidize the cost of implementation (Maryland General Assembly, 2007). WCCs were planted on the 475,560 acres of MD croplands in 2015 and this treatment was estimated to remove approximately 2.9 million pounds of N and 95,112 pounds of P (MDA, 2015). The WCC is planted after

harvest of summer crops and killed the following spring before planting summer crops in order to absorb remaining soil nutrients from summer crop production during winter seasons (Hievely et al., 2009; Dabney et al., 2001). Excessive nitrate in soil profiles sequestered by WCCs is immobilized by conversion to crop biomass. On the Coastal Plain of the CBW, remaining nitrate is easily delivered from agricultural lands to receiving water bodies during winter seasons due to low evapotranspiration (ET), high groundwater table, and fallow lands (Yeo et al., 2014) and therefore the importance of WCC treatment is highlighted in this region.

1.1.3.2 Wetland restoration and enhancement

Wetlands are unique ecosystems located on the transitional zone between aquatic and terrestrial systems (Fretwell et al., 1996). On the landscape, wetlands provide a wide array of ecosystem services (Hillman, 1998). For example, wetlands are capable of mitigating excessive N loads from agricultural lands. The majority of N entering into wetlands is removed via biochemical processes (Bowden, 1987). In aerobic conditions, organic N is converted to ammonium, which is a form of N usable for plants and microbes. Ammonium oxidized by bacteria is converted to nitrite and then nitrite is converted to nitrate through oxidation. This process is nitrification (ammonium to nitrate). Nitrate is assimilated by plants or microorganisms, or converted to gaseous N by anaerobic bacteria in anoxic conditions, which is denitrification (nitrate to N gas). In addition to water purification functions, their flooding mitigation and natural habitat benefits play a crucial role in maintaining the vitality of ecosystems (Cooper, 1990; Nygaard and Ejrnæs, 2009).

Expansion of urban and agricultural lands led to dramatic wetland loss in the CBW, resulting in increasing agricultural nutrient loads (Steven et al., 2011). The degradation of the Bay's ecosystem has drawn attention to the importance of wetland management. Due to the importance of wetland ecosystem services, wetland restoration and enhancement becomes a top priority. The CB Executive Order of 2009 has set a goal of restoring 30,000 acres of tidal and non-tidal wetlands and enhancing the function of an additional 150,000 acres of degraded wetlands by 2025 (Federal Leadership Committee for the Chesapeake Bay, 2010). To date these efforts have resulted in the restoration of the 18,217 acres and the enhancement of 97,738 wetland acres. Wetland water quality benefit is especially valuable on the Coastal Plain of the CBW. Wetlands are densely distributed over this region due to low topographic relief and a high groundwater table compared to other regions within the CBW (Tiner, 1995). This abundance of wetlands was found to be effective at reducing agricultural nutrient loads (Steven et al., 2011).

1.1.4 Necessity of a watershed modeling approach

To successfully achieve nutrient reduction goals using conservation practices, accurate assessment of the impacts of those practices is essential (Santhi et al., 2006). Assessment approaches are required to demonstrate the impacts of conservation practices at the spatial scale that corresponds to the management unit specified in current conservation strategies and plans, but also quantify their long-term impacts site by site in response to anthropogenic and natural stressors (e.g., agricultural activities and climate changes, respectively) (Santhi et al., 2006). *However, the long-*

term, cumulative effects of WCCs and wetland restoration and enhancement to improve water quality have not been fully examined at the watershed scale in the CBW. Most available data stem from field measurements, and therefore are not directly applicable to the current conservation strategies and planning due to the spatial mismatch. In other words, those field-scale data are not sufficient to demonstrate the impacts of conservation practices at the management scale because field-scale data cannot simply be scaled up or extrapolated for other sites due to the variability in landscape physical characteristics and land management practices (Hively et al., 2009).

A watershed modeling approach represents water and nutrient budgets at the multiple scales. A watershed is a basic management unit for evaluating the performance of conservation practices, and is the context where water and nutrient cycles take place. Accordingly, a watershed-scale analysis can accurately represent the effects of conservation practices on water and nutrient budgets at the management scale. The CB TMDL calls for watershed-level conservation practices, called watershed implementation plans (WIPs), by jurisdictions to accomplish the targeted water quality standards (USEPA, 2010b). The US Department of Agriculture (USDA) Conservation Effectiveness Assessment Project (CEAP) program emphasized that a watershed modeling approach is a promising method for accurate evaluation of conservation practices (Di Luzio et al., 2004; Van Liew et al., 2007). The USEPA also recommends a watershed modeling approach for monitoring water quality and its changes by conservation practices (USEPA, 2010b). *Hence, assessment of WCC and wetland water quality benefits using a watershed modeling approach can provide*

important information for current and future conservation policies and plans aimed at reducing nutrient loads from the Coastal Plain of the CBW.

A watershed modeling approach is a promising tool to evaluate conservation practices. This approach is also being regarded as a more feasible alternative to field monitoring due to its lower expense, including labor costs (Shirmohammadi et al., 2006). In the CBW, groundwater flow transports approximately half of the total annual N load of streams entering the Bay (Phillips et al., 1999). Nitrate leached into the groundwater has substantial residence time on the order of 5 – 40 years (McCarty et al., 2008; Meals et al., 2009). The relatively long and variable residence time of nutrient loads from their sources to receiving water bodies requires a computational modeling approach. Furthermore, there is a long lag time between implementing conservation practices and realizing water quality improvement. Agricultural nutrients cannot be tracked using field monitoring due to their complex transport. Therefore, the use of a watershed modeling approach is vital to evaluate the long-term impacts of conservation practices on reducing nutrient loads on the CBW.

1.1.5 Important considerations to assess conservation practices using a watershed modeling approach

Understanding of the physical processes of conservation practice in reality and the accurate characterization of conservation practices in a modeling context are imperative prior to assessment. To accurately demonstrate the impacts of conservation practices using a watershed modeling approach, it is important to

accurately represent the physical mechanism of conservation practices within the modeling context by enhanced parameterization or model structure.

In addition, the performances of conservation practices could vary by geophysical, climatic, and human factors because those have great impacts on hydrology and nutrient cycles and conservation practices. For effective use of conservation practices, it is also important to know how both water/nutrient cycles and the performance of conservation practices can vary under different conditions. Predictions of conservation practices that consider environmental and anthropogenic factors also help to identify more efficient ways to implement conservation practices. Those predictions can suggest alternative or additional conservation practices to deal with nutrient loads changed by multiple stressors (e.g., climate, land use, and agricultural activities changes).

Lastly, simulation results should provide the practical information to support conservation practices. For example, depending on planting timing and species of WCCs, varying WCC implementation methods are used. To effectively reduce nutrient loads, WCCs with a high nitrate uptake efficiency should be implemented on nutrient source areas. Therefore, the effectiveness of varying WCC implementation methods in reducing nutrient loads and their performances in different landscape settings would be important information. According to Lewis (1989), wetland restoration and enhancement are defined as follows: “restoration – returned from a disturbed or totally altered condition to a previously existing natural, or altered condition by some action of man” and “enhancement – the increase in one or more values of all or a portion of an existing wetland by man’s activities, often with the

accompanying decline in other wetland values”. An understanding of inundation pattern within multiple wetlands over the landscape is critical for effectively restoring and enhancing wetland functions. Inundation is the most important abiotic factor controlling wetland functions. Inundation information can be used to predict not only the water fluxes and hydrology of individual wetlands, but also their capability for pollutant removal (Lang et al., 2016), because the interactions between wetlands and pollutant loads can be inferred from wetland hydrology. Therefore, the spatial distribution and extent of inundation can suggest specific locations to be restored or enhanced.

1.1.6 Application of remotely sensed data within a watershed modeling approach

A typical watershed model consists of numerous equations and parameters describing the physical processes. Successful model application benefits from accurate characterization of input parameters (Fonseca et al., 2014). However, most parameters are not directly or easily obtainable from field measurements and therefore they are determined through model calibration using observations collected at the outlet of the watershed or use of default model values commonly provided by the model (Arnold et al., 2012). This general calibration may suffice to estimate watershed-scale water and nutrient loads, but unless physical processes are accurately represented, the contribution to improved understanding of the physical and biological mechanisms through which conservation practices influence water quality is extremely limited.

Remotely sensed data have also been used within watershed models to accurately represent the actual physical conditions. However, most studies applied remotely sensed data to improve input data quality, such as climate data, digital elevation model (DEM), and land use maps (Sexton et al., 2010; Yang et al., 2014; Ganasri and Ramesh, 2015). Little attention has been drawn to use of remotely sensed data for characterizing conservation practices, mainly due to data limitations. Recently available remotely sensed data demonstrated landscape-level WCC biomass and wetland inundation in the Coastal Plain of the CBW (Hively et al., 2009; Huang et al., 2014; Jin et al., 2017). These data accurately represented WCC biomass growth and changes in inundation areas of multiple wetlands on the landscape (Hively et al., 2009; Huang et al., 2014; Jin et al., 2017). Thus, the integration of these remotely sensed data into a watershed modeling approach can lead to enhanced characterization of both WCC biomass growth and the spatial distribution of wetland inundation that are useful for developing implementation plans for two conservation practices.

1.2 Research Objectives

The overarching goal of this dissertation is to characterize WCC nitrate uptake function and the spatial distribution of wetland inundation using a watershed modeling approach with remotely sensed data. Three specific objectives proposed to attain this goal are as follow:

1. To characterize and evaluate winter cover crop nitrate uptake efficiency at the watershed scale
2. To identify landscape characteristics affecting winter cover crop water quality benefits
3. To accurately characterize the spatial distribution of wetland inundation at the watershed scale

1.3 Outline of dissertation

This dissertation is comprised of five chapters:

Chapter 1 (this chapter) discusses the causes of the coastal ecosystem degradation at the study site and the need to better understand the effects of two conservation practices using a watershed modeling approach.

Chapter 2 suggests a novel approach to accurately simulate WCC nitrate uptake efficiency using a watershed model. WCC biomass growth is first calibrated based on landscape-level biomass observations derived from remotely sensed data and field measurements. This is because WCC nitrate uptake efficiency is highly dependent on WCC biomass growth. Representative WCC implementation methods widely adopted at the study site are taken into account to show how individual methods affect nitrate budgets and identify the most effective implementation methods in this region.

Chapter 3 focuses on assessing impacts of watershed characteristics and crop rotations on WCC nitrate uptake efficiency. The approach for biomass growth simulation developed in Chapter 2 was applied to simulate WCC nitrate uptake efficiency in two adjacent watersheds with contrasting land use and soil characteristics. The transport and fate of nitrate can vary by watershed characteristics and crop rotations because they have profound impacts on remaining soil nitrate immobilized by WCCs. Therefore, this chapter shows how two characteristics affect WCC nitrate uptake efficiency and proposes implementation methods that maximize WCC water quality benefits according to local landscape characteristics.

Chapter 4 presents an integrated wetland-watershed modeling approach framework that capitalizes on inundation maps and other geospatial data to improve spatial prediction of wetland inundation while reducing prediction uncertainty. Inundation is a key abiotic factor controlling wetland ecosystem functions including water purification. Thus, the accurate prediction of the spatial distribution of inundation can indicate the capacity of wetlands to remove nutrient loads at specific sites. This study outlines problems commonly arising from data preparation and parameterization used to simulate wetlands within a distributed watershed model. This study demonstrates how intra-watershed processes can be better captured by spatialized wetland parameters developed from remotely sensed data, because their use reduces the degree of model uncertainty (i.e., equifinality: many different parameter sets are equally good at reproducing an output signal; Beven, 2006). This spatial data-model integrated framework was tested using a watershed model with an improved riparian wetland extension. This study illustrates how spatially distributed information (i.e., remotely sensed data) on inundation reduces uncertainty of wetland hydrology function estimates at the local landscape scale, where monitoring and conservation decision making take place. The findings of this chapter exhibit the spatial distribution of wetland inundation within a watershed, which helps to identify the locations in need of wetland restoration and enhancement.

Chapter 5 summarizes major findings that are illustrated in Chapter 2 – 4, and describes the contributions of this dissertation. The future research direction is described based on key outcomes and limitations of this dissertation.

Chapter 2 Assessing winter cover crop nutrient uptake efficiency using a water quality simulation model¹

2.1 Introduction

The Chesapeake Bay (CB) is the largest and most productive estuary in the US. It is an international as well as a national asset. The Chesapeake Bay watershed (CBW) extends over 166,000 km² and covers parts of New York, Pennsylvania, Maryland, Delaware, West Virginia, Virginia and the District of Columbia. The importance of CB has been recognized by its designation as a Ramsar site of international importance (Gardner and Davidson, 2011). However, the Bay's ecosystems have been greatly degraded. Nearly 16 million people reside in the CBW, and its population is increasing rapidly, leading to accelerated land use and land cover change. High nitrogen (N) input to the Bay is the foremost water quality concern (Boesch et al., 2001).

It is particularly important to implement best management practices (BMPs) on agricultural lands in the Coastal Plain in order to improve water quality in the CB. N exports from agricultural lands are significantly higher than those from other land uses in the Coastal Plain of the CBW (Jordan et al., 1997; Fisher et al., 2010; Reckhow et al., 2011). Fisher et al. (2010) discussed that N export increases by a factor of ~10 as agriculture increases from 40 % to 90 % of land use within Coastal

¹ The material presented in this Chapter has been published in Yeo, I.Y, Lee, S., Sadeghi, A. M., Beeson, P. C., Hively, W. D., McCarty, G. W., & Lang, M. W. (2014). Assessing winter cover crop nutrient uptake efficiency using a water quality simulation model. *Hydrology and Earth System Sciences*, 18 (12), 5239–53.

Plain watersheds. Jordan et al. (1997) showed that N was exported from cropland at a rate of $18 \text{ kg N}\cdot\text{ha}^{-1}\cdot\text{yr}^{-1}$, 7 times higher than the rate from other land uses in the Coastal Plain. High nitrate exports from Coastal Plain watersheds have intensified CB water quality problems, due in part to short hydraulic distances (Reckhow et al., 2011).

The implementation of winter cover crops (WCCs) as a best management practice on agricultural lands has been recognized as one of the most important conservation practices being used in the CBW (CBC, 2000). WCCs can sequester residual N after the harvest of summer crops, reducing nitrate leaching to groundwater and delivery to waterways by surface runoff (Hively et al., 2009), and can also reduce the loss of sediment and phosphorus from agricultural lands. However, the overall efficiency of WCCs for reducing nitrate loads has not been fully evaluated. The influence of BMPs, such as WCCs, on nitrate flux to streams has not been measured *in situ* at scales larger than field, because of the substantial residence time of leached N in groundwater and the difficulty of monitoring over long time periods (McCarty et al., 2008). A few field studies have demonstrated cover crop nitrate reduction efficiencies at the field scale (e.g., Shipley et al., 1991; Staver and Brinsfield, 2000). Hively et al. (2009) used satellite remotely sensed images and field sampling data to estimate WCC biomass production and N uptake efficiency at the landscape scale. However, the catchment-scale benefits of WCC have not been fully understood. As the nutrient uptake and nitrate reduction efficiencies of WCC are primarily dependent upon crop biomass (Malhi et al., 2006; Hively et al., 2009), it is crucial to simulate plant growth accurately. The accurate simulation of the plant

growth would require field-based information and an improved calibration method to carefully account for the climate, soil characteristics, and site-specific nutrient management. Furthermore, the effectiveness of management practices, such as WCCs, has not been fully explored for coastal agricultural watersheds in the study region due to the challenge of accurately simulating hydrologic and nutrient cycling in lowland areas with high groundwater–surface water interaction (Lee et al., 2000; Sadeghi et al., 2007; Sexton et al., 2010; Lam et al., 2012).

This study utilized a physically-based watershed model, Soil and Water Assessment Tool (SWAT) (Arnold and Fohrer, 2005), to simulate hydrological processes and N cycling for an agricultural watershed in the Coastal Plain of the CBW. We examined the long-term impact (~10 years) of WCCs on water budget and nitrate loads under multiple cover crop implementation scenarios (e.g., species, timing and area planted). To accurately simulate the growth WCCs and their nutrient uptake and nitrate reduction efficiencies, we have developed a novel approach to calibrate model parameters that control WCC biomass, resulting in model estimates that closely approximate observed values. This study provided important information for decision making to effectively implement WCC programs and to target critical pollution source areas for future BMP implementation.

2.2 Data and Methods

2.2.1 Description of the study site

This study was undertaken in the German Branch (GB) watershed, located within the CBW. The GB is a third order Coastal Plain stream, located within the non-tidal zone of the Choptank River Basin (Figure 2.1). Its drainage area is approximately 50 km² and its land use is dominated by agriculture (~72 %) and forest (~27 %) (Figure 2.2). Agricultural lands are evenly split between corn and soybean cropping. The study site is relatively flat with elevations ranging from 1 to 26 m above sea level. Most of the soils are moderately well-drained (Hydrologic Soil Group (HSG)–B) or moderately poorly-drained (HSG–C). Soil groups B and C cover 52 % and 35 % of the study area, respectively. Well-drained (HSG–A) and poorly-drained (HSG–D) soils account for less than 1 % and 14 %, respectively, of the study area. Figure 2.2 presents information on land use, hydrologic soil types, and topography of the study site. The area is characterized by a temperate, humid climate with an average annual precipitation of 120 cm·yr⁻¹ (Ator et al., 2005). Precipitation is evenly distributed throughout the year, and approximately 50 % of annual precipitation recharges groundwater or enters streams via surface flow, while the remaining precipitation is lost to the atmosphere via evapotranspiration (ET) (Ator et al., 2005).

The Choptank River watershed has been identified as an “impaired” water body by the U.S. Environmental Protection Agency (USEPA) under Section 303(d) of the Clean Water Act due to excessive nutrients and sediments, and nutrient runoff from agricultural land has been identified as the main contributor of water pollution (McCarty et al., 2008). Since 1980, substantial efforts have been made to monitor

water quality in the Choptank River watershed to establish baseline information on nutrient loads from agricultural watersheds. Water quality in the GB watershed was intensively monitored between 1990 and 1995 as part of the Targeted Watershed Project, a multi-agency state initiative (Jordan et al., 1997; Primrose et al., 1997). In 2004, the Choptank River watershed was selected to become part of the U.S. Department of Agriculture (USDA) Conservation Effects Assessment Project (CEAP), which evaluates the effectiveness of various agricultural conservation practices designed to maintain water quality for the mid-Atlantic region of the US (McCarty et al., 2008).

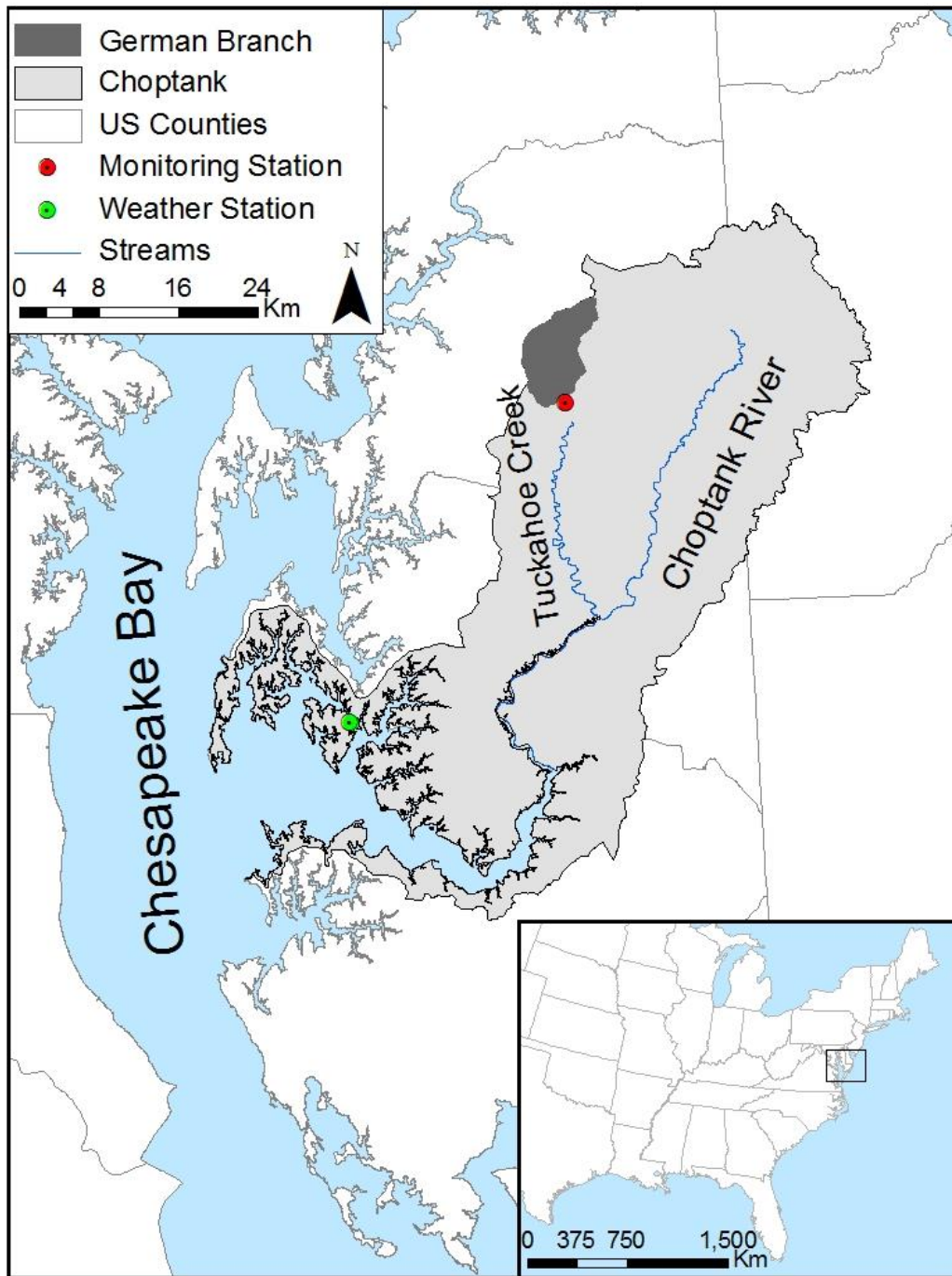


Figure 2.1. Geographical location of the study area (German Branch watershed, with the size of 50 km²)

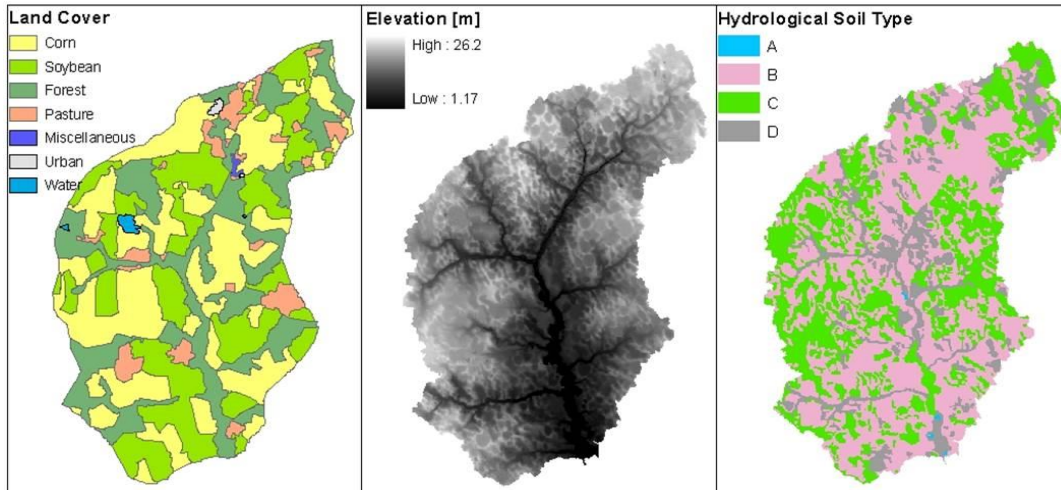


Figure 2.2. Characteristics of the study site: land cover, elevation, and hydrologic soil map map.

Note: (1) Miscellaneous land cover indicates agricultural lands used for minor crops, vegetables, and fruits; (2) Hydrologic soil group (HSG) is characterized as follows: Type A - well drained soils with $7.6-11.4 \text{ mm}\cdot\text{hr}^{-1}$ ($0.3-0.45 \text{ inch}\cdot\text{hr}^{-1}$) water infiltration rate; Type B - moderately well drained soils with $3.8-7.6 \text{ mm}\cdot\text{hr}^{-1}$ ($0.15-0.30 \text{ inch}\cdot\text{hr}^{-1}$) water infiltration rate; Type C - moderately poorly drained soils with $1.3-3.8 \text{ mm}\cdot\text{hr}^{-1}$ ($0.05-0.15 \text{ inch}\cdot\text{hr}^{-1}$) water infiltration rate; Type D - poorly drained soils with $0-1.3 \text{ mm}\cdot\text{hr}^{-1}$ ($0-0.05 \text{ inch}\cdot\text{hr}^{-1}$) water infiltration rate; (3) the land cover map shown is obtained from 2008 National Cropland Data Layer (NCDL). The time series NCDL maps (not shown here) indicate the areas grown with corn/soybean rotation are similar to the areas grown with soybean/corn rotation.

2.2.2 SWAT model: model description, data, calibration and validation

The SWAT was used to simulate the effects of WCCs on nitrate uptake with multiple WCC scenarios over the period of 1990-2000. The model simulation was run for the entire watershed (including forested, row croplands, and non-row croplands), and changes in both water budgets and nitrate loads to receiving waters under multiple scenarios were compared with baseline conditions (no WCCS) at the field and/or watershed scales. The overall modeling approach is presented in Figure 2.3. Since WCC N reduction efficiency is controlled by WCC biomass (Malhi et al.,

2006), we developed a new method to calibrate plant growth parameters that control leaf area development to produce simulation outputs close to observed values (discussed in Section 2.2.2.4).

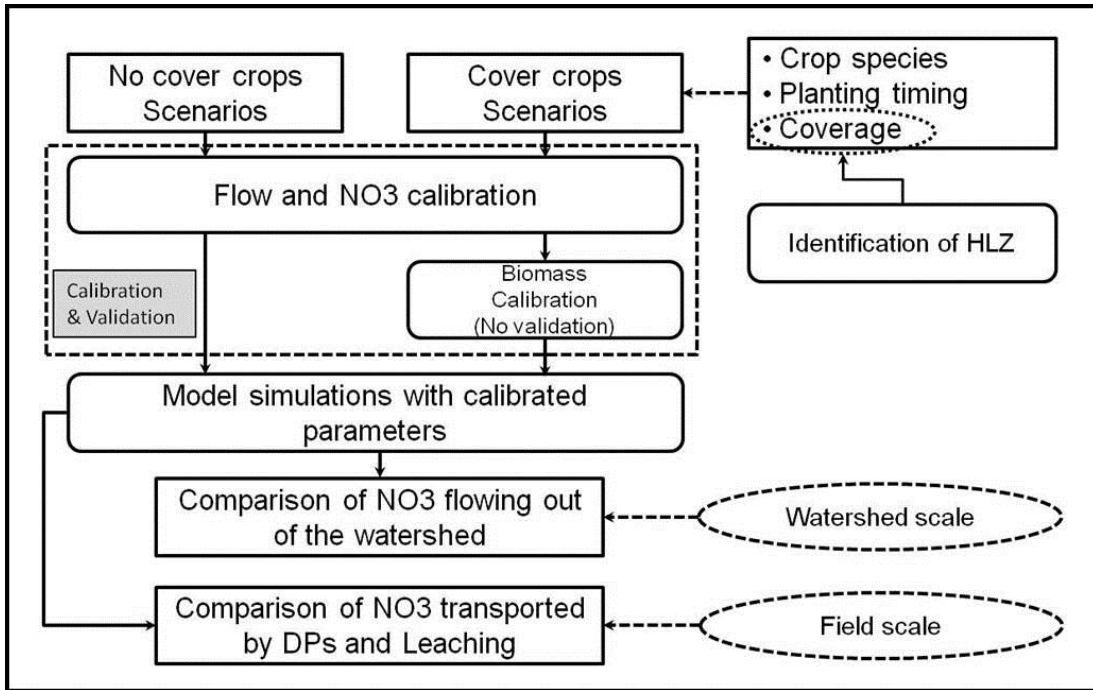


Figure 2.3. Schematic diagram of modeling procedure

Note: This shows the overall modeling procedure of the presented study and summarizes what simulation results are compared at the various spatial scales. HLZ (High Loading Zone) refers to those agricultural fields (hydrologic response units (HRUs)) with high nitrate export potential.

2.2.2.1 Description of SWAT Model

The SWAT is a continuous, physically-based semi-distributed watershed process model. The SWAT simulation runs on a daily time step. The SWAT includes and enhances modeling capabilities of a number of different models previously developed by the USDA Agricultural Research Service (ARS) and the USEPA. Arnold and Fohrer (2005) discuss the capabilities of SWAT in detail. Technical

documents on physical processes implemented in SWAT, input requirements, and explanation of output variables are available online (Neitsch et al., 2011). The key physical processes in SWAT relevant to this research are briefly discussed below.

The main components of SWAT include weather, hydrology, sedimentation, soil temperature, crop growth, nutrients, pesticide, pathogens, and land management (Neitsch et al., 2011). In SWAT, a watershed is subdivided into smaller spatial modeling units, sub-watersheds and hydrologic response units (HRUs). A HRU is the smallest spatial unit used for field-scale processes within the model. A HRU is characterized by homogeneous land cover, soil type, and slope. The overall hydrologic balance as well as nutrient cycling is simulated for each HRU, summed to the sub-watershed level, and then routed through stream channels to the watershed outlet. In SWAT model, a modification of the Soil Conservation Service (SCS) curve number (CN) method was used to simulate surface runoff for all land cover types including row crops, forests, and non-row croplands. The CN method determines runoff based on land use, the soil's permeability, and antecedent soil water conditions. The transformation and transport of N are simulated as a function of nutrient cycles within a HRU, comprising several organic and inorganic pools. Simulated loss of N can occur by surface runoff in solution and by eroded sediment and crop uptake. It can also take place in percolation below the root zone, in lateral subsurface flow, and by volatilization to the atmosphere.

2.2.2.2 Data and input preparation

Table 2.1 presents the list of data and other relevant information used in this study. Daily climate records on precipitation and temperature were obtained from the National Oceanic Atmospheric Administration (NOAA) National Climate Data Center (NCDC) (Royal Oak, Station ID: USC00187806). Daily solar radiation, relative humidity, wind speed, and missing precipitation and temperature information were derived using SWAT's built-in weather generator (Neitsch et al., 2011). Monthly streamflow and water quality information over the period of 1990 - 1995 was obtained from Jordan et al. (1997). Annual estimates of nitrate loads by sub-watershed areas within GB watershed were provided by Primrose et al. (1997).

The geospatial dataset needed to run SWAT simulations includes digital elevation model (DEM), hydrologic soil types, and land cover/land use. A Light Detection and Ranging (LiDAR)-based 2-m DEM, processed to add artificial drainage ditches by the USDA-Agricultural Research Service (ARS) at Beltsville, Maryland, (Lang et al., 2012) was used to extract topographic information. The DEM was used to delineate the drainage area, subdivide the study area into smaller modeling units, and define the stream network. Soil information was obtained from the Soil Survey Geographical Database (SSURGO) available from the USDA Natural Resources Conservation Service (NRCS).

A map of land use was prepared based on the comprehensive analysis of existing land use maps, including the U.S. Geological Survey's National Land Cover Database of 1992 and 2002, and 2006, the USDA National Agriculture Statistics Service (NASS) Cropland Data Layer (CDL) of 2002, 2008, 2009, and 2010 (Boryan

et al., 2012), and a high-resolution land use map developed from 1998 National Aerial Photography Program (NAPP) Digital Orthophoto Quad imagery (Sexton et al., 2012). These maps indicated a consistent pattern of land use distribution over the last two decades with little change. The spatial distribution of major croplands (e.g., soybean and corn) (Figure 2.2) was determined using 2008 CDL. As the two-year rotations of corn-soybean or soybean-corn were common practice and agricultural lands were used evenly for both crops, the placement of the crop rotations was simplified to alternate the locations of corn and soybean croplands every year using the 2008 CDL as a base map. While the placement of crop rotations between various years would vary, it was not possible to obtain the spatial distribution of major croplands for each simulation year. In addition, time series cropland patterns observed from recent CDL maps seem to support this generalized crop rotation pattern of interchanging the locations of corn and soybean fields.

Detailed agronomic management information was collected in the field, as well as through literature reviews and interviews with farmers and extension agents. Modeled agricultural practices and management reflects actual practices (i.e., no WCC practice, utilizing conservation tillage without irrigation) in the study region during the time of water quality monitoring (Sadeghi, et al., 2007), and the guidelines for WCC implementation practices were developed by the Maryland Department of Agriculture (MDA) cover crop program.

The GB watershed was subdivided into 29 sub-watersheds based on tributary drainage areas. Within each sub-watershed, the superimposing of similar land uses and soil type generated a total of 402 HRUs with 283 classified as agricultural HRUs.

The average size of HRUs ranged from 0.2 – 118.6 ha, with an average size of 11.8 ha and a standard deviation of 13.0 ha.

Table 2.1. List of data used in this study

Data	Source	Description	Year
DEM	MD-DNR	LiDAR-based 2 meter resolution	2006
	USDA-NASS	Land use map based on CDLs	2008
	USGS	NLCD	1992, 2002, 2006
Land use	USDA-ARS at Beltsville	Land use map developed through on-screen digitizing using NAPP digital orthophoto quad imagery (Sexton et al., 2012)	1998
Soils	USDA-NRCS	Soil Survey Geographic database	2012
Climate	NCDC	Daily precipitation and temperature	1990 – 2010
Streamflow	Jordan et al. (1997)	Monthly streamflow	1990 – 1995
Water Quality	Jordan et al. (1997)	Monthly nitrate	1990 – 1995

Note: MD-DNR stands for Maryland Department of Natural Resources

2.2.2.3 Calibration and validation of SWAT model

Although SWAT simulations were calculated on a daily basis, the calibration and validation were performed using the monthly water quality record available from the monitoring station located at the study watershed outlet. The calibration was performed manually under the baseline scenario with the 2-year crop rotations, following the standard procedure outlined in the SWAT user’s manual (Winchell et al., 2011). The key parameters and their allowable ranges were identified using the sensitivity analysis performed by Sexton et al. (2010) and previous studies (Table 2.2). The simulations included a 2-year warm up period (1990-1991) to establish the initial conditions. Model calibration was done using the next 2 years of water quality records (1992-1993), and the remaining records were used for validation (1994-1995). This short period of spin up and calibration could limit the model’s capability to capture the effects of inter-annual variability of weather on streamflow and nitrate

loads. The calibration was done as follows. We first adjusted the parameters related to the streamflow and then for nitrate, by making a small change in their allowable ranges (Table 2.2). The parameters were calibrated sequentially in order of their sensitivity as reported by Sexton et al. (2010). The calibration was run in a batch and the model performances statistics (discussed below) were computed for each run. We chose the parameter values that produce the best statistical outputs while meeting the model performance criteria as discussed by Moriasi et al. (2007). To assess longer-term effects, the model simulations were performed over the period of 1992 - 2000. We used ArcSWAT2009 with the 582 version of the executable file in the ArcGIS 9.3.1 interface.

Table 2.2. List of calibrated parameters

Parameter	Description	Range	Calibrated value
CN2*	Curve number	-20 to +20%	-16%
ESCO [†]	Soil evaporation compensation factor	0 – 1	1.000
SURLAG*	Surface runoff lag coefficient	0 – 10	1
ALPHA_BF ^{&}	Base flow recession constant	0 – 1	0.045
GW_DELAY ^{&}	Delay time for aquifer recharge	0 – 50	26
CH_K2*	Effective hydraulic conductivity	0 –150	2
CH_N2 ^{&}	Manning coefficient	0.02 – 0.1	0.038
NPERCO ^{&}	Nitrogen percolation coefficient	0.01 –1	1
N_UPDIS ^{\$}	Nitrogen uptake distribution parameter	5 – 50	50
ANION_EXCL ^{&}	Fraction of porosity from which anions are excluded	0.1 – 0.7	0.405
ERORGN ^{&}	Organic N enrichment ratio for load with sediment	0 – 5	0.497
BIOMIX [#]	Biological mixing efficiency	0.01 – 1.0	0.01
LAIMX1 [^]	Fraction of the maximum leaf area index corresponding to the first point on the leaf area development curve	-	0.01 (Wheat) 0.02 (Barley) 0.12 (Rye)
LAIMX2 [^]	Fraction of the maximum leaf area index corresponding to the second point	-	0.14 (Wheat) 0.31 (Barley) 0.35 (Rye)

Note: the ranges of parameters were adapted from existing literature [* Zhang et al. (2008), [†] Kang et al. (2006), [&] Meng et al. (2010), ^{\$} Saleh and De (2004), [#] Chu et al. (2004), and [^] Hively et al. (2009)]

Accuracy of the model calibration was assessed with three statistical model performance measures: Nash-Sutcliffe efficiency coefficient (NSE), root mean

squared error (RMSE)-standard deviation ratio (RSR), and percent-bias (P-bias) (Moriassi et al., 2007). They are defined as follows:

$$NSE = 1 - \left[\frac{\sum_{i=1}^n (O_i - S_i)^2}{\sum_{i=1}^n (O_i - \bar{O})^2} \right] \quad (2.1)$$

$$RSR = \frac{RMSE}{STDEV_{obs}} = \left[\frac{\sqrt{\sum_{i=1}^n (O_i - S_i)^2}}{\sqrt{\sum_{i=1}^n (O_i - \bar{O})^2}} \right] \quad (2.2)$$

$$P - bias = \left[\frac{\sum_{i=1}^n (O_i - S_i) \times 100}{\sum_{i=1}^n O_i} \right] \quad (2.3)$$

where O_i are observed and S_i are simulated data, \bar{O} is observed mean values, and n equals the number of observations. The values of those statistical measures were compared to the model evaluation criteria set for various water quality parameters (Moriassi et al., 2007).

2.2.2.4 Calibration of plant growth parameters

WCC plant growth parameters were calibrated to more realistically simulate cover crop growth during winter. Specifically, we modified the parameters that control the leaf area development curve using biomass estimates provided by Hively et al. (2009). Their study reported satellite-based biomass estimates for three commonly used WCCs categorized by various planting dates over the period of 2005-2006 in the Choptank River region. This information was analyzed to associate WCC

biomass estimates with heat units. Heat units were computed based on the potential heat unit (PHU) theory as implemented in SWAT, with the daily climate record over the cover crop monitoring period (2005 – 2006). The crop growth module of SWAT was then run with average daily climate data over 1990 – 2000 using the default parameter values to provide estimates of biomass and leaf area index (LAI) by growing degree days. This assumption should not have a significant effect on plant growth simulation, even if there is some inter-annual variability in weather conditions between the two periods. This is because the plant growth cycle in SWAT is simulated using heat unit theory, and there was little difference in heat units counted during two different time periods. Heat units are based on the accumulated number of growing days that have a daily temperature above the base temperature. Below the base temperature, no plant growth should occur.

Using this information, we then were able to relate simulated LAI values to the reported biomass estimates and heat units. These LAI values and the corresponding heat units were then normalized by the maximum LAI and total potential heat units required for plant maturity, and the relationship between these two normalized values (fractional LAI and heat units) was fitted using a simple regression model. This fitted model was extrapolated to identify two LAI parameter values (Table 2.2) required to adjust the leaf area development curve in the SWAT model.

2.2.2.5 Assessing the effectiveness of winter cover crops with multiple scenarios

We assessed the potential effects of WCCs on nitrate removal at the field and watershed scales under multiple implementation scenarios. Details of these scenarios are presented in Table 2.3. The MDA Cover Crop Program offers a varying cost share according to WCC planting species and cutoff planting dates. Following the program guidelines and county-level statistics of WCC implementation (MDA, 2012), we constructed multiple scenarios relevant to regional cover crop practices with three major cover crop species – i.e., wheat (*Triticum aestivum L.*), barley (*Hordeum vulgare L.*), and rye (*Secale cereale L.*) – and two planting date categories (early/late). Additional cover crop scenarios were developed to assess their effectiveness by varying extent of cover crop implementation. The average nitrate export was assessed at the field scale based on the simulation output over the period of 1992 – 2000 under the baseline scenario (i.e., no cover crop). Then, all agricultural HRUs were sorted by nitrate load and equally subdivided into five groups. Each group was then introduced incrementally for cover crop implementation, in order from the highest to the lowest nitrate load.

Table 2.3. List of winter cover crop scenarios

Scenario	Species	Planting timing	Abbreviations
1	None	N/A	Baseline
2	Winter wheat	Early planting (October 3)	WE
3	Barley	Early planting (October 3)	BE
4	Rye	Early planting (October 3)	RE
5	Wheat	Late planting (November 1)	WL
6	Barley	Late planting (November 1)	BL
7	Rye	Late planting (November 1)	RL

Note: early planting scenarios include 50 % of early planting on corn and 50 % of late planting on soybean. Soybean requires longer growing day, and actual practices and county statistics showed that early planting was generally allowed for corn only.

Table 2.4 summarizes agricultural practices and scheduling used for different scenarios. There was no difference between baseline and cover crop scenarios during the growing season. The croplands were managed with the typical 2-year corn–soybean or soybean–corn rotation, and fertilizer was only applied to corn cropping in the beginning of the growing season, due to its high demand for nutrients to support growth and yield. Instead of winter fallow, cover crop scenarios assumed placement of WCCs. The WCCs were planted after harvesting of summer crops either in the beginning of October (early planting) or November (late planting), and were chemically killed at the beginning of the following growing season (early April). The specific dates (3 October and 1 November) of cover crop planting were set according to MDA guidelines, with slight adjustment over the course of the simulation period to avoid days with substantial precipitation falling immediately prior to winter cover planting. Note that the harvest date of summer crops under the baseline was set for 15 October to make the model results from the baseline more comparable to the early and late cover crop scenarios by setting the harvesting date in between them. Actual practices and historical statistics indicate that early planting was generally allowed for corn only, as soybean requires later harvest in the Choptank River region. The MDA’s county level statistics over 2006 – 2011 showed that WCCs were generally planted later following soybean (in general, after mid-October), while two-thirds of cover crop implementation occurred prior to mid-October after corn. This difference could be due to late harvesting to allow for double planted soybean crops. In this study, early planting scenarios were considered to be more active conservative agricultural practices than late planting scenarios. Therefore, early planting scenarios

were set to apply the early planting date at 100 % where it could be applicable (i.e., corn fields), while the remaining fields (i.e., soybean fields) were assumed to be treated with 100 % of late plantings. As a result, these scenarios include 50 % of cover cropping with early planting on cornfields and the remaining 50 % with late planting on soybean fields, as both crop types have roughly an equal share of total croplands. Due to this mixed effect, the nitrate removal efficiency by different planting dates could not be fully assessed at the watershed scale, but evaluated at the field scale.

Table 2.4. Agricultural practices and management scheduling for the baseline and winter cover crop scenarios.

Baseline scenario (No winter cover crop)		
Year	Corn-Soybean rotation	Soybean-Corn rotation
First Year	Apr. 12- poultry manure; 4942 kg/ha (4413 lb/ac) Apr. 27- poultry manure; 2471 kg/ha (2206 lb/ac) April 30- Corn plant: no-till Jun. 15- sidedress 30% UAN; 112 kg/ha (100 lb/ac) Oct. 15- Corn harvest	May 20- Soybean plant: no-till Oct. 15 – Soybean harvest
Second Year	May 20- Soybean plant: no-till Oct. 15 – Soybean harvest	April 12- poultry manure; 4942 kg/ha (4413 lb/ac) April 27- poultry manure; 2471 kg/ha (2206 lb/ac) April 30- Corn plant: no-till Jun. 15- sidedress 30% UAN; 112 kg/ha (100 lb/ac) Oct. 15- Corn harvest
Winter cover crop scenario		
Year	Corn-Soybean rotation	Soybean-Corn rotation
First Year	April 12- poultry manure; 4942 kg/ha (4413 lb/ac) April 27- poultry manure; 2471 kg/ha (2206 lb/ac) April 30- Corn plant: no-till Jun. 15- sidedress 30% UAN; 112 kg/ha (100 lb/ac) Oct. 1 & Oct. 30- Corn harvesting Oct. 3 & Nov. 1 – Cover crops planting *	May 20- Soybean plant: no-till Oct. 30 – Soybean harvesting Nov. 1 – Cover crop planting**
Second Year	Apr. 1 – chemically kill cover crops May 20- Soybean plant: no-till Oct. 30 – Soybean harvesting Nov. 1 – Cover crop planting *	Apr. 1 – chemically kill cover crops April 12- poultry manure; 4942 kg/ha (4413 lb/ac) April 27- poultry manure; 2471 kg/ha (2206 lb/ac) April 30- Corn plant: no-till Jun. 15- sidedress 30% UAN; 112 kg/ha (100 lb/ac) Oct. 1 & Oct. 30- Corn harvesting Oct. 3 & Nov. 1 – Cover crop planting *

Note: the typical N content for poultry manure is 2.8 % (Glancey et al., 2012).

2.3 Results and Discussions

2.3.1 SWAT calibration and validation

The simulated results of monthly streamflow and nitrate were compared with the observed data for both the calibration and validation periods. Table 2.2 provides the list of the adjusted parameter values after model calibration. Overall, Figure 2.4 shows good agreement between measured and simulated monthly discharge of streamflow and nitrate. It illustrates the 95 percent prediction uncertainty (PPU, the shaded region) of the SWAT simulation model with the monthly observed and the best simulated streamflow and nitrates. The 95 PPU of streamflow seems to quantify most uncertainties as the interval includes most of the measured data. However, the 95 PPU of nitrate does not seem to represent all the uncertainty, particularly for the low-flow season when most of the simulated streamflow are not in good agreement with the observed streamflow. This could be caused by the limitations of SWAT itself and the large errors associated with calibration. The calibration was conducted over a short period and this could limit the capability of the calibrated model to capture the effects of weather variability on streamflow and nitrate. In addition, the nitrate load calculated based on the field sampling of nitrate stream concentration (i.e., the observed nitrate load) could be overestimated for the low flow season, if it is not based on sufficient coverage and consistency within the data set (e.g., continuous on-site measurements). The P factor values for streamflow ranges between 0.62 and 0.75 (as shown in Table 2.5), but most observed data outside the 95 PPU are not far off from this shaded region. These values could be well captured if a lower level of prediction interval (e.g., 90 %) is chosen. The nitrate simulation results produced a

much smaller P factor value than the streamflow, indicating much greater uncertainty. However, the R factor value of nitrate is smaller than that of streamflow, indicating the 95 PPU band for the nitrate is narrower (Table 2.5).

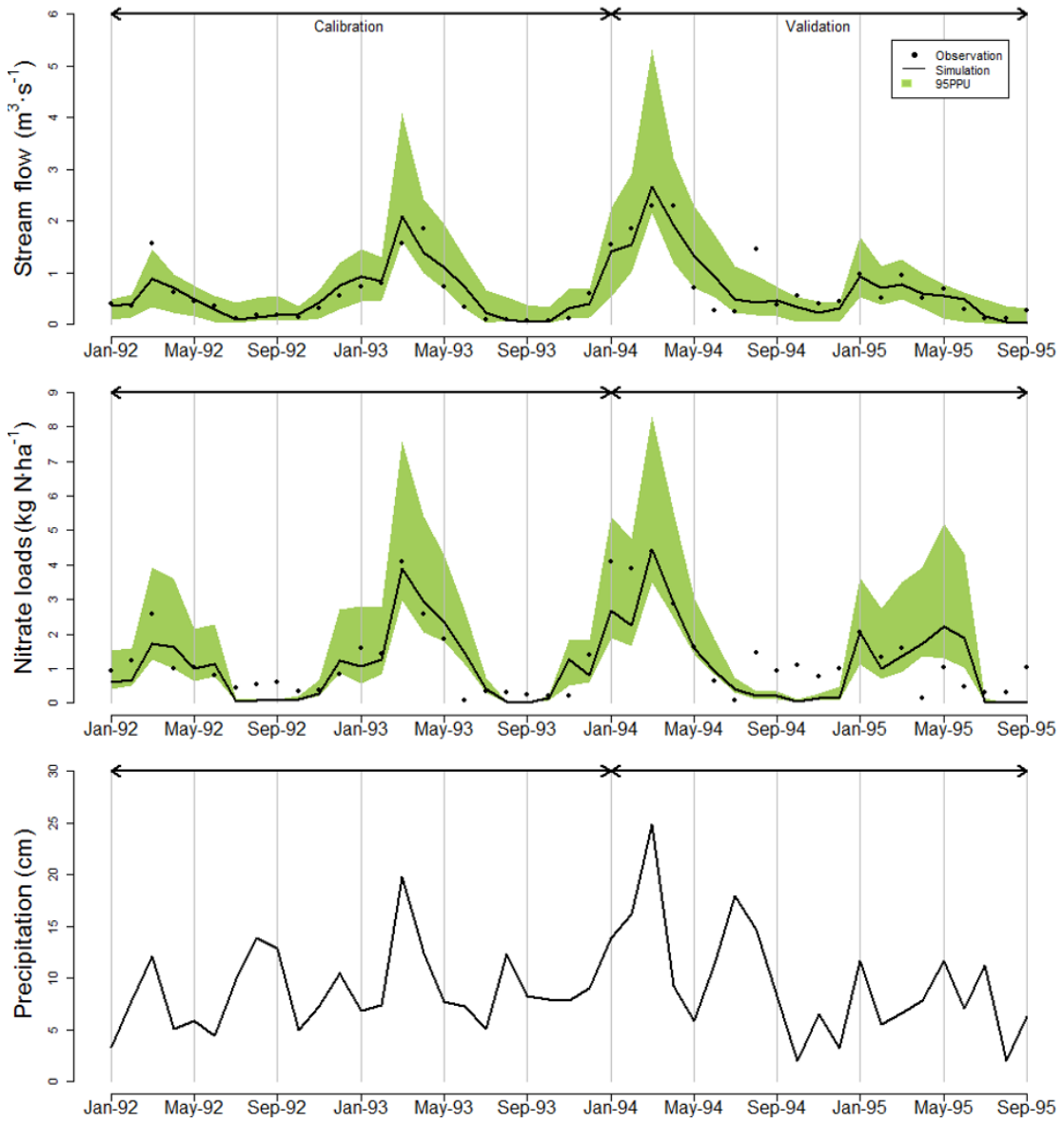


Figure 2.4. Observed and simulated streamflow and nitrate loads during the monitoring period (1992-1995) at the watershed scale

Table 2.5. Model performance measures for streamflow and nitrate.

Variable	Period	RSR	NSE	P-bias	P factor	R factor
Flow	Calibration	0.495 ^{***}	0.744 ^{**}	7.0 ^{***}	0.75	0.94
	Validation	0.517 ^{**}	0.718 ^{**}	-2.9 ^{***}	0.62	0.83
Nitrate	Calibration	0.550 ^{**}	0.684 ^{**}	-3.4 ^{***}	0.50	0.67
	Validation	0.688 [*]	0.503 [*]	-15.6 ^{***}	0.29	0.62

Note: performance rating indicates ^{*} satisfactory, ^{**} Good, and ^{***} Very Good. The performance rating criteria are adapted from Moriasi et al. (2009) and these statistics are computed based on the monthly water quality record.

Table 2.5 also presents a summary of model performance measures and their accuracy ratings based on the statistical evaluation guidelines reported by Moriasi et al. (2007). These performance measures are calculated based on a monthly water quality record. Overall, the model performance rating for streamflow and nitrate loads exceeded the “satisfactory” rating in both the calibration and validation periods. Model simulation results for streamflow were more congruent with the observed values than for nitrate, but the pattern of simulated nitrate was similar to the trend of simulated streamflow. Also, simulation results for the calibration period were in better agreement with the observed values, compared to the validation period. The largest discrepancy between simulated and measured streamflow and nitrate was in 1994. Unlike the simulation output, a high peak in stream- flow and consequently in nitrate load was observed in August. This relatively high flow and nitrate were somewhat unusual, as the weather record for this site did not show any dramatic change in precipitation during August of 1994 compared to the previous years. However, the reported streamflow in August of 1994 was much higher than observations from other years. In addition, the streamflow record from an adjacent watershed, with similar characteristics and size, did not produce high peak values for streamflow during the same period. This difference could perhaps be explained due to

unexpected agricultural practices, localized thunderstorms that did not occur at the weather station and nearby watershed, or human/measurement errors, although the exact cause of such error could not be determined. The SWAT simulation provided considerably improved results compared to previous studies conducted in the study area (Lee et al., 2000; Sadeghi et al., 2007; Sexton et al., 2010). These improvements may be due to different model choice (Niraula et al., 2013), the recent update of the SWAT model to more accurately predict nitrate in groundwater (USDA-ARS, 2012; Seo et al., 2014), and use of more accurate higher spatial resolution DEMs (Chaplot, 2005; Chaubey et al., 2005).

Accurate simulation of WCC growth and biomass at various stages of production is crucial to accurately estimating the potential of WCC to uptake residual N and reduce nitrate load. The WCC program was implemented in 2005 at this site and, therefore, no data were available to validate predicted WCC biomass over the period of 1992 – 2000. However, we are confident in our biomass simulation, as the simulated 8-year averaged WCC biomass estimates obtained at the HRU scale were comparable to the range of WCC biomass reported by Hively et al. (2009). It is to be noted that without calibration, WCC growth was simulated at a much faster growth rate, and the growth trend over winter months did not match field data as reported in Hively et al. (2009). This study calculated above-ground WCC biomass with a range of planting dates, based on field survey and satellite images acquired over the period of 2005 – 2006. For example, the modeled growth rate of rye before calibration was substantially lower in the early growth stage, producing much less biomass than observed values. Figure 2.5 shows the agreement between measured and simulated

biomass estimates after calibration, at the field (HRU) scale. Note that the simulated estimates of WCC biomass were at the upper end of the reported values, as the simulation output included both above- and below-ground biomass.

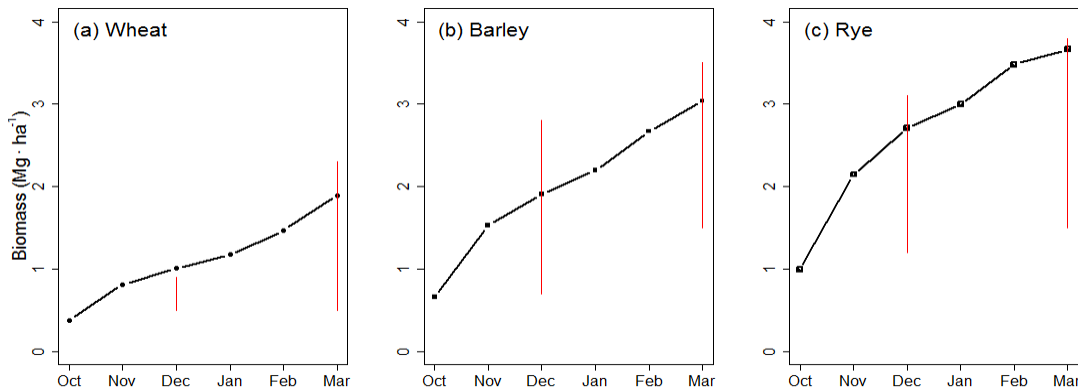


Figure 2.5. Estimation of winter cover crop biomass during the winter fallow period

Note: This figure presents monthly average total biomass (both above- and below-ground biomass) over the simulation period for three planting species obtained at the field (HRU) scale. The vertical red line represents the range of above-ground biomass estimates due to different growing/planting days from Hively et al. (2009). The simulated total biomass lies at the upper end of above ground biomass estimates.

2.3.2 Multiple scenario analysis

WCCs had little impact on catchment hydrology but a profound effect on nitrate exports. Figure 2.6 presents 9-year average annual mean streamflow, annual ET, and annual nitrate loads, under baseline and multiple cover crop scenarios. As reported from previous studies (Kaspar et al., 2007; Islam et al., 2006), the inclusion of a winter cover crop reduced streamflow only slightly (< 10 %). Similarly, our study found streamflow reductions of less than 8 %. Winter cover cropping reduced stream- flow from 8.5 to $7.8 \text{ m}^3 \cdot \text{s}^{-1}$ (RE) and $8.4 \text{ m}^3 \cdot \text{s}^{-1}$ (WL), and increased ET from 667 to 673 mm (WL) and 710 mm (RE), in comparison to the baseline scenario.

While the effects of winter vegetation on ET were relatively low, any water loss due to ET could be offset as cover cropping usually increases soil saturation by increasing water infiltration capacity (Dabney, 1998; Islam et al., 2006). Because the study site typically exhibits maximum streamflow during winter with rising groundwater levels (Fisher et al., 2010), the relative difference in streamflow due to WCCs remained small. Rye cover crops caused the most changes to the hydrologic budget followed by barley and winter wheat cover crops. Early planting scenarios produced slightly lower streamflow and higher ET, compared to those with the later planting date.

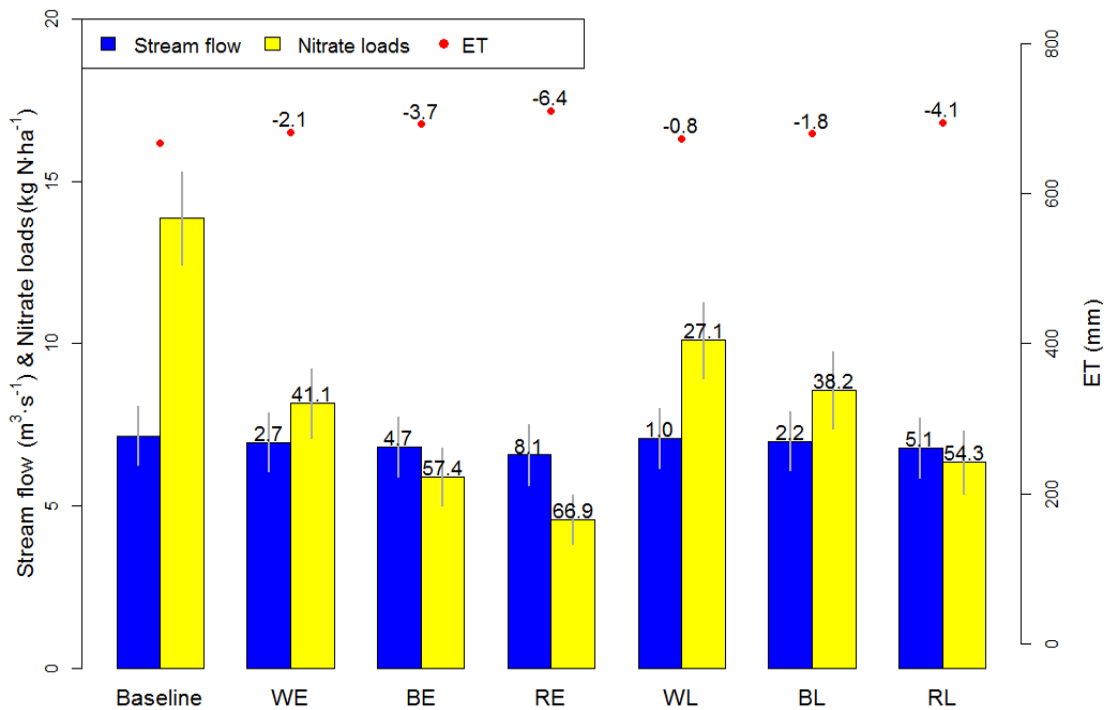


Figure 2.6. The 9-year average streamflow, annual actual evapotranspiration (ET), and annual nitrate loads at watershed scale under multiple cover crop scenarios

Note: Error bar (vertical line) represents standard deviation. The numeric value on the bar and dotted graphs indicates reduction rate (RR). RR is calculated by taking the relative difference in simulation outputs from the baseline and cover crop scenarios [RR = (Baseline – Cover crop Scenario) / Baseline].

Unlike its small hydrologic effect, winter cover cropping greatly reduced nitrate loads and there were large differences in nitrate loads by planting species and dates. Annual nitrate loads with WCC scenarios ranged from 4.6 (RE) to 10.1 kg N·ha⁻¹ (WL). The difference in nitrate loads under different WCC scenarios ranged from 1.3 (when RE was compared to BE, barley early) to 5.5 kg·ha⁻¹ (when RE was compared to WL). If the comparison of the removal efficiency was made within species, early cover cropping (3 October) lowered annual nitrate loads by 1.8 (rye and winter wheat) to 2.7 (barley) kg N·ha⁻¹, compared to late cover cropping (1 November). When compared with the baseline scenario (13.9 kg N·ha⁻¹), the WCC scenarios reduced nitrate loads by 27 (WL) – 67 % (RE) at the watershed scale. This finding compared well with the results of previous studies that reported the importance of early planting date (Ritter et al., 1998; Feyereisen et al., 2006; Hively et al., 2009). Shorter day lengths and lower temperatures could also limit the growth of WCC biomass during the winter season. Therefore, earlier planting could increase the amount of nitrogen uptake by WCCs because of longer growing seasons and warmer conditions (Baggs et al., 2000). Similar research in Minnesota also demonstrated that WCCs planted 45 days earlier reduced 6.5 kg N·ha⁻¹ more nitrogen than late planting (Feyereisen et al., 2006). Our simulation results are slightly lower than these published values, due to fewer growing days (~ 30 days). The earlier planting occurred ~ 30 days prior to the late planting.

The simulation results indicate that rye is the most effective cover crop at reducing nitrate loads. Rye is well adapted for use as a WCC due to its rapid growth and winter hardiness, and these characteristics enabled rye to consume a larger

amount of excessive nitrogen than other crops (Shipley et al., 1992; Clark, 2007; Hively et al., 2009). Barley is a cool-season crop and develops a strong root system during the winter season. Barley exhibits better nutrient uptake capacity than winter wheat (Malhi et al., 2006; Clark, 2007). Our simulation results were consistent with previous studies. As shown in Figure 2.5, rye grows faster than other WCCs particularly in the early growth stage, taking up higher levels of nitrate. Compared to the baseline scenario, rye removed more than 67 % of nitrate with early planting, and 54 % with late planting (Figure 2.6). Barley had a nitrate reduction rate of 57 % and winter wheat 41 % with early planting, but this removal efficiency drops to 38 % for barley and 27 % for winter wheat with late planting (Figure 2.6). Figure 6 illustrates that late-planted rye was nearly as effective as early-planted barley and more effective than early-planted winter wheat.

Simulated nitrate removal efficiency was greatly affected by different levels of cover crop implementation as shown in Figure 2.7. As expected, removal efficiency increased with increasing coverage of cover crop implementation, though the slope of removal efficiency slightly decreased at the 60 % extent. This finding seems to indicate that the nitrate reduction rate does not increase linearly with increasing coverage, but its relative efficiency could decrease after the coverage of cover crop implementation exceeds 50 % of the croplands. While this finding seems to be reasonable, further field-based studies are needed to verify this finding. It was noted that 60 % cover crop coverage with an early planting date would reduce more nitrate than 100 % cover crop coverage with late planting, emphasizing the

importance of early cover crop planting as indicated by other studies (Ritter et al., 1998; Hively et al., 2009).

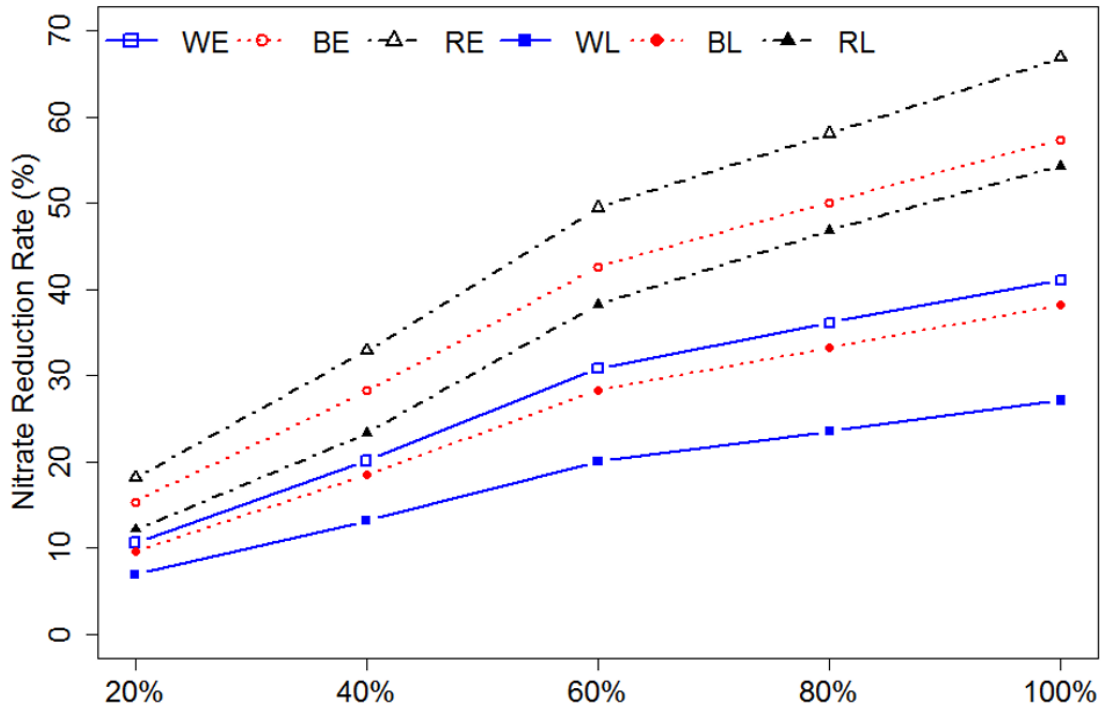


Figure 2.7. Nitrate reduction rates by varying degree of winter cover crop implementation evaluated at the watershed scale.

The effects of winter cover cropping were further assessed by quantifying the amount of nitrate transported from agricultural fields by different delivery pathways to waterways (surface runoff, lateral flow, and shallow groundwater) and nitrate leached to deep groundwater. Figure 2.8 presents nitrate loads per unit area leaving agricultural fields during the winter fallow period (October–March). The effectiveness of winter cover cropping to reduce nitrate leaching is particularly noticeable, as reported by earlier studies (McCraacken et al., 1994; Brandi-Dohrn et al., 1997; Francis et al., 1998; Bergstrom and Jokela, 2001; Rinnofner et al., 2008). At the field scale, the seasonal average of nitrate leaching (shown as “L” in Figure 2.8)

over the winter fallow period (October– March) without WCCs was estimated as 43 kg N·ha⁻¹. With WCCs, nitrate leaching decreased to 3.0 – 32.0 kg N·ha⁻¹, depending on planting species and timing, resulting in a reduction rate of 26 – 93 %, compared to baseline values. In addition, the amount of nitrate transported from fields to waterways by surface runoff, lateral flow, or shallow groundwater (referred to as DPs, direct pathways, in Figure 2.8) was greatly reduced from 2.9 to 10.7 kg N·ha⁻¹ with WCC scenarios, a reduction rate of 25 – 80 %. Similar to the watershed-scale analysis, rye with an early planting date produced the most effective result at the field scale with the highest reduction rate both through direct pathways and leaching.

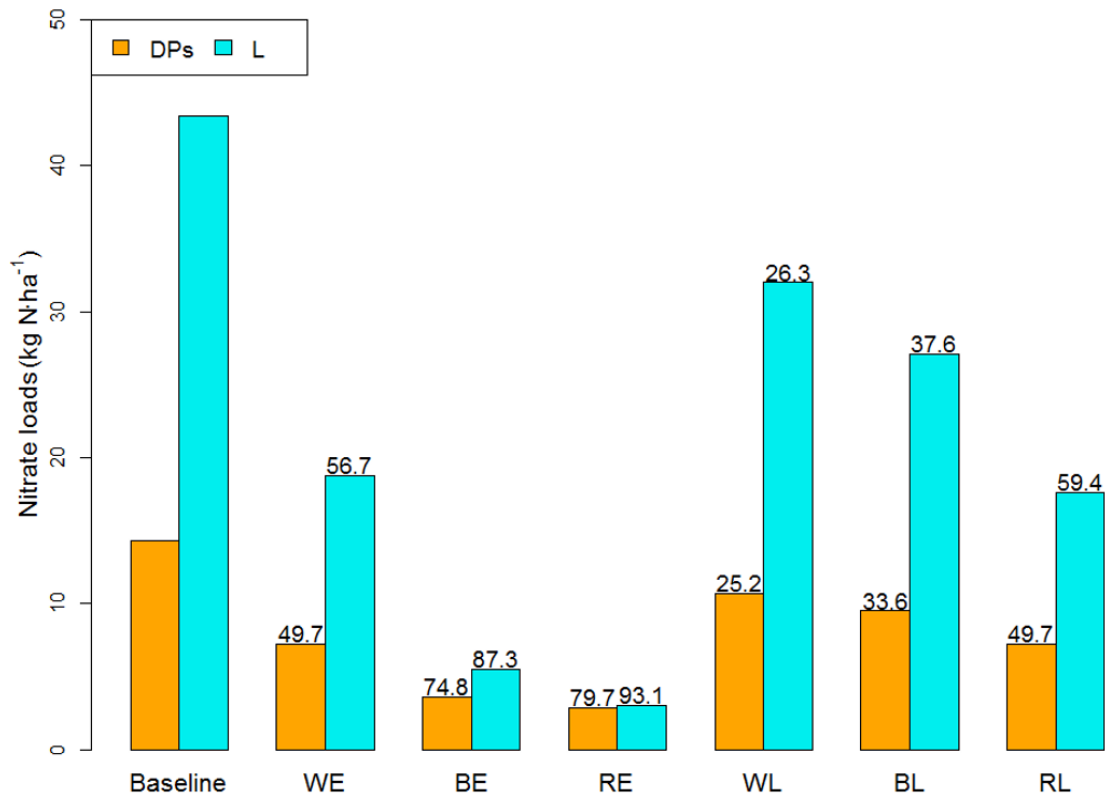


Figure 2.8. The 8-year average nitrate leaching and delivery to waterways during winter fallow assessed at the field scale under multiple winter cover crop scenarios.

Note: DPs (Direct pathways) refers to the amount of nitrate transported from agricultural fields (HRUs) to waterways by surface flow, lateral flow, and

groundwater; L is nitrate leaching to groundwater. The numeric value in parentheses, (), indicates reduction rate (RR). As the growth period of winter cover crop covers from October to March, results presented here were based on the eight years of simulation from October 1992 to March 2000.

2.3.3 Geospatial analysis to identify high nitrate load areas

The 9-year annual and monthly nitrate loads from agricultural fields (HRUs) simulated under the baseline scenario were analyzed to pinpoint those areas with a high potential for nitrate loads and better understand the characteristics and variability of these high load zones. We classified all agricultural HRUs into five classes according to different levels of nitrate export potential. Nitrate export potential was computed by summing up nitrate transported by direct pathways and leaching to groundwater. We observed consistent spatial patterns in nitrate loads at the inter-annual and monthly timescale. Figure 2.9 illustrates the geographical distribution of nutrient loads from all agricultural HRUs based on the 9-year annual and monthly average simulation results from selected months. Those selected months were chosen considering seasonal characteristics of climate and hydrology as well as the timing of agricultural practices and scheduling that may produce differences in nitrate loads (e.g., high precipitation and groundwater flow in March/April, killing WCC and fertilizer application in April, and cover crop application in November).

The location of high nitrate load areas was generally associated with moderately well-drained soils and agricultural fields more frequently used for corn over the simulation period. Nitrate leaching dominated the total nitrate loads from the fields (i.e., potential for nitrate export), as it outweighed nitrate transport by direct pathways (as shown in Figure 2.8). We hypothesize that areas with moderately well-

drained soils allowed high nitrate leaching due to their high infiltration capacity (Figure 2.2). Because of the high N demand for corn growth and yield, corn cropping requires a considerable amount of fertilizer application during the early growth stage, while soybean does not require any fertilizer application (Table 2.4). Consequently, nitrate export from agricultural fields more frequently used for corn over the simulation period was significantly greater than those used for soybean, as reported by Kaspar et al. (2012). Therefore, it would be important to prioritize winter cover cropping application for those areas with well-drained soils used for corn production.

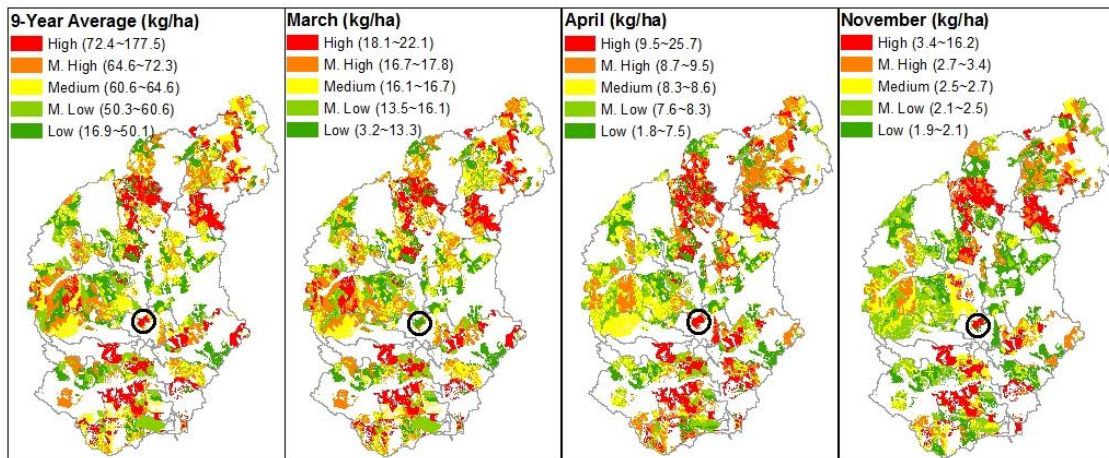


Figure 2.9. The spatial distribution of nitrate export potential from agricultural fields

Note: Nitrate export potential was computed by adding the annual or monthly averaged amount of nitrate leaching to the groundwater (L) and leaving to the streams by surface runoff, lateral flow, and groundwater (DPs) from the 9-year simulation results. Estimated nitrate loads from the HRUs were classified into five groups. In the legend M. High refers to Moderately High and M. Low Moderately Low. The HRUs within the black circle indicates outliers with extremely high nitrate loads. This area is characterized by poorly drained hydric soil (“Urban land”) and consistently produces extremely high nitrate loads throughout years and seasons. The white area is non-agricultural land as shown in Figure 2.2.

2.4 Conclusions

This study demonstrates the effectiveness of WCCs for reducing nitrate loads and shows that nitrate removal efficiency varies greatly by species, timing, and extent of WCC implementation. It also illustrates that nitrate exports vary based on edaphic and agronomic characteristics of the croplands upon which crops are planted. Therefore, it is important to develop management guidelines to encourage optimal planting species, timing, and locations to achieve enhanced water quality benefits. This study suggests that early-planted rye is the most effective cover crop practice, with the potential to reduce nitrate load by 67 % over the baseline at the watershed scale. We hypothesize that the relatively high nitrate removal efficiency of early-planted rye is due to the more rapid growth rate of rye, especially in the early growth stage, compared to other species. As expected, nitrate removal efficiency increased significantly with early planting of all species and increasing cover crop implementation. The study also illustrates that locations of high nitrate export were generally associated with moderately well-drained soils and agricultural fields more frequently used for corn. Therefore, it would be important to prioritize WCC application with early-planted rye for those areas with well-drained soils used for corn production.

This study also provides a new approach to calibrate WCC growth parameters. Growth parameters for WCCs need to be carefully calibrated for shorter day lengths and lower temperatures during the winter, to provide an accurate estimation of the nutrient uptake efficiency of WCCs. Unfortunately, at present there are limited data available on WCC growth and biomass estimation at the field or landscape scales.

However, this data limitation is expected to be resolved in the future, as the planting of WCCs becomes more common and monitoring programs are enhanced through the availability of no- or low-cost time series of remotely sensed data (e.g., Landsat). With multiyear cover crop biomass and growth data, the methodology presented in this paper could be extended to better calibrate growth parameters and validate WCC biomass, improving the accuracy of SWAT in estimating nitrate removal efficiency by WCCs.

Chapter 3 Impacts of Watershed Characteristics and Crop Rotations on Winter Cover Crop Nitrate-Nitrogen Uptake Capacity within Agricultural Watersheds in the Chesapeake Bay region²

3.1 Introduction

The Chesapeake Bay (CB) is the largest and most productive estuary in the United States (US). Eleven major rivers flow into the bay's 166,000 km² drainage basin. Despite significant restoration efforts, the health of the bay has continued to deteriorate primarily as a result of load of nutrients and sediments from agricultural land (Reckhow et al., 2011). Nitrate in soil and groundwater can be stored for a relatively long time before discharging to streams. The lag time between the implementation of land-based Best Management Practice (BMP) and the realization of nutrient reductions can cause uncertainty regarding the effect of BMPs (Reckhow et al., 2011). Nitrogen (N)-enriched groundwater on the eastern shore of the Chesapeake Bay Watershed (CBW) has significant implication on the Bay's ecosystem, as groundwater in the Mid-Atlantic Coastal Plain contributes a large portion of streamflow (~70%) (Reckhow et al., 2011). Previous studies have demonstrated that nitrate flux in groundwater is spatially related to the proportion of

² The material presented in this Chapter has been published in Lee, S., Yeo, I.-Y, Sadeghi, A. M., McCarty, G. W., Hively, W. D., & Lang, M. W. (2016). Impacts of Watershed Characteristics and Crop Rotations on Winter Cover Crop Nitrate-Nitrogen Uptake Capacity within Agricultural Watersheds in the Chesapeake Bay Region. PLoS ONE, 11(6), e0157637

agricultural land in coastal watersheds (Fisher et al., 2010). For example, Ator and Denver (2012) reported that a watershed dominated by agriculture exported 9-fold more nitrate flux from groundwater to streams than other watersheds dominated by non-agricultural lands in coastal regions.

Winter cover crops (WCCs) have been identified as a potentially important BMP for reduction of nitrate loads in the CBW (McCarty et al., 2008). Specifically, in the Coastal Plain of the CBW, in-stream nitrate concentration during the winter season from October (after harvest of summer crops) to the following March (before planting of summer crops) can be very high (Denver, 2004). An earlier study by Fisher et al. (2010) showed that winter nitrate concentration can be nearly five times greater than that during the late summer. During the winter season, rising groundwater level can also increase nitrate concentration. This collectively leads to higher in-stream nitrate loads to the bay (Fisher et al., 2010; Brinsfield and Staver, 1991). The WCCs can reduce residual soil N after harvest of summer crops and therefore N leaching by converting it to crop biomass N (Dabney et al., 2001; Hively et al., 2009). Therefore, WCCs have become a promising BMP for improving water quality in this region. Because of their potential to improve water quality, federal and state government agencies are providing technical assistance and financial incentives to local farmers to encourage planting WCCs in the agricultural lands within the watershed.

The potential of WCCs to reduce nitrate loads to the bay, however, has not been fully assessed at the watershed scale considering different land characteristics and agricultural practices. Field studies have demonstrated reduction in soil nitrate concentration after planting WCCs, but they were limited to plot-scale studies

(Brinsfield and Staver, 1991; Hively et al., 2009). Findings from these field studies do not necessarily reflect the long-term impacts of WCCs at the watershed scale and have limited ability to evaluate the performance of WCCs under various soil and weather conditions. Recently, Yeo et al. (2014) conducted a watershed-scale assessment of WCC efficiency in a small agricultural watershed. They, however, did not demonstrate the effects of drainage condition of soils and agricultural practices on WCC performance. Hydrogeological conditions and agricultural practices including crop rotations can affect nitrate loads and the performance of WCC. For instance, well-drained soils characterized by greater infiltration rates promote the downward movement of water and N leaching. With aerobic soils and aquifer conditions, nitrate tends to remain stable in groundwater and can later be transported to streams (Ator and Denver, 2012). Meanwhile, poorly-drained soils characterized by lower infiltration rates have water-saturated (i.e., anaerobic) conditions, favorable to denitrification (Denver et al., 2010). Agricultural production on poorly-drained soils often requires extensive artificial drainage system, which can shorten flow pathways and reduce the amount of time it takes for nitrate to reach nearby streams (Fisher et al., 2010; McCarty et al., 2008). In addition, soil residual N after harvest of previous crops can vary by crop species (Smith and Sharpley, 1990). Mineralization of crop residue and soil organic matter can also affect nitrate concentration in the soil (Gentry et al., 2001). The chemical composition (i.e., C/N ratio) and the amount of crop residue returned to the soil can also affect nitrate (Gentry et al., 2001). For example, Kaboneka et al. (1997) reported that soybean residue released greater N from mineralization than corn and wheat due to higher N concentration.

Despite similar climatic conditions, agronomic practices, and watershed size, in-stream nitrate concentrations (and therefore nitrate loads) are quite different in the Tuckahoe Creek and Greensboro watersheds, two adjacent agricultural watersheds located in the coastal plain of the CBW. The goal of this study was to assess the long-term (2001 – 2008) impact of WCC practices, watershed characteristics, and crop rotations on catchment hydrology and nitrate loads in the Tuckahoe Creek and Greensboro watersheds using the Soil and Water Assessment Tool (SWAT) model and statistical methods. Process-based water quality models, such as the SWAT, have been shown to be promising tools for the evaluation of long-term BMP effectiveness on water quality improvement at the watershed scale (Van Liew et al., 2007) and development of site-specific management plans. The SWAT model was applied to both watersheds under multiple WCC implementation scenarios (e.g., crop species and timing). Using this model, we 1) investigated how different soil and land use characteristics affect the generation and transport of nitrate fluxes, and the nitrate removal efficiency of WCC at the watershed and cropland scale, and 2) evaluated the effects of crop rotations on soil N and nitrate concentration. Following the SWAT modeling, multiple statistical analyses were performed to assess if the simulation outputs under the WCC scenarios were statistically different from those under the baseline scenario (no WCC). We integrated various time series geospatial data layers and county statistics to develop more realistic scheduling and placement of crop rotations, and used WCC reports to develop different WCC management scenarios. Extending the methodology used by Yeo et al. (2014), the plant growth model

embedded in the SWAT was further calibrated to accurately simulate WCC biomass and nutrient uptake.

3.2 Data and Methods

3.2.1 Study area

This study was undertaken in two adjacent watersheds defined by U.S. Geological Survey (USGS) gauge stations at Tuckahoe Creek near Ruthsburg (USGS#01491500) and the Choptank River near Greensboro (USGS#01491000) which are referred to as the Tuckahoe Creek Watershed (TCW, ~ 220.7 km²) and Greensboro Watershed (GW, ~ 290.1 km²), respectively (Figure 3.1). They are located on the headwaters of the Choptank River watershed in the coastal plain of the CBW (Figure 3.1). The Choptank River watershed is a U.S. Department of Agriculture (USDA) Conservation Effects Assessment Project (CEAP) Benchmark Watershed (McCarty et al., 2008). Due to high nutrient levels (in particular nitrate) in addition to sediments and bacteria, the Choptank River is listed as “impaired” by the U.S. Environmental Protection Agency (USEPA) under Section 303(d) of the 1972 Clean Water Act and is subject to extensive monitoring (McCarty et al., 2008).

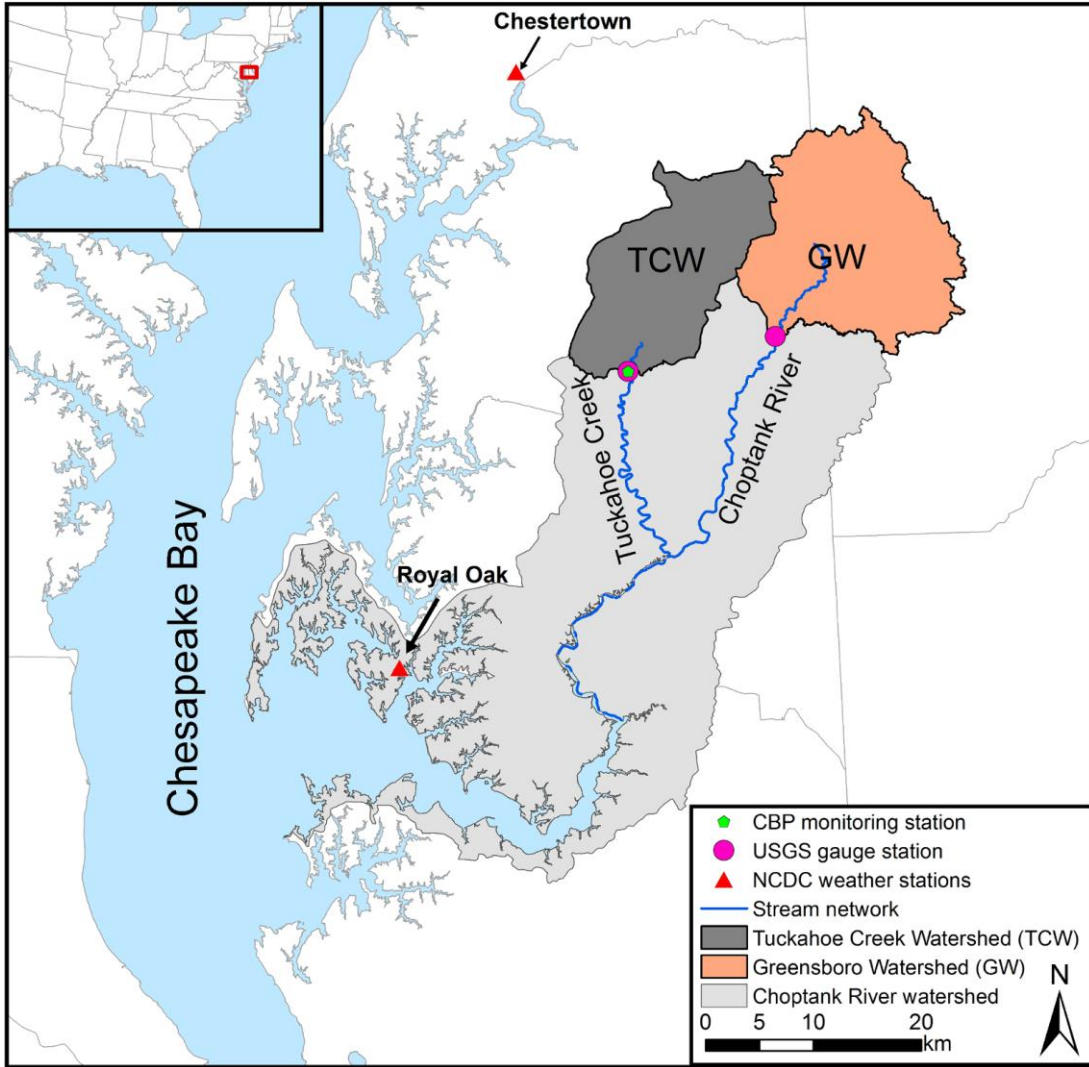


Figure 3.1. The location of the Tuckahoe Creek Watershed and Greensboro Watershed near Chesapeake Bay.

The two adjacent watersheds have very different characteristics in terms of soil properties and land use (Figure 3.2 and Table 3.1). In TCW, major land uses are agriculture (54.0%) and forestry (32.8%) dominated (56.1%) by well-drained soils (Hydrologic Soil Group, HSG-A&B) where 69.5% of the area are under croplands. In comparison, GW has a higher percentage of forest (48.3%) and a lower percentage of agricultural area (36.1%). A large portion of soils in GW (74.5%) is poorly-drained

(HSG-C&D) where 67.2% of croplands are located (Ator and Denver, 2015). In this region, drainage ditches have been established mostly on poorly-drained croplands for crop production. As a result, drainage ditches are widespread in GW compared to TCW (McCarty et al., 2008). Artificial subsurface drainage (e.g., tile drains) is less common in both watersheds. In general, well-drained soils have higher water infiltration capacity, produce little surface runoff, and facilitate the downward movement of water (Chiang, 1971). In comparison, poorly-drained soils have lower water infiltration capacity, substantial surface runoff, and limited water percolation (Chiang, 1971). Given the contrasting soil properties and land use in two watersheds, nitrate is expected to be lost mainly through leaching in TCW and near-surface runoff in GW (McCarty et al., 2008). Nitrate concentration in streamflow has been shown to vary with cropland soil properties according to regional water quality studies (Denver, 2004). Water quality records showed that the in-stream nitrate concentration in TCW is nearly two times higher than GW (McCarty et al., 2008). It is expected that nitrate removal by WCC would be greater in TCW due to greater area under crop production than GW.

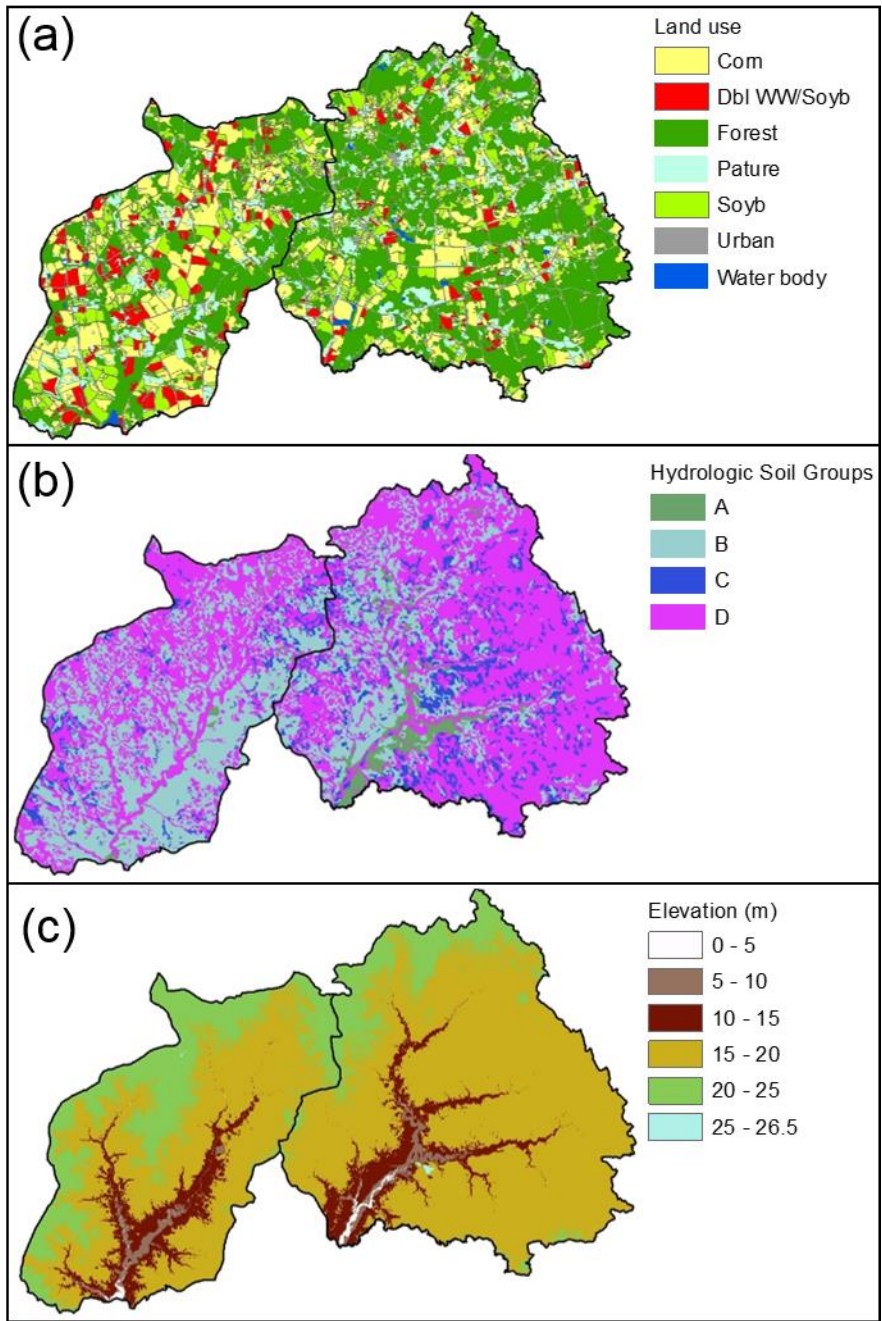


Figure 3.2. The physical characteristics of the Tuckahoe Creek Watershed (left) and Greensboro Watershed (right); (a) land use, (b) hydrologic soil groups, and (c) elevation.

Table 3.1. Soil properties and land use distribution of TCW and GW

Land use	TCW	GW
Agriculture	54.0 % [69.5% / 30.5 %]	36.1 % [32.8% / 67.2 %]
Forest	32.8 %	48.3 %
Pasture	8.4 %	9.3 %
Urban	4.2 %	5.6 %
Water body	0.6 %	0.7 %
HSG	TCW	GW
A	0.3 %	3.1 %
B	55.8 %	22.4 %
C	2.2 %	4.2 %
D	41.7 %	70.3 %

Note: Hydrologic soil groups (HSGs) are characterized as follows: Type A- well-drained soils with 7.6-11.4 mm·hr⁻¹ (0.3-0.45 inch·hr⁻¹) water infiltration rate; Type B - moderately well-drained soils with 3.8-7.6 mm·hr⁻¹ (0.15-0.30 inch·hr⁻¹) water infiltration rate; Type C - moderately poorly-drained soils with 1.3-3.8 mm·hr⁻¹ (0.05-0.15 in·hr⁻¹) water infiltration rate; Type D – poorly-drained soils with 0-1.3 mm·hr⁻¹ (0-0.05 inch·hr⁻¹) water infiltration rate. The values in the parenthesis [], denote the proportion of well-drained soils (HSG-A&B) and poorly-drained soils (HSG-C&D) used for agricultural lands, respectively.

3.2.2 SWAT watershed process model

The SWAT model has been widely used to evaluate water quality and assess effectiveness of BMPs (Neitsch et al., 2011). Major SWAT components include weather, hydrology, soil temperature, sedimentation, nutrients, pesticides, pathogens, plant growth, and land management (Neitsch et al., 2011). The model operates by partitioning a watershed into sub-watersheds, and then into hydrologic response units (HRUs) based on unique combinations of soil, land-use, and slope characteristics. Fluxes of water, sediment, nutrient, and other constituents of interest are simulated and computed at the HRU level and then aggregated to the sub-watershed and ultimately to the larger watershed through routing processes. Water balance within an HRU is determined based on precipitation, surface runoff, evapotranspiration (ET),

percolation, and groundwater recharge. Surface runoff is calculated using the Soil Conservation Service (SCS) Curve Number (CN) method (Neitsch et al., 2011). A daily CN is calculated based on soil permeability, land use, and antecedent soil water conditions. Once water enters the soil layers, it can evaporate, be taken up and transpired by plants, and flow into a surface water body through subsurface lateral flow, or percolate into groundwater through the vadose zone (i.e., unsaturated zone) between the bottom of soil layers (i.e., root zone) and the top of groundwater. Percolation, or downward flow, occurs when a soil layer exceeds its field capacity and the layer below is not saturated. The water entering the vadose zone flows into groundwater and its travel time in the vadose zone varies by the depth to the water table and hydraulic properties of the vadose and groundwater zones. The water in groundwater is partitioned into shallow groundwater, groundwater contribution to streamflow (i.e., groundwater flow), water discharge to the overlying unsaturated zone, and deep groundwater.

The N cycle is fully simulated in the SWAT model. Nitrogen is normally added by fertilizer, crop residue, N fixation, and wet and dry deposition, and removed by plant uptake, leaching, volatilization, denitrification, and surface runoff. Nitrate in the soil results from five processes: (1) nitrification (conversion of $\text{NH}_4\text{-N}$ to nitrate), (2) addition of manure and N fertilizer, (3) mineralization of soil organic N, (4) biological N fixation, and (5) mineralization of crop residue N.

3.2.3 Input data

The SWAT model requires detailed information on the climate, soils, and land use for the study site (Table 3.2). Daily precipitation and temperature were downloaded from the National Oceanic Atmospheric Administration (NOAA) National Climate Data Center (NCDC) at Chestertown and Royal Oak (USC00181750 and USC00187806, respectively) (Figure 3.1). Other climatic variables, such as daily solar radiation, relative humidity, and wind speed, were generated by the weather generator (WXGEN) embedded in the SWAT (Neitsch et al., 2011) due to data unavailability. Since the two watersheds are located side-by-side, we assumed that similar climate conditions prevail for both watersheds. By using the same climate inputs to both watersheds, we evaluated the impacts of soil properties and crop rotations on WCC performance. Monthly streamflow data for both watersheds were downloaded from USGS gauge stations on the Tuckahoe Creek near Ruthsburg (USGS#01491500) and the Upper Choptank River near Greensboro (USGS#01491000) (Figure 3.1). Nitrate concentration grab sample data were provided by the Chesapeake Bay Program (CBP, TUK#0181) for TCW and by USGS (USGS#01491000) for GW. These data were extrapolated to monthly NITRATE loads using the USGS LOAD ESTimator (LOADEST) program (Runkel, 2004) which has been widely used to estimate continuous water quality information from grab samples (Jha et al., 2007).

Table 3.2. List of data used in this study

Data	Source	Description	Year
DEM	MD-DNR	LiDAR-based 2 meter resolution	2006
Land use	USDA-NASS	Cropland Data Layer (CDL)	2008 - 2012
	MRLC	National Land Cover Database (NLCD)	2006
	USDA-FSA-APFO	National Agricultural Imagery Program Digital Orthophoto Quad Imagery	1998
	US Census Bureau	TIGER road map	2010
Soils	USDA-NRCS	Soil Survey Geographic database	2012
Climate	NCDC	Daily precipitation and temperature	1999 - 2008
Streamflow	USGS	Monthly streamflow	2001 - 2008
Water quality	USGS and CBP	Daily grab NITRATE samples	2001 - 2008

Note: MD-DNR stands for Maryland Department of Natural Resources. USDA-FSA-APFO stands for USDA-Farm Service Agency-Aerial Photography Field Office.

A soil map was prepared based on the USDA Natural Resources Conservation Service (NRCS) Soil Survey Geographic Database (SSURGO). Topography was delineated by resampling a 1 m Light Detection and Ranging (LiDAR)-based Digital Elevation Model (DEM, processed by the USDA-Agricultural Research Service (ARS) at Beltsville, Maryland) to 10 m using nearest-neighbor interpolation, since finer-scale DEMs have been found to overestimate slope parameter values in the SWAT (Beeson et al., 2014). The land use map and the scheduling of crop rotations were generated using 2008-2012 data from the USDA-National Agriculture Statistics Service (NASS) Cropland Data Layer (CDL), the Multi-Resolution Land Characteristics (MRLC) Consortium-National Land Cover Database (NLCD), digitized boundaries of agricultural fields, and the U.S. Census Bureau Topologically Integrated Geographic Encoding and Referencing (TIGER) road map. We assumed that there was no significant change in crop rotations (see Figure 3.3 and Table 3.3) between the period of our SWAT simulation (1999 – 2008) and the period of USDA-NASS CDLs coverage (2008 – 2012). The boundaries of agricultural fields were

digitized based on National Agricultural Imagery Program Digital Orthophoto Quad Imagery (1:12,000) and other land use types were delineated using the NLCD. The TIGER road map buffered out by 40 m was intersected with land use maps to better represent urban (i.e., impervious land cover) areas. For each agricultural boundary, the major crop types and their rotations were identified. From the resulting sequence of observed crop rotations, we applied five most frequent crop rotations to the SWAT simulation years used in this study (Table 3.3). The placement and sequence of crop rotations for the two watersheds are provided in Figure 3.3 and Table 3.3. Corn, soybean, and double crop winter wheat/soybean were the most frequently grown crops in this region (Figure 3.3).

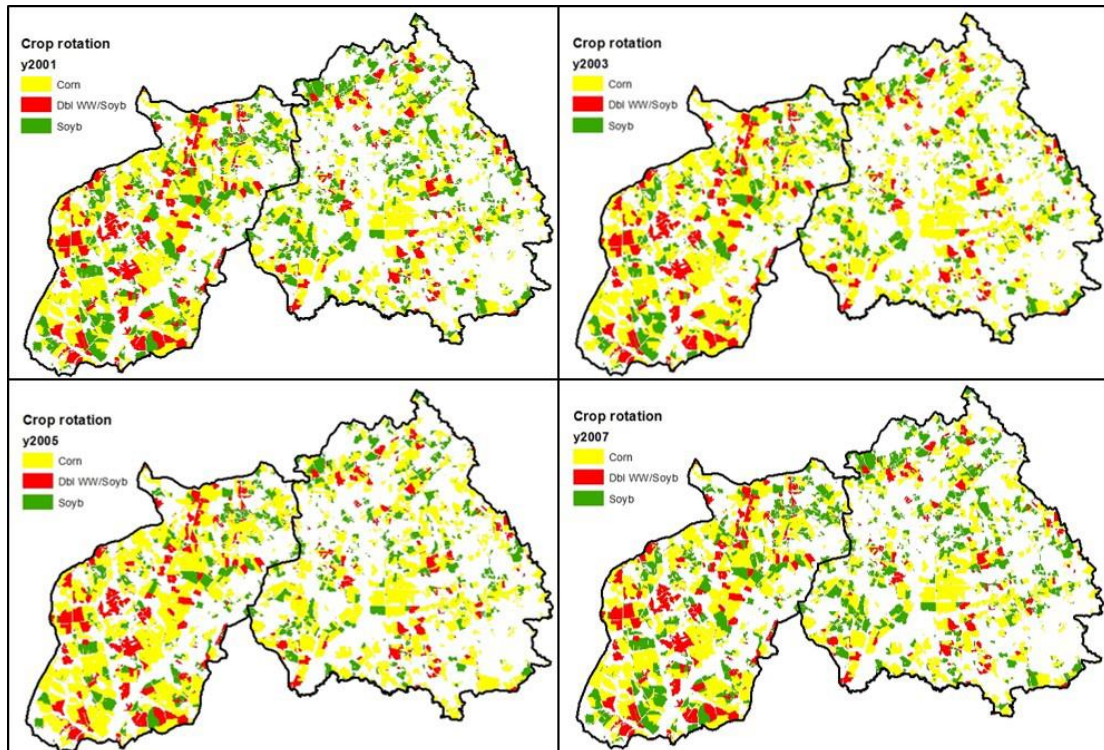


Figure 3.3. The spatial distribution of crop rotations in agricultural fields over the simulation period.

Note: Dbl WW/Soyb stands for double crops of winter wheat and soybean.

Table 3.3. Representative crop rotation information and distribution of corn and soybean fields

Type	2001	2002	2003	2004	2005	2006	2007	2008	Proportion (%)		
									TCW	GW	
AGA1	Corn	Dbl WW/Soyb	Corn	Dbl WW/Soyb	Corn	Dbl WW/Soyb	Corn	Dbl WW/Soyb	14.5	12.8	
AGA2	Dbl WW/Soyb	Corn	Dbl WW/Soyb	Corn	Dbl WW/Soyb	Corn	Dbl WW/Soyb	Corn	21.9	11.1	
AGAB	Corn	Soyb	Corn	Dbl WW/Soyb	Corn	Soyb	Corn	Dbl WW/Soyb	7.7	11.6	
AGB1	Corn	Soyb	Corn	Soyb	Corn	Soyb	Corn	Soyb	11.3	17.5	
AGB2	Soyb	Corn	Soyb	Corn	Soyb	Corn	Soyb	Corn	9.8	10.8	
AGC1	Corn	Corn	Corn	Corn	Corn	Corn	Corn	Corn	17.1	10.8	
AGD1	Soyb	Corn	Soyb	Soyb	Corn	Soyb	Soyb	Corn	10.2	12.0	
AGD2	Soyb	Soyb	Corn	Soyb	Soyb	Corn	Soyb	Soyb	7.5	13.4	
TCW	Corn (%)	50.6	59.0	58.1	48.8	60.8	56.3	50.6	59.0	-	-
	Soyb (%)	49.4	41.0	41.9	51.2	39.2	43.7	49.4	41.0	-	-
GW	Corn (%)	52.7	44.7	66.1	32.7	64.7	46.1	52.7	44.7	-	-
	Soyb (%)	47.3	55.3	33.9	67.3	35.3	53.9	47.3	55.3	-	-

Note: The last two columns indicate the relative area (%) of each crop rotation applied to croplands. The bottom four rows indicates the relative area (%) of corn and soybean fields resulted from different rotations applied concurrently. Dbl WW/Soyb is regarded as double crop winter wheat and soybean.

Detailed agronomic management information for field crops was collected through literature reviews and extension agent familiar with the watersheds. Based on collected data, we established the most representative management practices for these regions. We reduced N fertilization rate by 45 kg N·ha⁻¹ for corn after soybean compared with corn after corn, due to N credit from soybean residue, based on local expert knowledge (Table 3.4). The specific agronomic practices, including the timing of planting and harvest of summers crops and the amount and type of fertilizer applications (Table 3.4 and Figure 3.4), were provided by personal communication with R. J. Kratochivil (Assoc. Prof., Dept. of Plant Science & Landscape Architecture, University of Maryland, MD) in May 2014.

Table 3.4. The management schedules for baseline and winter cover crop scenarios

Baseline scenario (no winter cover crop)			
Crop	Planting	Fertilizer	Harvest
Corn (after corn)	Apr. 30 (no-till)	157 kg N·ha ⁻¹ (140 lb N·acre ⁻¹) of poultry manure on Apr. 20 45 kg N·ha ⁻¹ (40 lb N·ha ⁻¹) of sidedress 30% UAN on Jun. 7	Oct. 3
Corn (after Soybean and Double crop soybean)	Apr. 30 (no-till)	124 kg N·ha ⁻¹ (110 lb N·acre ⁻¹) of poultry manure on Apr. 20 34 kg N·ha ⁻¹ (30 lb N·ha ⁻¹) of sidedress 30% UAN on Jun. 7	Oct. 3
Soybean	May 20 (no-till)		Oct. 15
Double crop winter wheat (Dbl WW)	Oct. 10	34 kg N·ha ⁻¹ (30 lb N·acre ⁻¹) of sidedress 30% UAN on Oct. 8 45 kg N·ha ⁻¹ (40 lb N·acre ⁻¹) of sidedress 30% UAN on Mar. 1 67 kg N·ha ⁻¹ (60 lb N·acre ⁻¹) of sidedress 30% UAN on Apr. 5	Jun. 27
Double crop soybean (Dbl Soyb)	Jun. 29		Nov. 1
Winter cover crop scenario			
Crop	Planting	Fertilizer	Harvest
Corn (after corn)	Apr. 30 (no-till)	157 kg N·ha ⁻¹ (140 lb N·acre ⁻¹) of poultry manure on Apr. 20 45 kg N·ha ⁻¹ (40 lb N·acre ⁻¹) of sidedress 30% UAN on Jun. 7	Oct. 1 or 30
Corn (after Soybean and Double crop soybean)	Apr. 30 (no-till)	124 kg N·ha ⁻¹ (110 lb N·acre ⁻¹) of poultry manure on Apr. 20 34 kg N·ha ⁻¹ (30 lb N·ha ⁻¹) of sidedress 30% UAN on Jun. 7	Oct. 1 or 30
Soybean	May 20 (no-till)		Oct. 1 or 30
Double crop winter wheat (Dbl WW)	Oct. 10	34 kg N·ha ⁻¹ (30 lb N·acre ⁻¹) of sidedress 30% UAN on Oct. 8 45 kg N·ha ⁻¹ (40 lb N·acre ⁻¹) of sidedress 30% UAN on Mar. 1 67 kg N·ha ⁻¹ (60 lb N·acre ⁻¹) of sidedress 30% UAN on Apr. 5	Jun. 27
Double crop soybean (Dbl Soyb)	Jun. 29		Nov. 1
Winter cover crop	Oct. 3 & Nov. 2		Mar. 31 (Killing)

Note: The typical nitrogen content for poultry manure is 2.8% (Glancey et al., 2012).

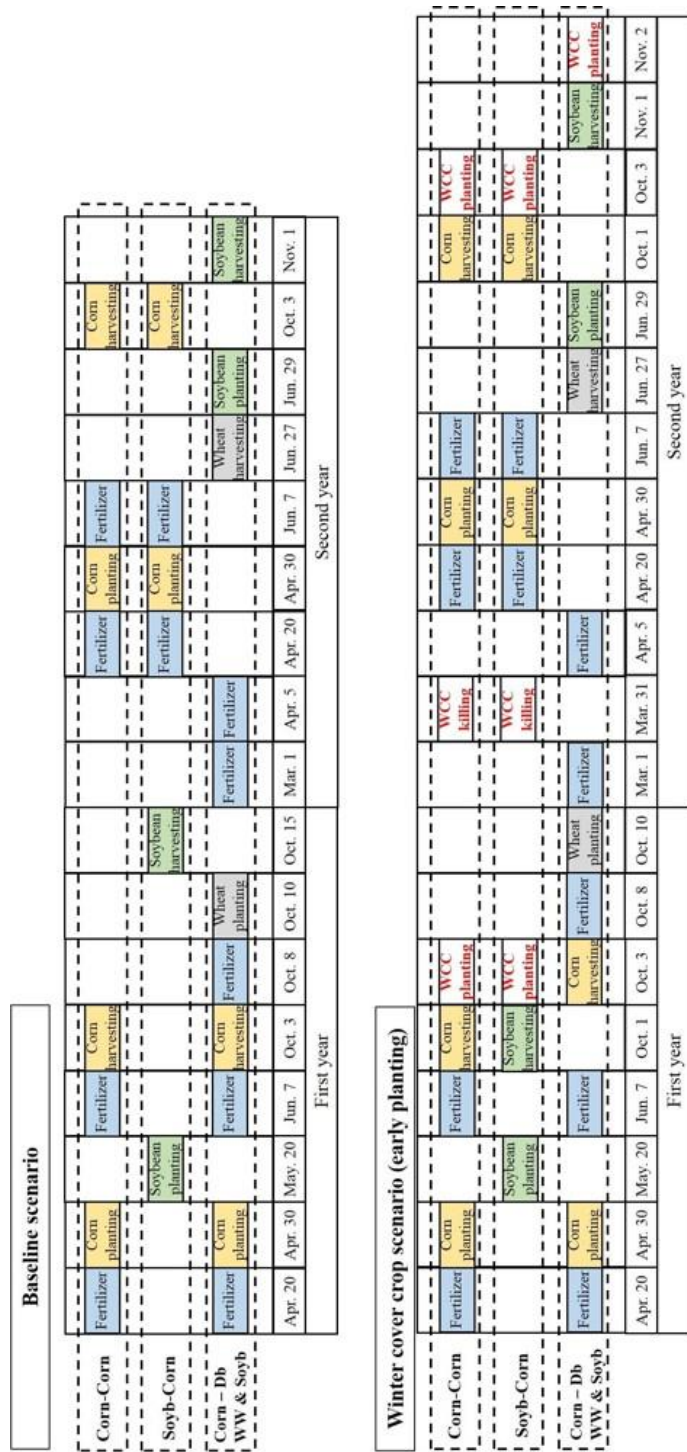


Figure 3.4. The temporal sequence of crop rotations under baseline and winter cover crop scenarios.

Note: Db WW & Soyb stands for double crops of winter wheat and soybean.

Guidelines for WCC implementation practices including recommended planting dates and species were developed by the Maryland Agricultural Water Quality Cost-Share (MACS) cover crop program (MDA, 2015a). The MACS offers varying incentives for planting winter cover crops, primarily depending on species and planting date (MDA, 2015a). Farmers can gain more incentives when they plant WCCs earlier because early-planted WCCs can reduce residual soil N content more effectively than late-planted WCCs. Based on the guideline of the MACS, WCC expert knowledge, and country-level statistics, we established typical early (October 1) and late (October 30) planting dates for WCCs, two harvest dates of summer crops corresponding to the two WCC planting dates (Table 3.2), and three most commonly used planting species (i.e., wheat (*Triticum aestivum* L.), barley (*Hordeum vulgare* L.), and rye (*Secale cereale* L.) in our WCC scenarios (See Table 3.4). In our SWAT model, summertime agronomic practices were kept the same for both baseline (no WCC) and WCC scenarios, but management differed during winter seasons when WCCs were planted on fallow croplands. The WCCs were planted after harvesting summer crops, either in the beginning of October (early planting) or November (late planting), and were killed at the beginning of the subsequent growing season (March 31) (Table 3.4). It was assumed that WCCs could not be placed concurrently with double crop winter wheat, but they could be planted late after harvest of double crop soybean. We did not predict differences in N uptake by summer crops due to shorter versus longer season varieties caused by the two WCC planting dates. The SWAT modeled the maturity for summer crops occurring by the end of September and

demonstrated that both early- and late-harvested summer crops (due to two WCC planting dates) have similar biomass and N uptake by the end of September.

Note that the evaluation of WCC effects on water and nitrate budgets was carried out at two spatial scales. First the overall impacts of different WCC species and planting dates were assessed at the watershed scale. Then the effects of WCC placement on different soils and interaction with N availability based on modeled crop rotations were analyzed at the cropland scale, using the SWAT model results for only cropland areas.

3.2.4 Calibration and validation of the SWAT model

The SWAT simulations were conducted at a monthly time step over the period of 1999 – 2008. Cumulative daily water and nitrate fluxes delivered to streams by surface runoff, lateral flow, groundwater flow, and percolation/leaching over a month were represented as monthly outputs. The simulations included a 2-year warm-up (1999 – 2000), 5-year calibration (2001 – 2005), and 3-year validation (2006 – 2008) time periods. The model was carefully calibrated based on information from previous SWAT modeling studies in the region (Yeo et al., 2014) and literature values (Table 3.3). We first calibrated the parameters pertaining to streamflow and then nitrate loads. The model calibration was conducted manually by adjusting parameter values within an allowable range, following the technical guideline of the SWAT model. Parameter values were selected yielding the best statistical performance measures while satisfying the SWAT performance criteria suggested by Moriasi et al. (2007) (Moriasi et al., 2007). The following statistical performance measures were

considered: Nash-Sutcliffe efficiency coefficient (NSE), root mean square error (RMSE)-standard deviation ratio (RSR), and percent bias (P-bias), shown as in Eq. (3.1 – 3.3):

$$NSE = 1 - \left[\frac{\sum_{i=1}^n (O_i - S_i)^2}{\sum_{i=1}^n (O_i - \bar{O})^2} \right] \quad (3.1)$$

$$RSR = \frac{RMSE}{STDEV_{obs}} = \left[\frac{\sqrt{\sum_{i=1}^n (O_i - S_i)^2}}{\sqrt{\sum_{i=1}^n (O_i - \bar{O})^2}} \right] \quad (3.2)$$

$$P - bias = \left[\frac{\sum_{i=1}^n (O_i - S_i) \times 100}{\sum_{i=1}^n O_i} \right] \quad (3.3)$$

where O_i are observed and S_i are simulated data, \bar{O} is observed mean values, and n equals the number of observations. In addition, the model uncertainty was assessed using the 95 percent prediction uncertainty (95 PPU) range suggested by Singh et al. (2014). This was computed using all simulation outputs obtained during the manual calibration process. The 95 PPU value was calculated at the 2.5 and 97.5 percentiles of the cumulative distribution of simulation outputs (Singh et al., 2014).

The SWAT parameters affecting summertime crop growth, N fixation, and soil N mineralization were at the default values. However, the parameters related to the growth of WCCs were adjusted to more realistically replicate observed WCC growth in the local region as N uptake by WCC is primarily dependent upon cover crop biomass (Hively et al., 2009). We used the method employed by Yeo et al.

(2014) to simulate “representative” biomass growth at the field scale per species, considering substantial variation. This method adjusts the plant growth parameters that control the leaf area development curve using the potential heat unit (PHU) theory as implemented in the SWAT to match estimates of biomass (simulated at the HRU scale) with those observed at the field scale as described by Hively et al. (2009). They reported landscape-level biomass estimates for three commonly used winter cover crop species categorized by various planting dates in the Choptank River region using multi-temporal satellite remotely sensed observations and field sampling data (133 sites) over the winter season (October – March) by including relative growth observations for a single winter growth period (2005 – 2006) (Hively et al., 2009). The SWAT cover crop growth was calibrated to produce 7-year average biomass outputs estimated at the HRU scale to be consistent with the 1-year observation. The WCC results, therefore, did not capture any inter-annual variation in biomass and N accumulation resulting from annual climatic conditions. However, this should not considerably affect plant growth simulation even if there is some inter-annual variability in weather conditions during the monitoring period. The plant growth cycle in the SWAT was simulated using the heat unit theory. It predicts plant growth based on the heat unit. Heat units are estimated based on the cumulative daily temperature above the base temperature relative to potential heat units required for the plant maturity. Not only significant changes in cumulative heat units normalized by potential heat units during the monitoring period, but also the small difference in heat units did not produce substantial variation in WCC biomass growth. See Yeo et al. (2014) for further discussion. Note that the simulated WCC biomass outputs were

analyzed for 7 years, as there are 7 full winter terms (October – March) over the eight calendar year (January – December) simulation period.

Table 3.5. The list of calibrated parameters

Parameter	Description (unit)	Range	Calibrated value	
			TCW	GW
CN2 ¹	Curve number	-50 - 50 %	-30 %	0%
ESCO ¹	Soil evaporation compensation factor	0 - 1	1	0.95*
SURLAG ¹	Surface runoff lag coefficient	0.5 - 24	0.5	0.5
SOL_AWC ¹	Available water capacity of the soil layer (mm H ₂ O·mm soil ⁻¹)	-50 - 50 %	- 10%	- 1%
SOL_K ¹	Saturated hydraulic conductivity (mm·hr ⁻¹)	-50 - 50 %	50 %	-50 %
SOL_Z ¹	Depth from soil surface to bottom of layer (mm)	-50 - 50 %	-20 %	-31 %
ALPHA_BF ¹	Base flow recession constant (1·days ⁻¹)	0 - 1	0.07	0.051
GW_DELAY ¹	Groundwater delay time (days)	0 - 500	120	40
GW_REVAP ¹	Groundwater “revap” coefficient	0.02 - 0.2	0.10	0.02*
RCHRG_DP ¹	Deep aquifer percolation fraction	0 - 1	0.01	0.01*
GWQMN ¹	Threshold depth of water in the shallow aquifer required for return flow to occur (mm)	0 - 5000	1.9	1.0
CH_K2 ¹	Effective hydraulic conductivity (mm·hr ⁻¹)	0 - 150	0*	25
CH_N2 ¹	Manning coefficient	0.01 - 0.3	0.29	0.025
NPERCO ^{&}	Nitrogen percolation coefficient	0.01 - 1	0.5	0.15
N_UPDIS ^{&}	Nitrogen uptake distribution parameter	5 - 50	50	50
ANION_EXCL ^{&}	Fraction of porosity from which anions are excluded	0.1 - 0.7	0.59	0.6
ERORGN ^{&}	Organic N enrichment ratio for load with sediment	0 - 5	4.92	4.1
BIOMIX ^{&}	Biological mixing efficiency	0.01 - 1	0.01	0.01
SOL_NO3 ^{\$}	Initial NO ₃ concentration in soil layer (mg N·kg ⁻¹)	0 - 100	11.23	0
CDN [#]	Denitrification exponential rate coefficient	0 - 3.0	0.3	2.9
SDNCO [#]	Denitrification threshold water content	0.1 - 1.1	1.0	1.0
LAIMX1 [^]	Fraction of the maximum leaf area index corresponding to the first point on the leaf area development curve		0.01 (Wheat) 0.02 (Barley) 0.12 (Rye)	
LAIMX1 [^]	Fraction of the maximum leaf area index corresponding to the first point on the leaf area development curve		0.14 (Wheat) 0.31 (Barley) 0.35 (Rye)	

Note: *(an asterisk) refers to a default value. The ranges of parameters were adapted from previous literature [¹ Citau and Chaubey (2010), [&] Yeo et al. (2014), ^{\$} Seo et al. (2014), [#] Neitsch et al. (2011), and [^] Hively et al. (2009)].

3.2.5 Statistical analysis of WCC impacts

Following the SWAT modeling, several statistical analyses were conducted to compare treatment effects (no WCC versus WCCs) on water and nitrate budgets within and between watersheds, using either annually or seasonally (winter season) simulated water and nitrate loads. We first asked if the two watersheds showed significantly different hydrological responses as hypothesized, using a one-way multivariate analysis of variance (MANOVA) and a two-sample t-test. A three-way analysis of variance (ANOVA) and the Bonferroni procedure were then used to investigate if the WCC N uptake efficiency varied by site characteristics (i.e., dominant soils in watershed), WCC planting species, WCC planting timing, and their interactions. The effects of cropland soils on nitrate delivery mechanisms were further investigated by performing a one-way ANOVA and the Bonferroni procedure which compared the overall WCC effects on the seasonal nitrate loads against the baseline. Note that the effect of the two crop rotations (i.e., continuous corn and corn-soybean rotation) on WCC performance in nitrate reduction was analyzed only for the early-planted rye (RE) scenario in TCW, which resulted in the greatest reduction in nitrate budgets. A paired sample t-test was used to assess crop rotation effects on nitrate loads as compared to the baseline. As the statistical methods we employed were sensitive to the outliers, we carefully inspected the sample distribution of the hydrological variables and removed outliers prior to statistical testing. An outlier was identified when an observation point fell more than 1.5 times the interquartile range above the 3rd quartile or below the 1st quartile. The annual and seasonal hydrological variables obtained in 2003 were extremely high and thus were determined to be

outliers. This was most likely due to the extremely high precipitation that occurred in 2003. The annual and seasonal precipitation in 2003 ranked the highest over the last 30 years.

3.3 Results

3.3.1 SWAT calibration and validation

Overall, monthly streamflow and nitrate loads simulated from the calibrated model were in good agreement with corresponding observed values (Figure 3.5). Seasonal variations in both the streamflow and nitrate loads were well depicted by the SWAT simulations. However, the 95 PPU band (shown by interval in Figure 3.5) did not capture observed peak streamflow for TCW and GW. The CN surface runoff method used in the SWAT limited predicting storm effect, because the duration and intensity of precipitation were not considered in surface runoff calculation. This resulted in underestimation of peak streamflow (Qiu et al., 2012). Precipitation obtained from remote weather stations (~ 35 km away from the outlet of the watersheds) may not have provided accurate values for the watershed (Larose et al., 2007). Accordingly, localized storm effect might not be reflected in simulations. In addition, poorly simulated ET might increase water loss, resulting in underestimation of streamflow during summer periods (Larose et al., 2007).

The SWAT underestimated nitrate loads during low-flow seasons, particularly for TCW. Underestimation of nitrate loads during the low-flow seasons in TCW have also been reported by several studies (Yeo et al., 2014; Lee et al., 2000; Sadeghi et

al., 2007). Previous studies (Yeo et al., 2014; Boithias et al., 2014) attributed lower estimates of nitrate loads to the underestimation of streamflow, inherent limitation of the SWAT's capacity to simulate N cycle in lowlands, and inaccurate simulation of summer crop growth relative to N uptake by plants. The residence time of groundwater nitrate in the eastern shore region of the CBW range from a few years to several decades (McCarty et al., 2008). Fertilizer application rates in the 1970's to 1990's were much higher than current rates (Ator and Denver, 2015) and 2 years of the model warm-up (1999 – 2000) might not be sufficient to represent this background nitrate from the past fertilization. Considering long residence time, N fertilizer applied several decades ago could presently be discharged to streams and lead to substantially higher in-stream nitrate concentration, lowering model predictability. Also nitrate loads based on field sampling of stream concentration (i.e., the observed nitrate load) could be inaccurate if field samples were not collected frequently over the long-term, leading to the extrapolation of misleading “observed” nitrate loads (Ullrich and Volk, 2010).

Model performance measures and accuracy ratings under the baseline scenario are summarized in Table 3.6. Accuracy ratings were based on statistical evaluation guidelines from Moriasi et al. (2007). Overall model calibration and validation results were satisfactory for both watersheds. Simulations for streamflow were better matched with observations than for nitrate loads. Model performances for nitrate loads under the baseline condition were classified as satisfactory, good, and very good (Table 3.6).

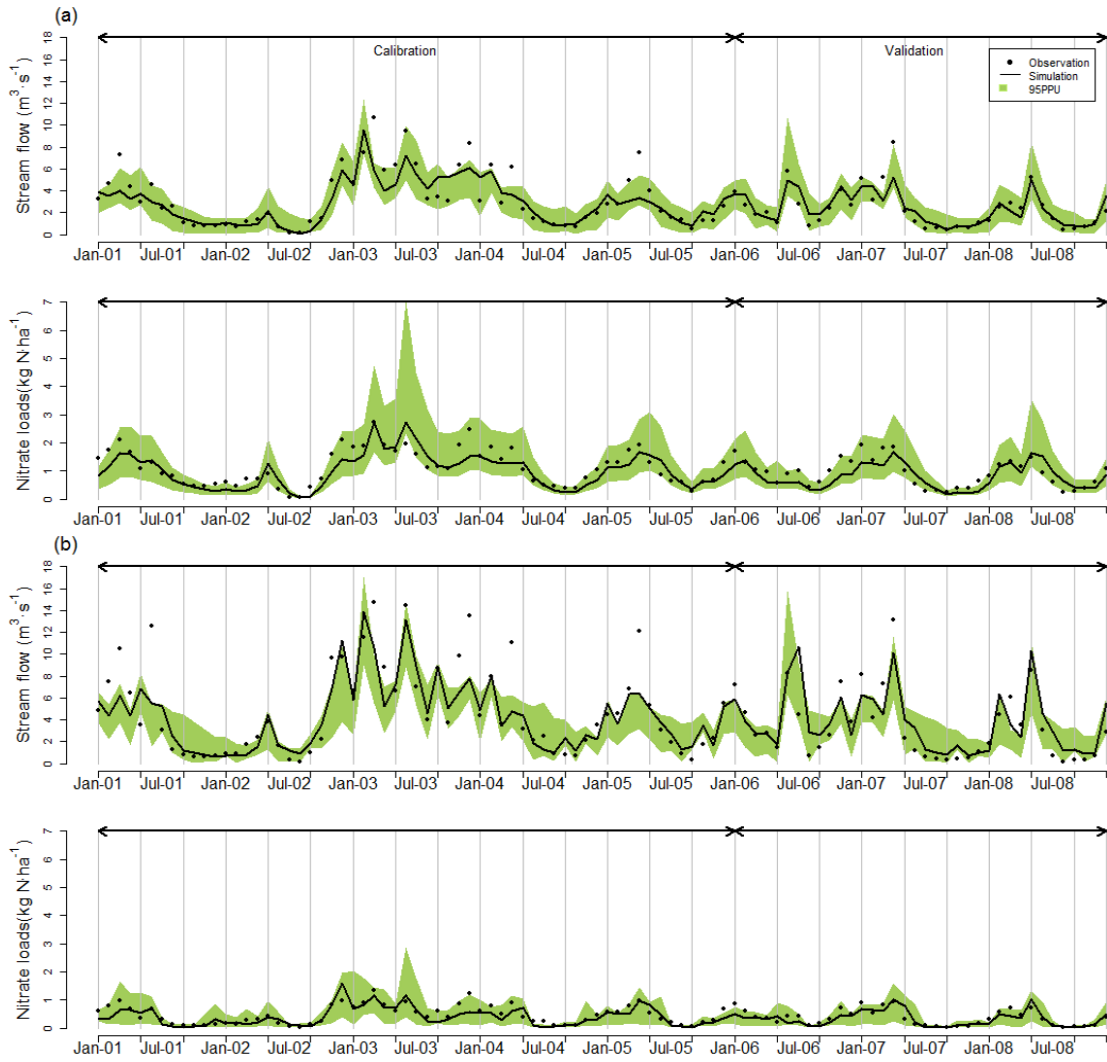


Figure 3.5. Comparison of observed and simulated monthly streamflow and nitrate loads for the (a) Tuckahoe Creek Watershed and (b) Greensboro Watershed

Table 3.6. Model performance measures for streamflow and nitrate loads

Period	Variable	Streamflow		nitrate loads	
		TCW	GW	TCW	GW
Calibration	NSE	0.705**	0.703**	0.687**	0.594*
	RSR	0.537**	0.540**	0.554**	0.631*
	P-bias (%)	-9.4***	-9.4***	-10.8***	-13.7***
Validation	NSE	0.759***	0.661**	0.561*	0.631*
	RSR	0.483***	0.573**	0.652*	0.598**
	P-bias (%)	2.7***	12.8***	-12.9***	-9.8***

Note: model performances were rated based on the criteria of Moriasi et al. (2008); * Satisfactory, ** Good, and *** Very Good.

Nitrate reduction by WCCs is achieved by the transformation of soil N into WCC biomass N. Therefore, accurate simulation of WCC biomass accumulation could lead to enhanced prediction of WCC N uptake and its effect on nitrate loads. The WCC growth was calibrated within the SWAT model to match with the actual regional growth pattern in the winter of 2005 – 2006 following methods used by Hively et al. (2009) (Figure 3.6). Note that in this region rye grows quickly and often has the greater biomass than barley and wheat (Hively et al., 2009). In contrast, pre-calibrated simulation outputs (results not shown in this paper) using default SWAT growth parameters would have estimated greater winter wheat and barley biomass than rye biomass because their growth was considered during summer compared to winter growing season. Note that WCC biomass during 2001 – 2008 was calibrated to the specific remotely sensed observations made for 2005 – 2006 (Hively et al., 2009). An inter-annual assessment of WCC biomass could not be undertaken in this study due to data unavailability. However, the method described by Yeo et al. (2014) calibrated data over a limited timeframe (2005 – 2006) well represented the typical WCC performances in this region. Simulated WCC biomass growth patterns from Yeo et al. (2014) were consistent with field observations made for different years (Hively et al., 2009; Staver et al., 1989; Prabhakara et al., 2015). Furthermore, the estimates of Yeo et al. (2014) were consistent with cover crop N uptake assumed by the Chesapeake Bay Program Watershed Model version 5.3.2 (CBP, 2014). As the MACS cover crop program collected field WCC biomass data and longer term field observations became available, the WCC biomass calibration can be improved to

represent the inter-annual variations in WCC biomass and N uptake under various climate conditions and agricultural practices.

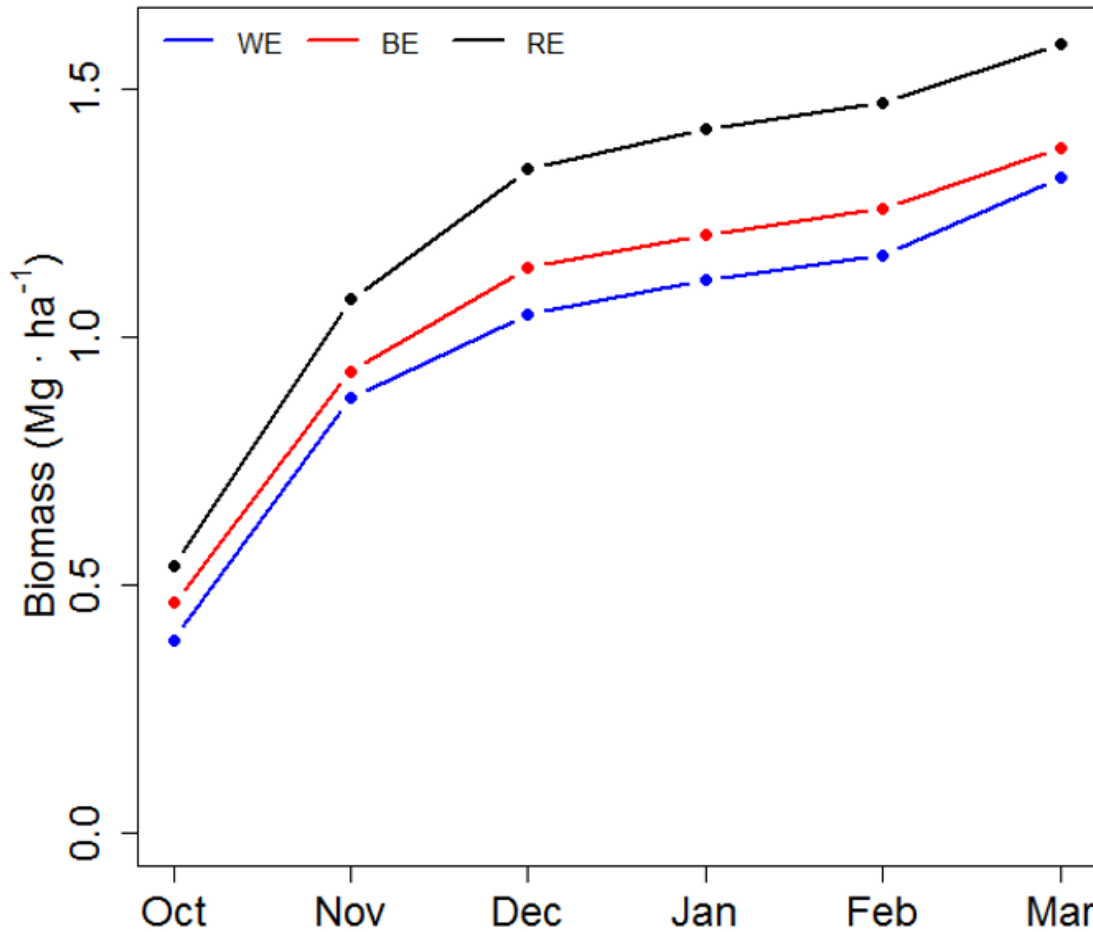


Figure 3.6. 7-year average of early-planted winter cover crop biomass over winter seasons (October – March) calibrated to the field observation collected from 2005-2006

3.3.2 Watershed-scale assessment of winter cover crop effects on water budget and nitrate loads

The 8-year average annual SWAT model outputs were calculated at the watershed scale and summarized by WCC scenarios (Figure 3.7). Streamflows, ET, and transported nitrate were utilized for the watershed-scale assessment. As hypothesized, the two watersheds showed significantly different hydrological responses (p -value < 0.001 from the one-way MANOVA). A previous regional study showed that WCCs had negligible impacts on streamflow and ET, but greatly affected nitrate loads (Yeo et al., 2014). Similarly, our simulation results also showed small changes in streamflow and ET regardless of WCC implementation for both watersheds. Our findings showed that the slightly greater changes in streamflow and ET were caused by rye compared to barley and wheat due to its relatively higher growth rate and biomass yield. Early planting of cover crops induced a slight increase in ET and decrease in streamflow relative to late planting (Figure 3.7a).

The impacts of WCCs on nitrate loads were much more noticeable than the effects on streamflow (Figure 3.7b). Compared to the baseline, annual nitrate loads after WCC treatments were significantly different for the two watersheds (p -value < 0.000) by WCC planting timing (p -value < 0.013) and species (p -value < 0.036) (Table 3.7). Annual nitrate loads decreased from 11.2 (Baseline) to 5.7 (RE) $\text{kg N}\cdot\text{ha}^{-1}$ for TCW and from 4.5 (Baseline) to 3.3 (RE) $\text{kg N}\cdot\text{ha}^{-1}$ for GW. This is equivalent to nitrate load reductions of 0.9 to 5.8 $\text{kg N}\cdot\text{ha}^{-1}$ or from 33.8 % (WL) to 49.3 % (RE) for TCW and from 18.0 % (WL) to 26.5 % (RE) for GW. Relative to late planting, early-planted WCCs lowered nitrate loads by 0.5 $\text{kg N}\cdot\text{ha}^{-1}$ on average (95 %

confidence interval: 0.1 to 0.8 N·ha⁻¹). The difference in N uptake by WCC between two planting timings was greater in TCW (8.8 %, 0.6 – 1.0 kg N·ha⁻¹), than in GW (5.3 %, 0.1 – 0.2 kg N·ha⁻¹). Overall, this occurred most effectively in RE. The longer growing days and warmer conditions for early-planted WCCs promoted growth and biomass and therefore resulted in higher N uptake than late-planted ones (Feyereisen et al., 2006). Rye is a hardy species and establishes its root system more rapidly, thereby resulting in greater N uptake than other crops (Clark, 2007). The TCW showed higher nitrate loads and WCC N uptake compared to GW (95 % CI for the differences in nitrate loads between two watersheds: 3.35 to 4.06 kg N·ha⁻¹), likely due to larger area of croplands mainly located on well-drained soils.

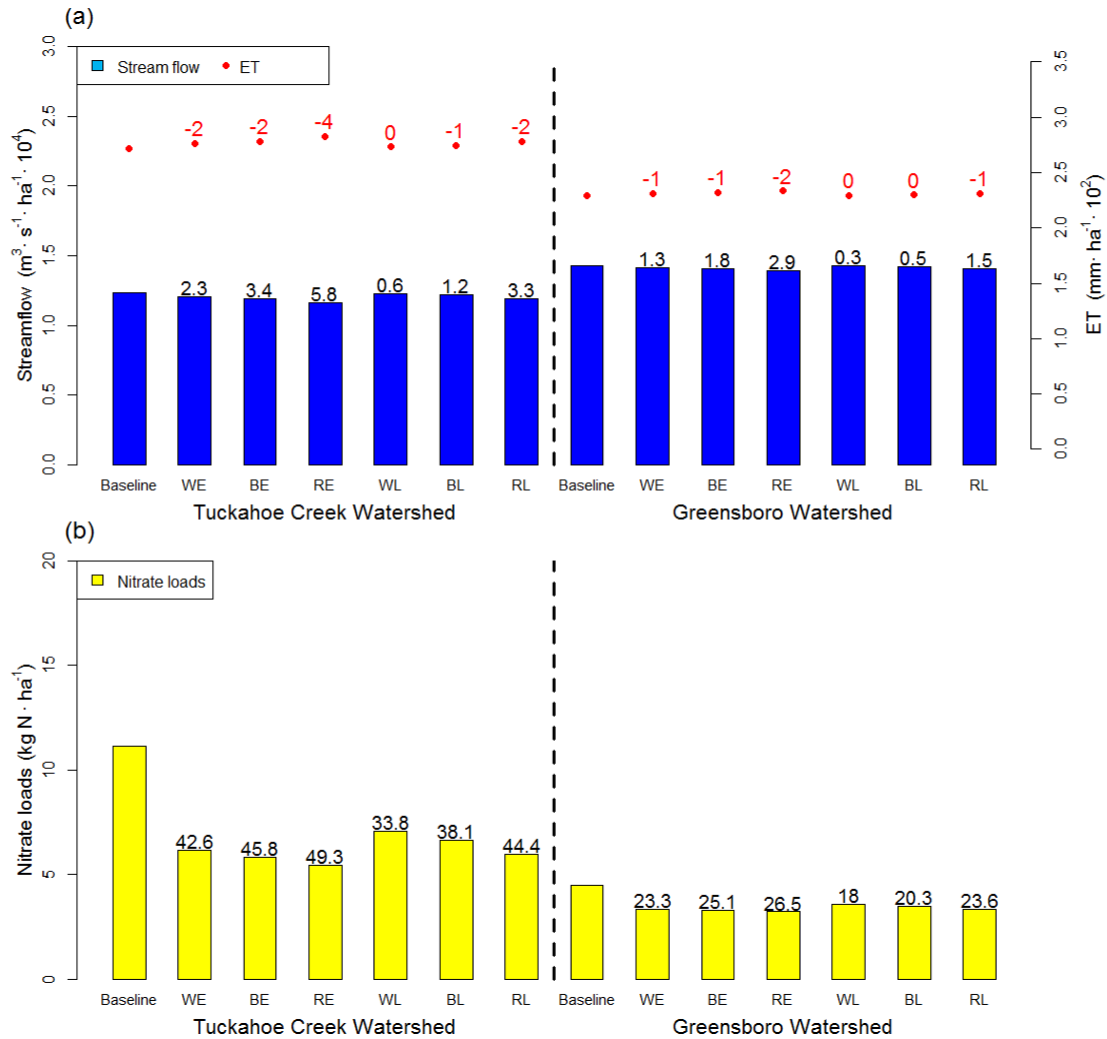


Figure 3.7. 8-year average of annual hydrologic variables under winter cover crop scenarios at the watershed scale: (a) streamflow and evapotranspiration (ET) and (b) nitrate loads normalized by the total watershed area.

Note: The numeric values on the bar and dotted graphs indicate reduction rate (RR) of ET, streamflow, and nitrate loads, respectively. RR is calculated by taking the relative difference in simulation outputs from the baseline and WCC scenarios [RR (%) = (Baseline – WCC Scenario) / Baseline × 100]. Table A.3.3 summarizes the finding from the three-way ANOVA for the nitrate reduction by the watershed, WCC planting timing, and species.

Table 3.7. Analysis of variance for the reduction of annual nitrate loads by watershed, WCC planting species and timing

Source of Variation	Sum Squares	Degree of freedom	Mean Square	F-Statistics	p-Value
Watershed (Wshd)	287.939	1	287.939	438.43	0
WCC Planting Species (Species)	4.576	2	2.288	3.48	0.036
WCC Planting Timing (Timing)	4.228	1	4.228	6.44	0.0133
Wshd × Species	2.019	2	1.01	1.54	0.2219
Wshd × Timing	1.52	1	1.52	2.31	0.1326
Species × Timing	0.212	2	0.106	0.16	0.8513
Wshd × Species × Timing	0.082	2	0.041	0.06	0.9397
Error	47.286	72	0.657		
Total	347.862	83			

3.3.3 Site characteristic impacts on nitrate fate and winter cover crop performance

Differences in water and nitrate fluxes and WCC performances between the two watersheds were further explained by the cropland-scale outputs (i.e., cropland HRU), excluding other watershed land use over the fall and winter (October to March) of each year (Figure 3.8). The outputs described the amount of water and nitrate fluxes) delivered to streams by surface runoff and lateral and groundwater flow from croplands and 2) entering the groundwater (e.g., percolation from the bottom of soil profile or nitrate leaching). This partitioning elucidated the overall effects of different soil properties on the fate and transport of nitrate and on WCC performance.

The simulation results illustrated that two watersheds have different water and nitrate delivery mechanisms (p -value < 0.000 from the one-way MANOVA). In TCW, croplands are mainly located on well-drained soils with high conductivity (Figure 3.8 & Table 3.1). Under the baseline condition, a large amount of water flux moved into deeper soils, passing the bottom of the soil profile and ~78.8 % of water

fluxes transported to streams by groundwater flow (Figure 3.8a). Because nitrate in TCW remains stable in subsurface soils and groundwater under aerobic conditions, high nitrate fluxes entered into groundwater ($19.5 \text{ kg N}\cdot\text{ha}^{-1}$) and delivered to the streams by groundwater flow ($8.9 \text{ kg N}\cdot\text{ha}^{-1}$) (Figure 3.8b). In contrast, 75.7 % of water fluxes delivered to streams from GW croplands was attributed to surface runoff, due at least in part to the abundance of poorly-drained soils and high-density ditch systems, while the subsurface flow contribution to streams (e.g., lateral flow and groundwater flow) was 24.3 % (Figure 3.8a). The anaerobic condition in poorly-drained soils is expected to reduce nitrate export through denitrification. Our simulation results also indicated that the amount of nitrate removed by denitrification was $13.0 \text{ kg N}\cdot\text{ha}^{-1}$ greater in GW croplands during winter seasons compared to TCW croplands. These hydrologic characteristics in GW croplands might contribute to lowering nitrate leached into groundwater ($6.5 \text{ kg N}\cdot\text{ha}^{-1}$) and nitrate fluxes delivered to streams by groundwater flow ($4.5 \text{ kg N}\cdot\text{ha}^{-1}$) compared to TCW croplands. In both watersheds, nitrate leaching was a dominant transport mechanism. The amount of nitrate leached into groundwater was much higher than the amount delivered to the streams from the croplands under the baseline condition.

Compared to the baseline, WCCs were effective at reducing nitrate fluxes delivered to streams (p -value < 0.0001 from the one-way ANOVA) and nitrate fluxes leached to ground water (p -value < 0.0000 from the one-way ANOVA) for both watersheds. The WCCs were more effective in TCW croplands than in GW croplands (Figure 3.8b) (one-sided p -value < 0.0000 from a two-sample t -test). Overall, WCCs were more effective in TCW croplands with increased reduction in nitrate fluxes of ~

2.5 kg N·ha⁻¹ delivered to streams and ~ 10.1 kg N·ha⁻¹ leached into groundwater compared to GW croplands. Compared to the baseline values, nitrate fluxes delivered to streams were lowered by from 3.5 (WL) to 5.5 (RE) kg N·ha⁻¹ in TCW croplands and from 1.9 (WL) to 3.0 (RE) kg N·ha⁻¹ in GW croplands. The WCCs reduced water percolation by up to ~ 37.2 mm·km⁻² and ~ 20.6 mm·ha⁻¹·10⁴ in TCW and GW croplands, respectively, compared to the baseline scenario (no-WCC). This hydrological effect on percolation, combined with WCC effects on nitrate concentration in soils and groundwater, greatly reduced nitrate leaching for both watersheds, by up to ~ 15.7 kg N·ha⁻¹ and ~ 5.6 kg N·ha⁻¹ for TCW and GW croplands, respectively. Seven-fold greater reduction of nitrate fluxes transported to streams by surface runoff was achieved in GW croplands (~ 1.4 kg N·ha⁻¹) compared to TCW croplands (~ 0.2 kg N·ha⁻¹) (Table 3.8). Surface runoff accounted for the majority of water fluxes delivered to streams in GW croplands. Therefore, the WCC impact on reduction of nitrate fluxes delivered to streams by surface runoff was more effective in GW croplands than in TCW croplands. The simulated outputs were in good agreement with field observations (Singer, 2015). Rye cover crop was shown to reduce nitrate leaching by 70.3 – 86.1 % (Table 3.8) and field observations reported N reduction rate by rye cover crop ranging from 60 to 94 %. The results indicated that WCCs were more effective in reducing subsurface flow and nitrate leaching than in reducing nitrate losses to surface runoff. They also emphasized the importance of WCC implementation on well-drained agricultural soils, since these soils were shown to have higher nitrate levels and a greater potential for nitrate leaching than poorly-drained agricultural soils.

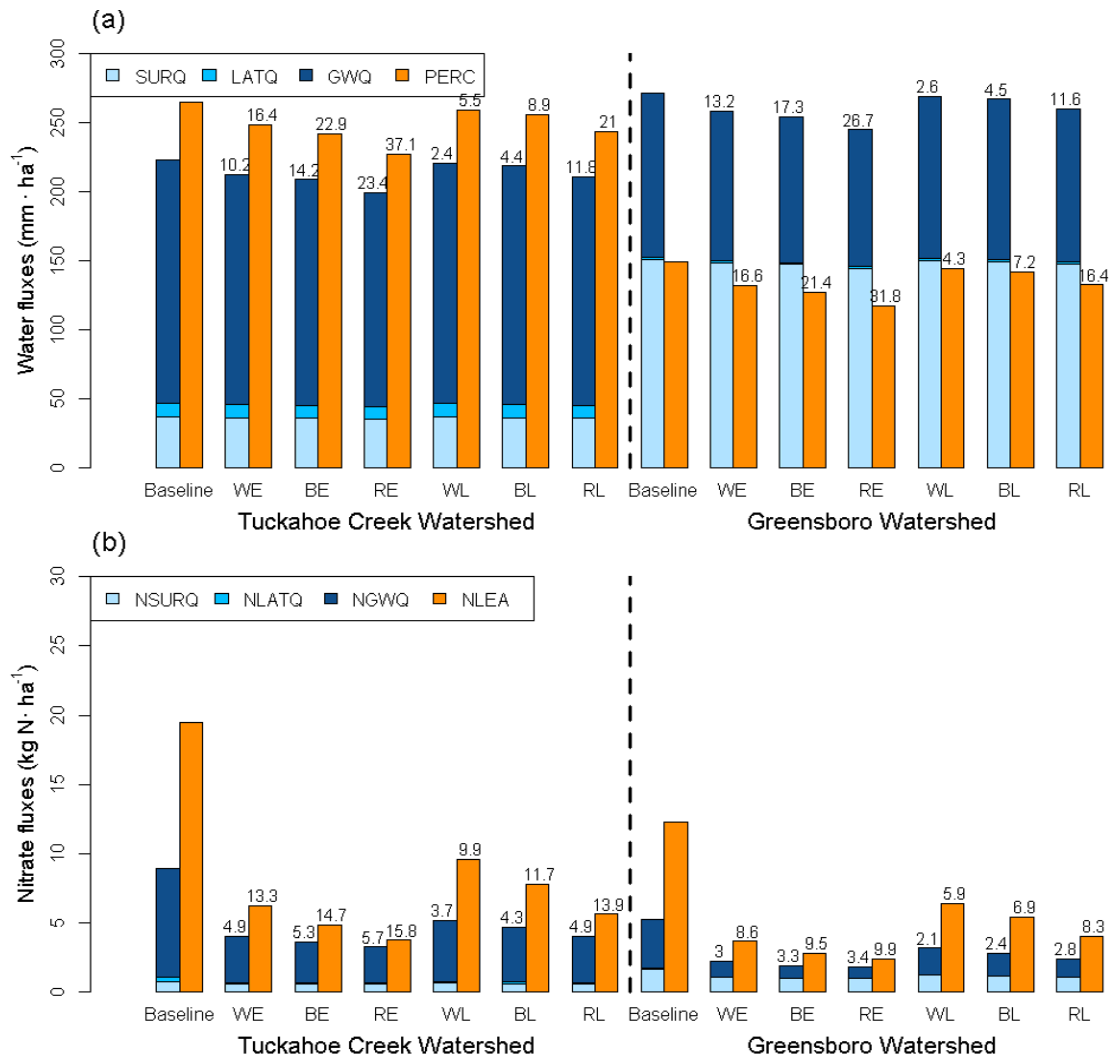


Figure 3.8. 7-year average of annual (a) water and (b) nitrate fluxes at the cropland scale under winter cover crop scenarios over winter seasons (October-March) normalized by the total cropland area.

Note: The SURQ, LATQ, and GWQ in (a) refer to water fluxes delivered to streams by surface runoff, lateral flow, and groundwater flow, respectively. The PERC refers to water percolation entering to groundwater from the bottom of the soil profile. The NSURQ, NLATQ, and NGWQ in (b) refer to nitrate fluxes delivered to streams from croplands by surface runoff, lateral flow, and groundwater flow, respectively. The LEA is nitrate leaching to groundwater. The PERC and LEA eventually affect the groundwater contribution to streams and nitrate loads in the groundwater flow over time, respectively. The numeric values on the top of the bar graph indicate the reduction amount of water and nitrate fluxes under winter cover crop scenarios relative to the baseline scenario. The reduction amount by each pathway is available in Table 3.8.

Table 3.8. The reduction amount and rate of water and nitrate fluxes by winter cover crops

Watershed	Scenario	Water fluxes, mm·ha ⁻¹ (%)				NO ₃ -N fluxes, kg N·ha ⁻¹ (%)			
		SURQ	LATQ	GWQ	PERC	NSURQ	NLATQ	NGWQ	NLEA
TCW	WE	0.9 (2.3)	0.4 (4.4)	8.7 (4.9)	16.0 (6.0)	0.2 (21.7)	0.2 (63.1)	4.4 (56)	13.2 (67.5)
	BE	1.2 (3.2)	0.6 (6.2)	12.2 (7.0)	22.8 (12.6)	0.2 (23.8)	0.2 (70.5)	4.8 (60.6)	14.6 (74.8)
	RE	1.9 (5.0)	1.0 (9.9)	20.6 (11.7)	37.2 (12.6)	0.2 (25.8)	0.2 (73.8)	5.1 (65.1)	15.7 (80.5)
	WL	0.4 (1.0)	0.1 (1.3)	1.4 (0.8)	4.8 (12.6)	0.1 (16.6)	0.1 (50.3)	3.2 (41)	9.5 (48.9)
	BL	0.5 (1.3)	0.2 (2.2)	3.2 (1.8)	8.2 (12.6)	0.1 (19.9)	0.2 (58.7)	3.7 (47.2)	11.4 (58.4)
	RL	1.1 (2.8)	0.6 (5.6)	9.9 (5.6)	20.7 (12.6)	0.2 (24.3)	0.2 (67.7)	4.4 (55.5)	13.7 (70.3)
GW	WE	4.6 (2.4)	0.2 (4.5)	7.3 (12.6)	11.0 (12.6)	1.3 (48.9)	0.1 (64)	1.3 (71.4)	4.9 (74.9)
	BE	6.2 (3.3)	0.2 (6.2)	9.3 (16.0)	14.4 (12.6)	1.4 (53.5)	0.1 (71.4)	1.4 (78.3)	5.4 (82.4)
	RE	9.7 (5.1)	0.3 (8.6)	13.4 (23.1)	20.6 (12.6)	1.4 (55.9)	0.1 (72.6)	1.5 (81.4)	5.6 (86.1)
	WL	1.2 (0.6)	0.0 (1.2)	0.6 (1.1)	2.3 (12.6)	1 (38.2)	0.1 (53.1)	0.9 (46.9)	3.3 (50.1)
	BL	1.9 (1.0)	0.1 (2.2)	1.7 (3.0)	4.3 (12.6)	1.1 (44.1)	0.1 (60.5)	1 (55.6)	3.9 (59.9)
	RL	4.2 (2.2)	0.2 (5.5)	5.7 (9.8)	10.8 (12.6)	1.3 (51.6)	0.1 (68.3)	1.2 (66.2)	4.7 (71.8)

Note: The numeric values show the reduction amount and rate (%) of water (mm·ha⁻¹) and NO₃-N fluxes (kg N·ha⁻¹), relative to the baseline. Pairwise comparisons (with the Baseline) showed that all reduction amounts were statistically significant (one-sided *p*-value <0.05 from a paired t-test).

3.3.4 Crop rotation impacts on winter cover crop performance over winter seasons

Data from the 7-year average annual nitrate fluxes after corn-soybean rotation and continuous corn were compared to evaluate the effects of crop rotations and summer crop species on WCC nitrate uptake. To illustrate differences in the performance of WCC by crop rotations, we used simulation outputs from the RE scenario in TCW, as they had the largest relative reduction rate in comparison to the baseline values. When postharvest nitrate fluxes in two crop rotations were compared under the baseline scenario, corn-soybean rotation exported 4.0 kg N·ha⁻¹ more nitrate fluxes than continuous corn (Figure 3.9a) (one-sided *p*-value = 0.10 from a paired t-test). Nitrate fluxes after the harvest of soybean in corn-soybean rotation were higher than after the harvest of corn, accounting for ~68.5 % of the total fluxes (Figure 3.9a). This is likely because soybean often leaves a greater amount of nitrate

in the soil due to the rapid rate of residue mineralization (Gentry et al., 2001). Mineralization is controlled by the C/N ratio of crop residue (Stevenson and Cole, 1999). As the C/N ratio of residue decreases (i.e., greater N content), the rate of residue mineralization increases (Stevenson and Cole, 1999). Crops with higher N content (e.g., soybean) typically generate more nitrate than lower N content like corn (Smith and Sharpley, 1990). Therefore, crop rotations with soybean are expected to have more residual soil N than continuous corn. Our simulation outputs during winter seasons supported these assumptions (Figure 3.9b). They showed that corn-soybean rotation left $6.3 \text{ kg N}\cdot\text{ha}^{-1}$ more nitrate from mineralization of N in residue compared to continuous corn. Approximately 77.5 % of mineralized N originated from soybean residue in corn-soybean rotation (Figure 3.9b). The simulation results on postharvest nitrate fluxes after two crop rotations were consistent with the findings from previous observations (Weed and Kanwar, 1996; Klocke et al., 1999). Indeed, Figure 3.10ab shows that mineralized N was greater following earlier harvest than following late harvest when temperatures were relatively high compared to other winter months. This climate condition likely also influenced the amount of mineralized nitrate based on harvesting timing of summer crops (i.e., WCC planting dates). The simulation results showed early-harvested crops (October 1) had substantial N mineralization occurring in October, followed by reduced amounts of mineralization in subsequent months. In contrast, late-harvested crops (October 31) showed highest mineralization in November, with decreased monthly mineralization rates thereafter (Figure 3.10ab). Overall, the residue from early-harvested crops exhibited approximately $3.7 \text{ kg}\cdot\text{ha}^{-1}$ more N from mineralization than late-harvested crops over winter seasons.

Because simulated residual mineralized N was substantially greater in soybean than in corn, the efficiency of the RE scenario at reducing nitrate was greater in corn-soybean rotation compared to in continuous corn (one-sided p -value = 0.007 from a paired t-test). The RE scenario decreased nitrate fluxes from 32.4 kg N·ha⁻¹ to 3.6 kg N·ha⁻¹ in corn-soybean rotation and from 28.4 kg N·ha⁻¹ to 5.4 kg N·ha⁻¹ in continuous corn (Figure 3.9a). The temporal distribution of nitrate fluxes differed considerably between the baseline and RE scenarios (Figure 3.10cd). With increasing biomass (Figure 3.6) and nitrate uptake, a smaller amount of nitrate fluxes was exported to streams and groundwater. This result illustrated the effect of crop rotations on postharvest residual soil nitrate and the WCC nitrate uptake efficiency. Overall, this result suggested that WCCs may have a greater impact on water quality when planted on fields under crop rotations that produce greater amounts of leachable nitrate.

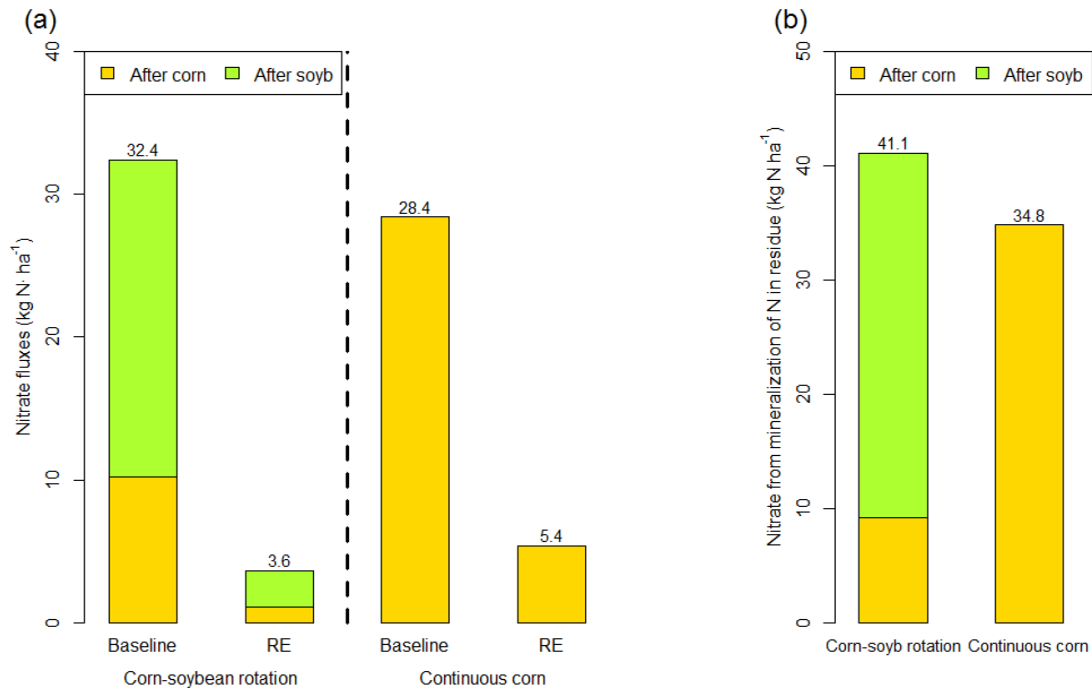


Figure 3.9. 7-year average of annual (a) nitrate fluxes (delivered to streams and leached into groundwater), and (b) nitrate from mineralization of N in residue in two crop rotations at the cropland scale under the baseline and rye early scenarios over winter seasons (October-March).

Note: Nitrate values are normalized by the total croplands used for these two crop rotations. Monthly values are represented in Figure 3.8.

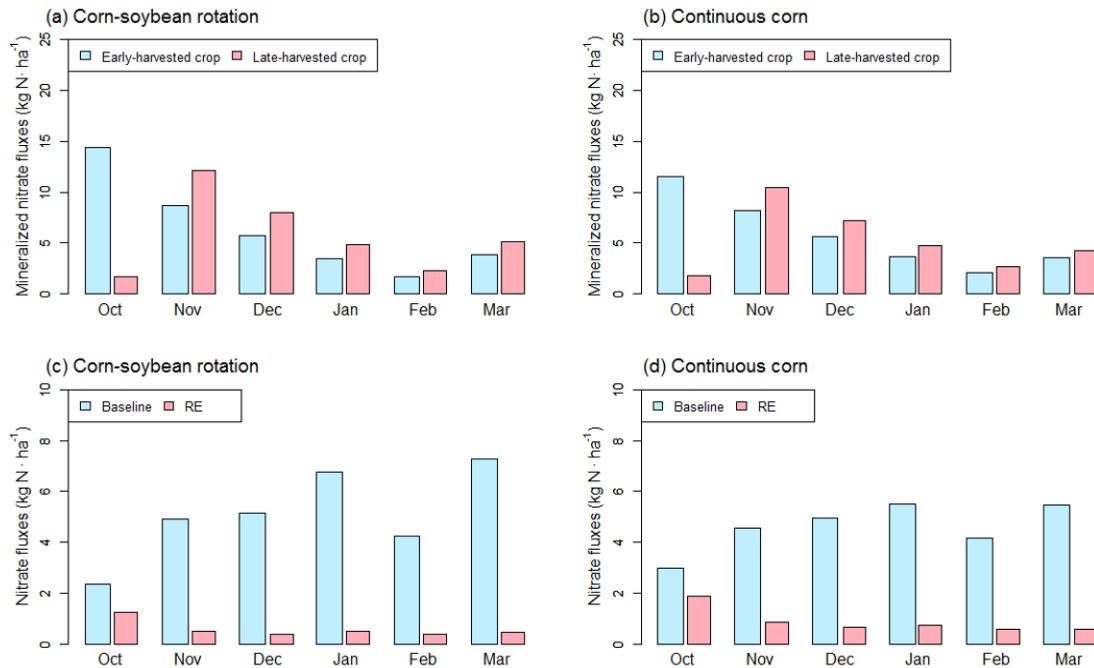


Figure 3.10. Temporal distribution of 7-year average of (a & b) nitrate from mineralization of N in residue and (c & d) nitrate fluxes (delivered to streams and leached into groundwater) in two crop rotations at the cropland scale under early-planted rye scenario over winter seasons (October-March).

Note: Nitrate values are normalized by the total croplands used for these two crop rotations. Cumulative values are represented in Figure 3.7.

3.4 Conclusions

A physical model (SWAT) paired with statistical analysis was used to investigate the efficiency of WCCs for reducing nitrate loads under different WCC planting dates, species, soil characteristics, and crop rotations. Overall, the WCCs were more effective when baseline nitrate loads were high due to high leaching potential and/or high availability of residual and mineralized soil nitrate, resulting from soil characteristics and crop rotations. The WCC efficiency varied by planting time and species. Therefore, for the water quality improvements, it is crucial to establish an appropriate WCC treatment depending on local edaphic, hydrologic, and

agronomic characteristics. For example, well-drained areas used for frequent cultivation of soybean should adopt a more robust WCC practice (e.g., rye with early planting), while areas with lower infiltration rates, increased denitrification capacity, and lower available soil residual and mineralized N could achieve the same water quality standards with less robust WCC practices (e.g., barley and wheat). The findings of this study can provide key information to aid decision making and to develop effective WCC implementation plans suitable for local characteristics at the watershed scale.

Chapter 4 Reducing uncertainty of an integrated wetland-watershed hydrologic model using remotely sensed data³

4.1 Introduction

Wetlands provide important ecosystem services, such as mitigating flood damage (Hillman, 1998), improving water quality by reducing pollution loads (Cooper, 1990), and serving as natural habitats to support biodiversity (Nygaard and Ejrnæs, 2009). These functions highly depend on wetland hydrology determined by its interactions with surrounding areas (Tiner, 2005; Kettlewell et al., 2008). For example, the denitrification process is triggered by anaerobic condition within a wetland and incoming nitrate loads, which are driven by water inflow to wetlands from the surrounding landscape (Cooper, 1990). Wetlands, in turn, exert a strong influence on the characteristics and functioning of downstream waters (USEPA, 2015). Therefore, it is important to understand wetland hydrology as it relates to upstream and downstream landscapes to assess the cumulative benefits of wetlands at the watershed scale (USEPA, 2015).

It is challenging to predict wetland hydrology owing to complex hydrologic connections between wetlands and surrounding areas via surface and subsurface pathways (Ranalli et al. 2010). Computational models have been developed to simulate wetland hydrology at the individual site scale. For example, MODFLOW

³ The material presented in this Chapter is under review: Lee, S., Yeo, I.-Y, Lang, M. W., McCarty, G. W., Sadeghi, A. M., Sharifi, A., Jin, H. & Liu, Y. (2016). Reducing uncertainty of an integrated wetland-watershed hydrologic model using remotely sensed data. *Environmental Modelling & Software*

was used to simulate hydro-dynamics of wetlands induced by surface flow and interactions with aquifers (Restrepo et al. 1998), and its groundwater recharge function under different weather conditions (Bradley, 2012). WETLAND (Lee et al., 2002) and Wetland Solute Transport Dynamics (WETSAND, Kazezyilmaz-Alhan et al., 2007) were developed to simulate plant uptake and denitrification process within a wetland. These models were able to simulate water and nutrient cycling at the site, but the results were confined to individual wetlands. Thus, they could not represent the cumulative impacts of multiple wetlands on downstream waters at the watershed scale.

Recently, spatially distributed watershed models have been applied to examine catchment-scale benefits of wetland by including a wetland module as a component in a distributed watershed model. Vining (2002) simulated the Devils Lake Basin wetlands model to estimate water storage capacity of wetlands and its effects on downstream water balance at the watershed scale. Padmanabhan and Bengtson (2001) used the Hydrologic Engineering Center (HEC)-1 model to evaluate the integrated impacts of wetlands on mitigating flooding in a large drainage area (~4150 km²). Hattermann et al. (2006) predicted the impacts of wetlands on overall water and nutrient budgets for an agricultural watershed using the Soil and Water Integrated Model (SWIM). The Soil and Water Assessment Tool (SWAT) has been applied to investigate various water quality and hydrological benefits of wetlands for agricultural watersheds (Gassman et al., 2007). For example, SWAT was applied to assess wetland effects on streamflow during wet and dry periods (Wu and Johnston, 2008), to predict the impacts of wetland restoration and losses on water quantity and

quality (Wang et al., 2010; Yang et al., 2010; Records et al., 2014; Martinez-Martinez et al., 2014 and 2015), and to identify optimal locations for wetland restoration to improve water quality and mitigate flood damage (Babbar-Sebens et al., 2013; Comín et al., 2014).

SWAT, similar to other semi-distributed watershed models, oversimplified physical processes and representation of wetlands in a watershed context. SWAT simulates the lumped effect of multiple wetlands within a sub-watershed (Neitsch et al., 2011), using the concept known as “equivalent wetland area” (Wang et al., 2008). For example, multiple wetlands within a sub-watershed are spatially aggregated, and simulated as one. The size of this hypothetical wetland is assumed to be equivalent to the aggregated areal extent of multiple wetlands located within a sub-watershed. Its upland area is set by the relative proportion of aggregated drainage areas of multiple wetlands to a sub-watershed, and its location is positioned at the outlet of the sub-watershed. Hence outflow from an aggregated wetland is directly transported to the next downstream sub-watershed. This simplification significantly reduces computational demands. However, it disregards spatially variable wetland interactions with surrounding areas and local groundwater systems, such as recharge (Feng et al., 2013, McLaughlin et al., 2014, Evenson et al., 2015 and 2016), and the hydrological exchange with streams and groundwater along stream channels within a sub-watershed (Liu et al., 2008). Conceptually and spatially agglomerated representation of wetlands can be a large source of uncertainty in model prediction (Zhang et al., 2011). Several attempts are being made to improve wetland processes by disaggregating and modifying wetland representation by different types (Feng et

al., 2013), while considering hydrological connection with surrounding areas (Evenson et al., 2015 and 2016) and nearby streams (Liu et al., 2008).

However, it still remains unclear if enhanced model capabilities would reduce wetland function prediction uncertainty. This is because simulation results with enhanced capabilities have been evaluated against “aggregate” hydrological variables (e.g., streamflow, nutrient and sediment loads referred to as “hard data” in Seibert and McDonnell, 2002) collected at the watershed outlet (Liu et al., 2008; Evenson et al., 2015), while changes were made to improve spatial processes and patterns. The relative improvement in aggregated response cannot offer any insight into intra-watershed responses. Thus wetland hydroperiod (i.e., change in inundation or root-zone saturation through) and associated wetland functions affecting downstream waters should not be evaluated using aggregated response variables at various spatial scales.

SWAT, similar to other wetland models, estimates change in inundation extent (i.e., water levels) using a wetland water volume-surface area relationship. This relationship is specified by four wetland parameters: i.e., surface area and volume within a wetland at normal and maximum water levels. Spatially explicit information that describes the geomorphic and inundation characteristics of individual wetlands is required. However, such data rarely exist, and thus these parameters have often been set uniformly for all wetlands, regardless of spatial locations and site characteristics (Liu et al., 2008; Wu and Johnson, 2008; Babbar-Sebens et al., 2013; Comín et al., 2014; Records et al., 2014). Furthermore, spatially explicit *in-situ* data that can be used to evaluate simulated inundation within multiple

wetlands under various weather conditions rarely exist. To cope with data scarcity, it has been suggested that qualitative data (i.e., “soft data” in Seibert and McDonnell, 2002), derived from expert knowledge, literature, and extensive field monitoring of similar sites, be used. These data have been used to constrain a range of model parameter values for calibration (Seibert and McDonnell, 2002 and 2013; Vaché and McDonnell, 2006; Julich et al., 2012) or to qualitatively evaluate if modeled behaviors and intra-watershed responses are reasonable (Seibert and McDonnell, 2002).

Remotely sensed data provide synoptic information on the spatial distribution of various hydrological variables (e.g., precipitation, soil moisture, and inundation) at multiple spatial and temporal scales (Nielsen et al., 2008; Huang et al., 2014). With improved technology and increasing coverage, significant efforts are being made to integrate remotely sensed data products (e.g., soil moisture and vegetation) into various land surface models. The aim is to reduce the degree of equifinality (i.e., many different parameter sets are equally good at reproducing an output signal; Beven, 2006) using observed spatial patterns to reduce ambiguity in the input data, change states/condition, parameters, and represented processes, and improve model prediction (e.g., soil moisture and streamflow) via data assimilation (Loumagne et al., 2001). The results seem to be promising, particularly at the regional or global scale, when coupled with conceptual models. However, data assimilation was shown to be unsatisfactory when tested with more complex spatially distributed, process-based models, such as SWAT, at a local catchment scale (Chen et al., 2011). Moreover, most routinely collected remotely sensed data products of hydrological variables

(e.g., soil moisture) are acquired at a coarse spatial resolution (tens of kilometers; Lakshmi, 2013) and therefore are limited in their utility for characterizing small to moderate size wetlands which are dominant on the landscape. On the other hand, commonly available wetland mapping products are categorical maps at much higher spatial resolutions (e.g., US Fish and Wildlife Service (USFWS) National Wetland Inventory (NWI), US National Land Cover Database (NLCD) by the Multi-Resolution Land Characteristics (MRLC) Consortium, US National Oceanic and Atmospheric Administration (NOAA) Coastal Change Analysis Program (C-CAP)). However, they cannot provide information on inundation changes in a wetland over time.

The potential to routinely map inundated wetlands at a 30-m resolution with high accuracy (> 92%) was recently demonstrated using Light Detection and Ranging (LiDAR) and time series Landsat data (Lang and McCarty, 2009; Lang et al., 2013, Huang et al., 2014; Jin et al., 2017). The mapping algorithm was applied to detect inundated area for small seasonal forested wetlands, which are densely distributed in the Coastal Plain of the Mid-Atlantic Region of the US (Huang et al., 2014). Forested wetlands are difficult to map, due to the presence of the forest canopy and the fact that inundation and saturation in these wetland is often ephemeral. Inundation maps were produced annually using LiDAR intensity data and Landsat images acquired in early spring (Jin et al., 2017), when most standing water within a wetland was viewable due to the leaf-off status of the forest canopy (Lang et al., 2012, Huang et al., 2014). When applied to watersheds in the Coastal Plain Physiographic Province of the Chesapeake Bay Watershed (CBW), spatial patterns of inundation reflected

different weather conditions and followed the change trend of streamflow (Huang et al., 2014; Jin et al., 2017).

In this paper, we present an integrated wetland-watershed modeling framework that capitalizes on time series inundation maps, with an aim to improve prediction of wetland inundation patterns at a landscape scale. We outline problems commonly arising from input data preparation and parameterization to represent spatially aggregated wetlands within a distributed watershed model. We demonstrate how intra-watershed processes can be better captured by setting spatialized wetland parameters developed from remotely sensed data, as doing so reduced the degree of equifinality. We then place particular emphasis on assessing model prediction using spatial maps of inundation under different weather conditions. This spatial data-model integrated framework was tested with SWAT and the Riparian Wetland Module (RWM), an improved SWAT extension for riparian wetlands (RWs). The effects of improved parameterization and process representation on predicted inundation are demonstrated using a case study conducted in the upper river basin of Choptank Watershed, located in the Coastal Plain of the CBW.

4.2 Data and Methods

4.2.1 Study area

The Tuckahoe Creek Watershed (TCW, ~ 220.7 km²) is located on the upper region of the Choptank River Watershed in the Coastal Plain of the CBW (Figure 4.1). The Choptank River Watershed is on the list of “impaired watersheds”

designated by the US Environmental Protection Agency (USEPA), due to excessive sediment and nutrient loads from agricultural lands (McCarty et al., 2008). The site has been selected as one of the US Department of Agriculture (USDA) Conservation Effects Assessment Project (CEAP) benchmark watersheds, and extensively monitored and studied (McCarty et al., 2008; Yeo et al., 2014; Lee et al., 2016; Sharifi et al., 2016). It is characterized by a relative flat topography (Figure 4.2a), with humid and temperate climate (Ator et al., 2005). Overall, soils are evenly split between well-drained (USDA classification of Hydrologic Soil Group (HSG) – A or B) and poorly-drained soils (HSG – C or D) (Figure 2b). Land use is mainly comprised of agriculture (51.3%) and forest (38.4 %), followed by pasture (8.5%), urban areas (1.4%), and water bodies (0.3%) (Figure 4.2c). The study site includes abundant forested wetlands, such as wetland depressions (e.g., Delmarva bays), wetland flats, and riparian wetlands (Lang et al., 2012). According to the NWI map, most forested areas are indeed forested wetlands and the total coverage of wetlands is about 34.5 km², accounting for 15.5% of the entire TCW (Figure 4.2d). The majority of forested wetlands are known to be seasonally inundated for a relatively short time period in early spring, when ET is low leading to seasonally high groundwater (Tiner and Burke, 1995).

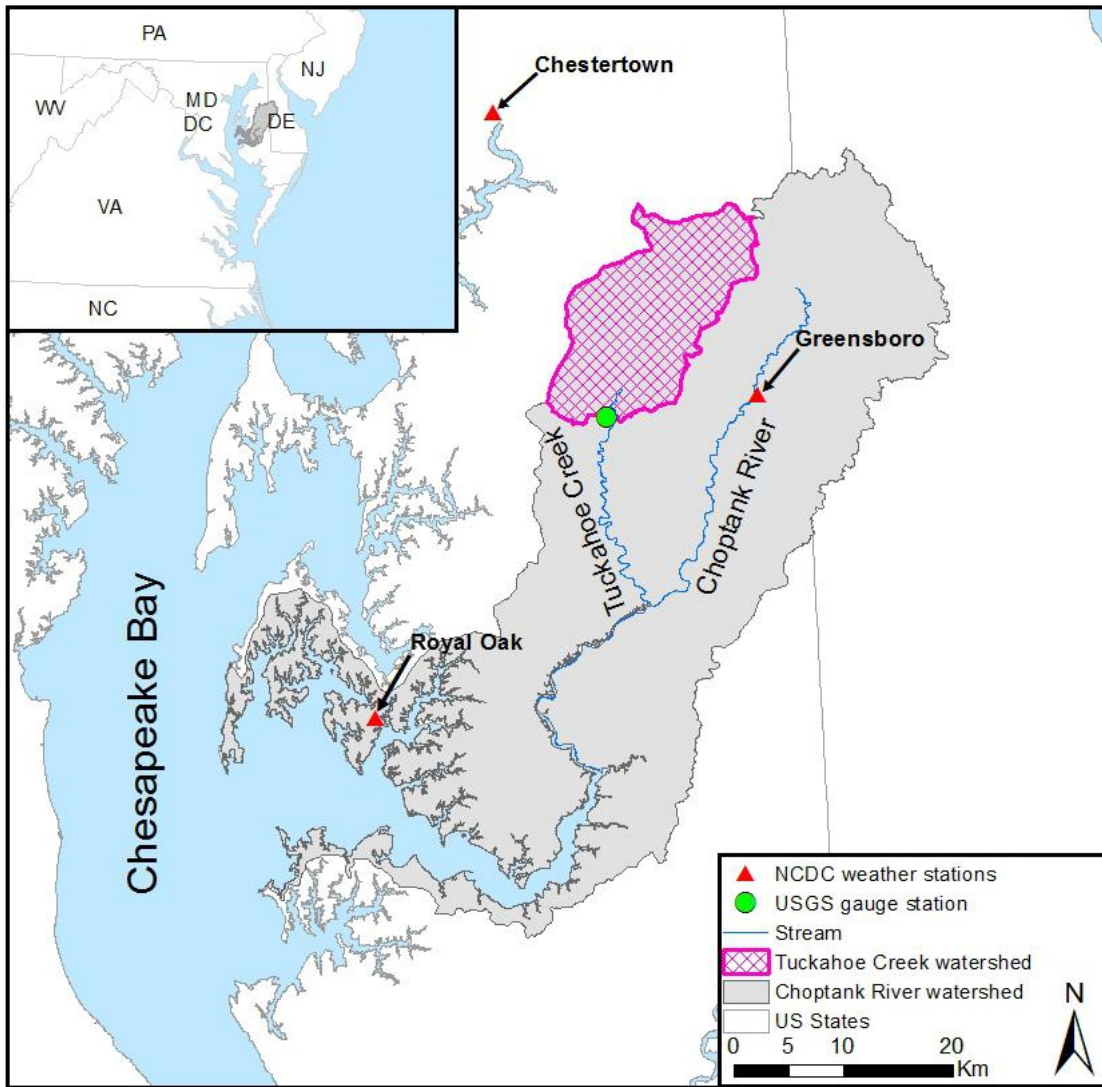


Figure 4.1. The location of the Tuckahoe Creek Watershed and Greensboro Watershed near Chesapeake Bay.

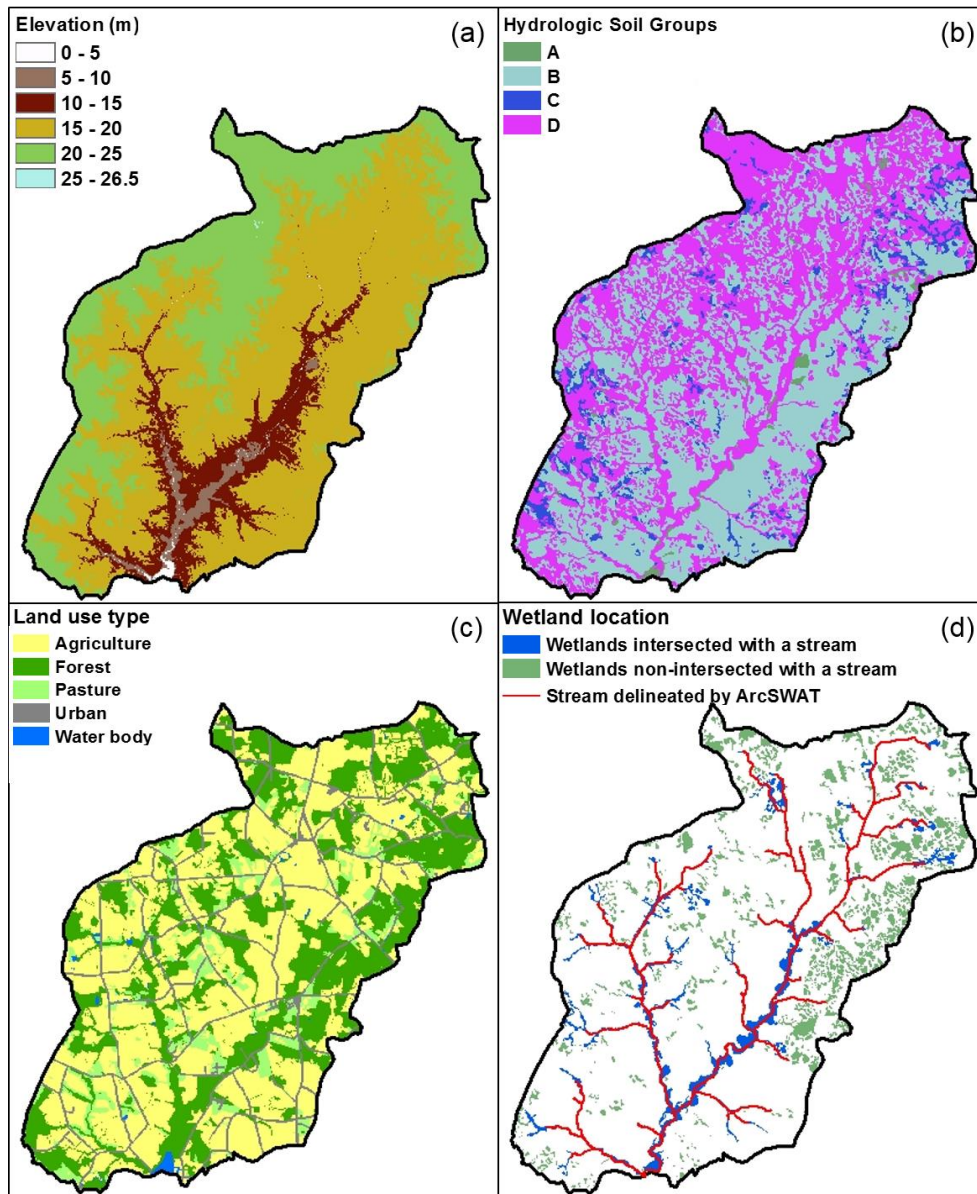


Figure 4.2. The physical characteristics of the TCW: (a) elevation, (b) soil properties, (c) land use, and (d) wetlands identified by the NWI map (adapted from Lee et al. 2016)

Note: Hydrologic soil groups (HSGs) are characterized as follows: Type A- well-drained soils with $7.6-11.4 \text{ mm}\cdot\text{hr}^{-1}$ ($0.3-0.45 \text{ inch}\cdot\text{hr}^{-1}$) water infiltration rate; B - moderately well-drained soils with $3.8-7.6 \text{ mm}\cdot\text{hr}^{-1}$ ($0.15-0.30 \text{ inch}\cdot\text{hr}^{-1}$) water infiltration rate; C - moderately poorly-drained soils with $1.3-3.8 \text{ mm}\cdot\text{hr}^{-1}$ ($0.05-0.15 \text{ in}\cdot\text{hr}^{-1}$) water infiltration rate; and D – poorly-drained soils with $0-1.3 \text{ mm}\cdot\text{hr}^{-1}$ ($0-0.05 \text{ inch}\cdot\text{hr}^{-1}$) water infiltration rate (Neitsch et al., 2011). The NWI polygons connected to the stream map are represented as “blue” and others as “green” in Figure 4.2d. See section 4.2.4.1 for further details.

4.2.2 Soil and Water Assessment Tool (SWAT) model: an overall approach to watershed simulation

SWAT is a distributed, continuous, process-based watershed model. It has been widely used to simulate hydrology, nutrient cycling, and sediment loads in an agricultural watershed (Neitsch et al., 2011). SWAT partitions a watershed into sub-watersheds, the draining area of the stream segment, and further into Hydrologic Response Units (HRUs) based on unique combination of land use, soil type, and slope. The mass balance, transport, and cycling of hydrologic and water quality variables are simulated at each HRU, whose outputs aggregated for the sub-watershed, and then routed to the outlet of the watershed through channel processes. SWAT uses the Soil Conservation Service (SCS) Curve Number (CN) method to compute surface runoff and infiltration, which is determined based on soil's permeability, land use and antecedent soil water conditions. The Penman-Monteith method was used to simulate ET. Refer to Neitsch et al. (2011) for further details.

SWAT input data consist of various geospatial and climate data (Table 4.1). A high resolution LiDAR-based Digital Elevation Model (DEM), land use map and Soil Survey Geographical Database (SSURGO) were used to characterize the study site and delineate stream network, sub-watersheds, and HRUs. In total, the watershed was divided into 71 sub-watersheds and further into 573 HRUs, by applying the threshold (%) of 10, 20, and 20 to land use, soil use, and slope, respectively. Delineation processes are fully described in Winchell et al. (2010).

Daily precipitation and temperature were obtained from three weather stations located near the TCW, operated by NOAA National Climate Data Center (NCDC)

(Chestertown: USC00181750, Royal Oak: USC00187806, and Greensboro: US1MDCL0009). Daily solar radiation, relative humidity, and wind speed were not monitored, so they were generated using SWAT's built-in weather generator (Neitsch et al., 2011). Daily streamflow data collected at the outlet of the TCW was obtained from the US Geological Survey (USGS) gauge station (#01491500, Figure 4.1). A commonly available drought index (i.e., Palmer Drought Severity Index [PDSI]) was used to characterize weather conditions (e.g., drought, normal, and wet) based on historic climate records. It was downloaded from the NOAA NCDC for the climate division (MD Region 5) within where the study watershed is situated.

Table 4.1. List of input data

Data	Source	Description	Year
DEM	MD-DNR	LiDAR-based 1 meter resolution	2006
Land use	USDA-NASS	Cropland Data Layer (CDL)	2008 - 2012
	MRLC	National Land Cover Database (NLCD)	2006
	USDA-FSA-APFO*	National Agricultural Imagery Program digital Orthophoto quad imagery	1998
Soils	US Census Bureau	TIGER road map	2010
	USDA-NRCS	Soil Survey Geographical Database (SSURGO)	2012
Climate	NCDC	Daily precipitation and temperature	1999 - 2008
Streamflow	USGS	Daily streamflow	2001 - 2008
Wetland	NWI	National Wetlands Inventory	
Stream map			
Sub-watershed boundary	ArcSWAT	DEM-based delineation method using the threshold of a drainage area	N/A
Inundation map	Huang et al. (2014)	Annual time series inundation map developed from Landsat images and LiDAR intensity data	2001-2008
Drought Index	NOAA-NCDC	Palmer Drought Severity Index	2001-2008
High resolution image	USDA-FSA	1-meter aerial imagery acquired at 8/15/2013 from the national agriculture imagery program available through ArcGIS online	2015

MD-DNR: Maryland Department of Natural Resources, USDA-NASS: USDA-National Agriculture Statistics Service, USDA-FSA-APFO: USDA-Farm Service Agency-Aerial Photography Field Office, USDA-NRCS: USDA-National Resources Conservation Service, and USDA-FSA: USDA-Farm Service Agency

4.2.3 Representation of wetland processes

This study used the built-in ‘conventional’ wetland module in SWAT to simulate non-riparian wetlands (NRWs) and the improved riparian wetland module, RWM (Liu et al. 2008), for riparian wetlands (RWs). This sub-section briefly describes the two modules.

4.2.3.1 Non-riparian wetland (NRW) module

SWAT treats a wetland like an impoundment and simulates its hydrological effects at the sub-watershed scale (Neitsch et al., 2011). It aggregates wetlands distributed within a sub-watershed. Then this lumped wetland is assumed to be located at the outlet of the sub-watershed (Neitsch et al., 2011) and its water balance is calculated at a daily time step, as (Eq. 4.1):

$$V = V_{stored} + V_{flowin} - V_{flowout} + V_{pcp} - V_{evap} + V_{seep} \quad (4.1)$$

where V is the volume of water stored in a wetland at the end of the day, V_{stored} the volume of water stored in the wetland at the beginning of the day, V_{flowin} the volume of water entering the wetland during the day, $V_{flowout}$ the volume of water flowing out of the wetland during the day, V_{pcp} the volume of precipitation falling onto the wetland during the day, V_{evap} the volume of water removed from the wetland by ET during the day, and V_{seep} the volume of water lost from the wetland by seepage during the day. Note that V_{flowin} is calculated based on the fraction of water draining into a wetland from a sub-watershed (including surface runoff, lateral flow and groundwater

flow). SWAT assumes outflow, $V_{flowout}$ to occur whenever water stored in a wetland exceeds its normal storage volume (V_{nor}), as:

$$V_{flowout} = 0 \quad \text{if } V < V_{nor} \quad (4.2)$$

$$V_{flowout} = \frac{V - V_{nor}}{10} \quad \text{if } V_{nor} \leq V \leq V_{mx} \quad (4.3)$$

$$V_{flowout} = V - V_{mx} \quad \text{if } V > V_{mx} \quad (4.4)$$

where V_{mx} and V_{nor} are the volume of water held in a wetland at maximum and normal water levels, respectively.

Based on the daily volume of water stored in a wetland (i.e., V in Eq. 4.1), the surface area of a wetland (A_{wet}) is calculated at the daily time step, as:

$$A_{wet} = \beta \cdot V^\alpha \quad (4.5)$$

where α and β are coefficients. These coefficients are estimated as:

$$\alpha = \frac{\log_{10}(SA_{mx}) - \log_{10}(SA_{nor})}{\log_{10}(V_{mx}) - \log_{10}(V_{nor})} \quad (4.6)$$

$$\beta = \left(\frac{SA_{mx}}{V_{mx}} \right)^\alpha \quad (4.7)$$

where SA_{mx} and SA_{nor} are the surface water area of a wetland at maximum and normal water levels, and V_{mx} and V_{nor} the volume of water held in the wetland at maximum and normal water levels, respectively. Further details are available from Neitsch et al. (2011).

4.2.3.2 Riparian wetland module (RMW)

The riparian Wetland Module (RWM) developed by Liu et al. (2008) explicitly simulates the “bi-directional” exchange of water flow and sediments between a RW and the main stream segment in a sub-watershed. For example, RWM calculates the water balance of a RW (V_r) as:

$$V_r = V_{r,stored} + V_{r,flowin} + V_{r,flowout} + V_{r,pcp} - V_{r,evap} + V_{r,seep} \pm V_{r,rchflow} \quad (4.8)$$

All the components in Eq (4.8) are identical to Eq (4.1), except that Eq (4.8) includes $V_{r,rchflow}$, the volume of surface and sub-surface water exchange between RWs and reach. The subscript, r , denotes simulation of riparian wetlands. Note that the RWM simulates water flows from upland into a stream segment, NRWs, and RWs separately, as it divides the sub-watershed into three drainage zones (i.e., riparian wetland, non-riparian wetland, and stream drainage zones, Figure 4.3). The RWM estimates the amount of inflow (i.e., contributing upland flow) into three drainage zones according to its areal fraction relative to the total sub-watershed area. Note that $V_{r,flowin}$ can be estimated from surface runoff, lateral flow, and groundwater flow. Surface area within a RW is estimated similar to the NRW module (Eq. 4.5 – 4.7) after a slight modification (Liu et al., 2008).

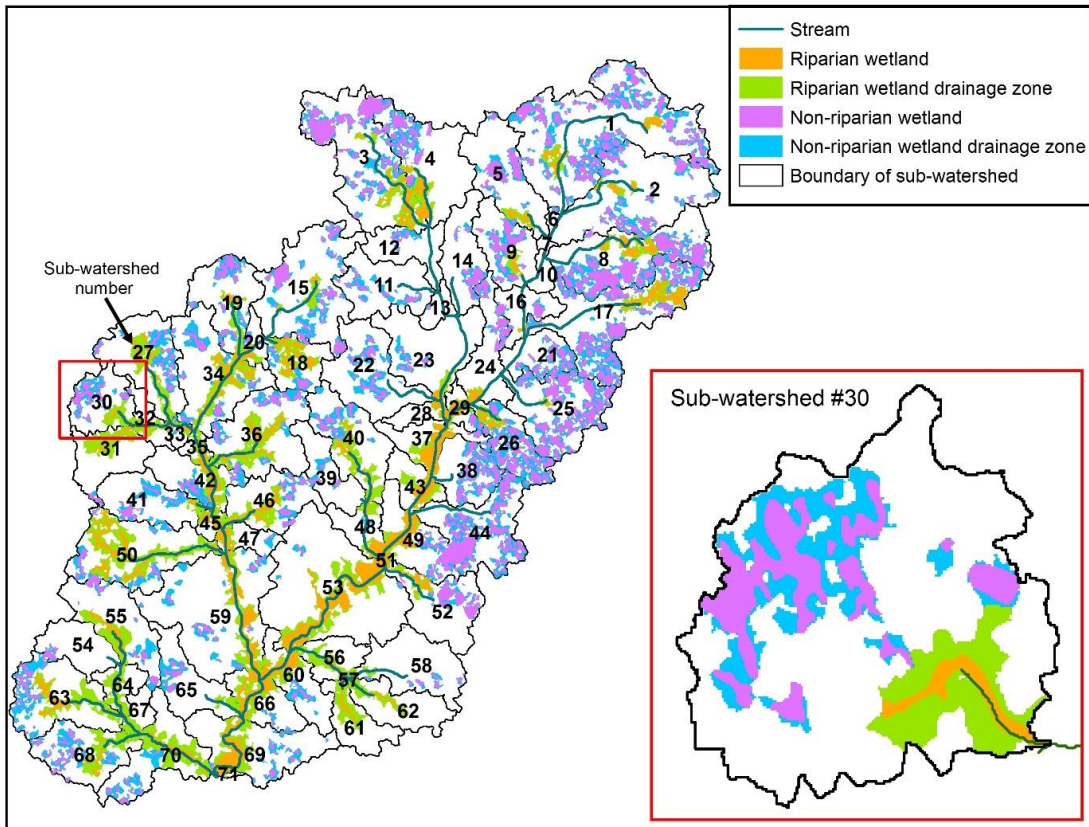


Figure 4.3. The representation of riparian wetlands and non-riparian wetlands, and wetland drainage zones delineated by the ArcGIS geo-processing tools.

Note: The inset map provides an enlarged view of the spatial arrangement of two wetland types and their drainage zones relative to the stream, within a selected sub-watershed boundary (# 30). A wetland drainage zone indicates an upland area. The white background areas, which do not fall within riparian wetland and non-riparian wetland drainage zones, directly drain into the stream.

Figure 4.4 illustrates the conceptual scheme that outlines the lateral exchange of water flows between a RW and a stream segment as in Liu et al. (2008). RWM assumes that wetland water level at its normal depth is equivalent to reach water level at its bank full depth. Then, the lateral surface flow exchange occurs under high flow conditions, when wetland water level is higher than its normal depth and/or the channel water level is higher than the bank full depth. Liu et al. (2008) describes how

the channel water depth can be estimated using rating curves based on channel geometry, watershed drainage characteristics, and Manning’s equation as in SWAT. The lateral subsurface flow exchange occurs when the water level is between the bottom and the bankfull level for both the wetland and stream reach, and the groundwater flow exchange was estimated by Darcy’s Law (Liu et al., 2008). Lateral subsurface flow exchange follows similar iterative algorithm as the lateral surface flow exchange illustrated in Figure 4.4 Groundwater flow from upland areas is assumed to pass under RWs (i.e., no groundwater inflow to RWs from upland areas) and directly contributes to streams, if water level in the stream is lower than the bottom of the RWs (Liu et al., 2008). See Liu et al. (2008) for further details.

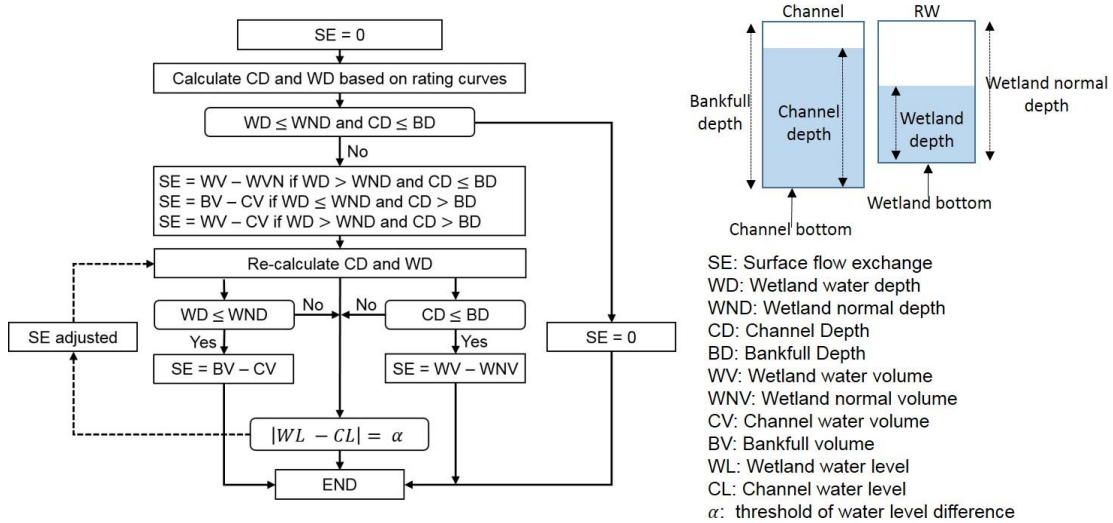


Figure 4.4. The conceptual model that illustrates lateral surface flow exchange between riparian wetlands and streams (adapted from Liu et al. (2008)).

4.2.4 Parameterization of wetlands

4.2.4.1 Delineation of RWs and NRWs

RWM defines RWs as those wetlands that intersect nearby streams, and assumes RWs to have bi-directional exchange with nearby streams (see discussion in 4.2.3.2). We identified RWs within the study watershed by following this “operational definition” in Liu et al. (2008). This operational definition requires the exclusion of two particular groups of RWs, which are most unlikely to have bi-directional exchange with streams. The first is headwater wetlands. These are initiating, intermittent headwater streams that typically have “one directional flow” into the stream (McDonough et al., 2015). The other is wetlands directly connected to artificial ditches, which are extensively developed in the region to drain wetlands to local streams during periods of low ET (Denver et al., 2014).

Instead of using commonly available stream maps (e.g., USGS National Hydrography Dataset (NHD)) that are known to underrepresent streams and ditch length in the study site (Lang et al., 2012), we used a high resolution LiDAR DEM to delineate a more detailed, accurate stream network. A high resolution LiDAR DEM and the built-in “Stream Definition” function in ArcSWAT (Winchell et al., 2010) with multiple drainage density thresholds were used to create detailed drainage networks. The finer high resolution stream map helped to identify and isolate those NWI polygons that belong to two particular groups described above. We delineated stream maps by applying different drainage area thresholds and then selected one that did not intersect these two particular groups of NWI polygons. The delineation was done based on our local knowledge, field observation, and visual inspection of the

study site with high-resolution images. The selected stream map was overlaid with NWI polygons which were processed to aggregate wetlands in close proximity (with <10 cm threshold) using the ArcGIS Cartography Tool (ESRI, Redlands CA, ArcGIS v 10.2). Those NWI polygons which intersect with the stream map were considered RWs and the remaining as Non-Riparian Wetlands (NRWs). Aggregated areas of RWs and NRWs identified through this procedure were 13.4 km² and 21.1 km², accounting for 6.0 % and 9.5 % of the TCW, respectively.

4.2.4.2 Model parameterization for wetlands: data and geospatial processing

As aforementioned, wetland modules compute a daily water balance within a wetland (Eq. 4.1 and 4.8), and then update its surface water area using the nonlinear volume-surface area relationship (Eq. 4.5) specified by two parameters (i.e., α and β). To estimate them, detailed information on the surface area and volume of wetlands at normal and maximum water levels (Eq. 4.6 and 4.7) is required. However, such data rarely exist, especially from field monitoring. We used three geospatial datasets (i.e., NWI map, inundation maps, and DEM) to calculate surface area under the two conditions, and applied the GIS-based methods shown in Lane and D'Amico (2010) to estimate the water volume of wetlands. This GIS-based method takes the average elevation of each wetland polygon boundary as the maximum stage height of a wetland, and then estimates the maximum water storage volume using the ArcGIS 3D Analyst Tool (Lane and D'Amico, 2010).

The NWI was used to calculate surface water area at the maximum water level. The NWI shows the spatial distribution and extent of wetlands (Tiner, 1997).

Developed from high resolution aerial photographs or multispectral satellite images commonly collected on multiple dates, the NWI dataset undergoes an extensive validation process (Tiner, 1997). NWI polygons located within a close proximity were spatially aggregated, and then partitioned into sub-watersheds based on the spatial distribution and positioning. This partitioning resulted in “slivers”, i.e., the extremely small portion of the NWI polygon to a sub-watershed (see examples from Figure 4.5a). Those slivers were removed for further processing. We used the median elevation value, instead of the average as shown in Lane and D’Amico (2010), of the polygon boundary as the maximum water stage and calculated the maximum water volume. We then aggregated the maximum surface area and storage volume separately, for NRWs and RWs, at the sub-watershed scale.

Surface water area at the normal water level was estimated from the inundation map derived with the Landsat image acquired in early spring of 2007 (Huang et al., 2014, Jin et al., 2017). The inundation maps showed surface water fraction (SWF), or percent inundation, within a 30-m Landsat pixel in early spring. We selected the 2007 inundation map to capture typical patterns of surface water area at the normal spring water level, as weather condition and seasonal streamflow was shown to be “normal” according to the PDSI and the long-term records of streamflow and precipitation over last 30 years. In addition, the 2007 map was evaluated with extensive field data collected at the study site, providing confidence for this spatial dataset (Lang et al., 2009; Huang et al., 2014; Jin et al., 2017). Surface area at the normal water level was estimated by calculating a weighted sum of inundation pixels (using SWF as a weight). The normal water volume was computed after we

delineated contiguous inundated polygons which show the edge of the flooded area. This data processing involved multiple steps, as follows: (1) conversion of inundation pixels into polygons, (2) aggregation of inundation polygons in a close proximity (with a threshold < 10 cm), and (3) filling holes ('island polygon', if any) inside aggregated inundation polygon (Figure 4.5b). We applied the GIS-based method by Lane and D'Amico (2010) to estimate normal water volume using the 2007 map and DEM. The normal depth of RW required for simulating the lateral water exchange between RWs and streams (Figure 4.4) was estimated by simply dividing the aggregate water volume by the aggregate surface area at the sub-watershed scale, assuming the geometry of this hypothetical wetland as a cubic (Liu et al., 2008). The spatial distribution of inundated areas could be irregular and uneven, relative to the NWI polygon coverage (Figure 4.5c). For example, some sub-watersheds (e.g., #22 and #23 in Figure 4.5c) contained a very small portion of wetlands (aggregated NWI), which did not show any sign of inundation. In this case, we estimated inundated area using the original NWI polygon prior to aggregation (Figure 4.5d).

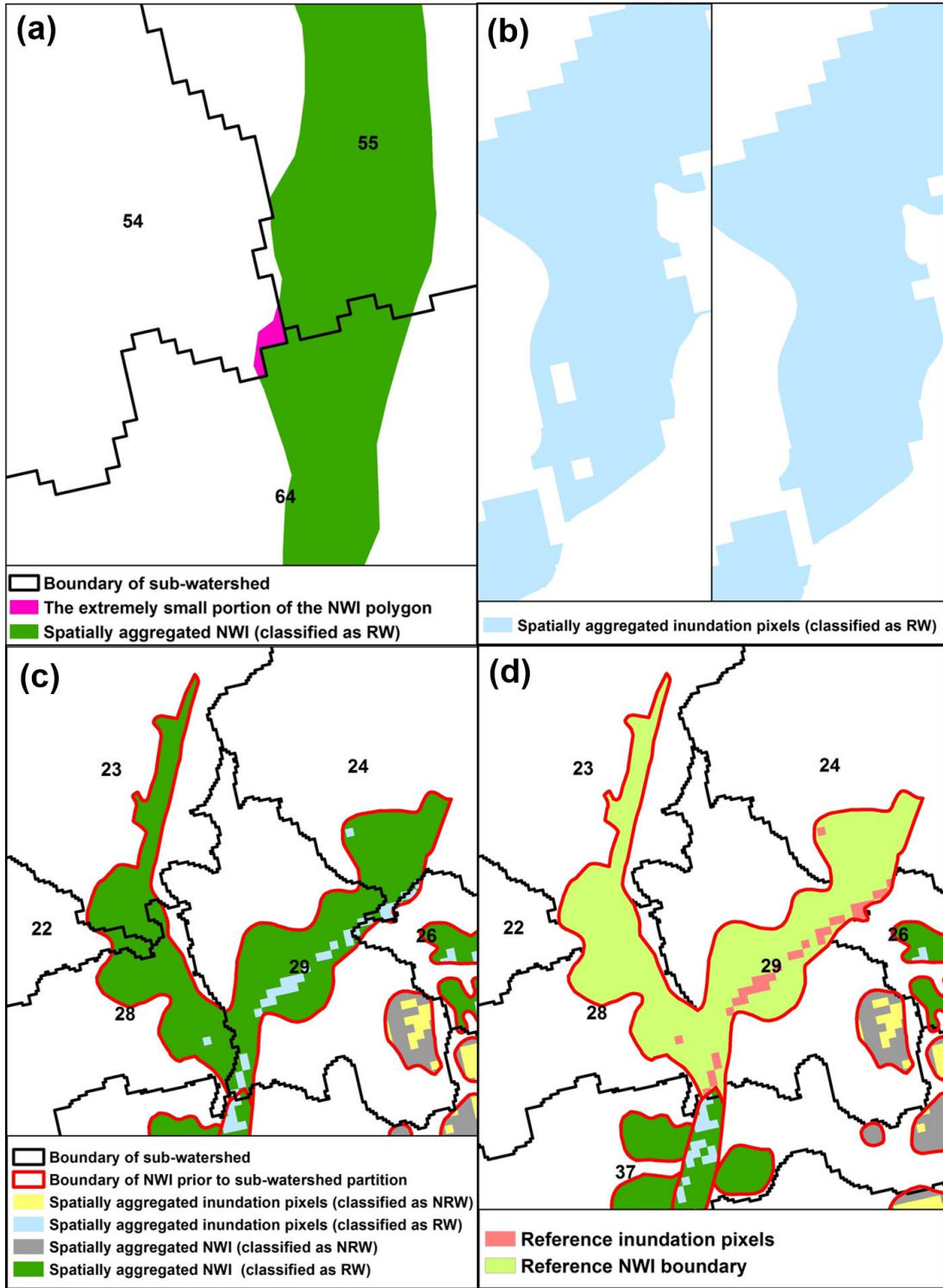


Figure 4.5. Estimation of the proportion of the inundated area at the normal and maximum water level using NWI and the 2007 inundation map: (a) the sub-watershed including the extremely small portion (“slivers”) of the NWI polygon after partitioning (# 54), (b) gaps inside inundation polygon created after vectorizing inundation pixels, (c) spatially aggregated NWI polygons and inundation pixels, and

(d) the aggregated NWI polygon (in C) ungrouped into original NWI polygons to estimate the relative inundated areas for the NWI (# 22 and 23).

Note: A numerical value is used to label the sub-watershed. For those sub-watersheds that do not include inundation pixels (# 22 and 23 in Figure 4.5d), the proportion of normal to maximum wetland area was assumed to be same as the proportion of inundation pixels (red area in Figure 4.5d) within the original NWI to the original NWI polygon (light green area in Figure 4.5d). The normal wetland depth derived from the red area in Figure 4.5d was used to calculate the normal wetland volumes (area \times depth).

4.2.5 Model calibration and validation

SWAT was simulated at a daily time step over 10 years, including 2-year warm-up (1999-2000), 5-year calibration (2001-2005), and 3-year validation (2006-2008). We calibrated SWAT twice against observed streamflow collected at the outlet of the watershed (Figure 4.6) following Liu et al. (2008). For the first calibration, wetland modules were turned off (referred to as Flow_WO), and 18 parameters deemed to be most sensitive to streamflow were manually calibrated based on previous SWAT modeling studies conducted in the study watershed (Sexton et al., 2010, Yeo et al., 2014, Lee et al., 2016) (Table 4.2). Model calibration was conducted manually by adjusting parameter values within an allowable range, following the SWAT model technical guideline. Selected were those parameter values that produced the best model performances while meeting SWAT performance criteria outlined by Moriasi et al. (2007) (Table 4.2). For the second calibration, wetland modules (referred to as Flow_W) were turned on, for the second calibration, and five parameters (Table 4.2) that control the routing processes, including surface water and groundwater routing to stream segments and then to watershed outlet via the main channels, were refined (Liu et al., 2008). Wetland parameters developed in section

4.2.4.2 were introduced in the second step, and other parameters required for wetland modules (e.g., saturated hydraulic conductivity of the wetland bottom and an evaporation coefficient) were set as the default values in SWAT (Arnold et al., 2012). The following statistical performance measures were considered to assess model performance during the calibration: Nash-Sutcliffe efficiency coefficient (NSE), root mean squared error (RMSE)-standard deviation ratio (RSR), and percent bias (P-bias; Moriasi et al., 2007). They were computed as:

$$NSE = 1 - \left[\frac{\sum_{i=1}^n (O_i - S_i)^2}{\sum_{i=1}^n (O_i - \bar{O})^2} \right] \quad (4.9)$$

$$RSR = \frac{RMSE}{STDEV_{obs}} = \left[\frac{\sqrt{\sum_{i=1}^n (O_i - S_i)^2}}{\sqrt{\sum_{i=1}^n (O_i - \bar{O})^2}} \right] \quad (4.10)$$

$$P - bias = \left[\frac{\sum_{i=1}^n (O_i - S_i) \times 100}{\sum_{i=1}^n O_i} \right] \quad (4.11)$$

where O_i are observed and S_i are simulated data, \bar{O} is observed mean values, and n equals the number of observations.

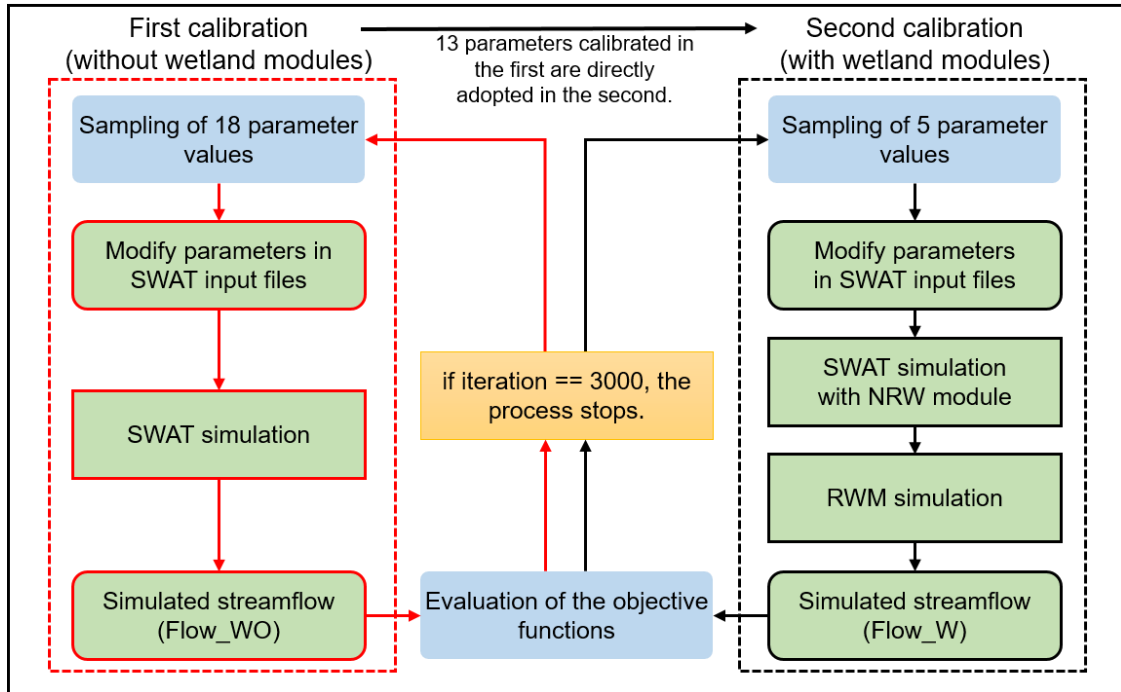


Figure 4.6. Flow diagram illustrating SWAT wetland module calibration procedures.

Note: The objective functions are shown in Eq. 4.9 – 4.11. 18 parameters used in the first calibration are listed in Table 4.2, and 5 parameters re-adjusted in the second calibration are highlighted in Table 2. “==” stands for “equal”.

Table 4.2. List of calibrated parameters

Parameter	Description (unit)	Range	First calibration (Flow_WO)	Second calibration (Flow_W)
CN*	SCS runoff curve number	-50 – 50 %	- 15 %	- 15 %
ESCO*	Soil evaporation compensation factor	0 – 1	0.89	0.89
OV_N#	Manning's "n" value for overland flow	0.01 – 30	1.81	1.90
SLSUBBSN*	Average slope length (m)	-50 – 50 %	-37 %	-37 %
EPCO*	Plant uptake compensation factor	0 – 1	0.63	0.63
CANMX#	Maximum canopy storage (mm H ₂ O)	0 – 100	0.18	0.18
GW_DELAY*	Groundwater delay (days)	0 – 500	53.60	55.61
ALPHA_BF*	Baseflow alpha factor (1·days ⁻¹)	0 – 1	0.73	0.73
GWQMN*	Threshold depth of water in the shallow aquifer required for return flow to occur (mm H ₂ O)	0 – 5000	0	0
GW_REVAP*	Groundwater "revap" coefficient	0.02 – 0.2	0.06	0.06
REVAPMN*	Threshold depth of water in the shallow aquifer for "revap" to occur (mm H ₂ O)	0 – 500	1	1
RCHRG_DP*	Deep aquifer percolation fraction	0 – 1	0.05	0.05
SOL_AWC*	Available water capacity of the soil layer (mm H ₂ O ·mm soil ⁻¹)	-50 – 50 %	- 6 %	- 6 %
SOL_K*	Saturated hydraulic conductivity (mm·hr ⁻¹)	-50 – 50 %	- 47 %	- 47 %
SOL_Z*	Depth from soil surface to bottom of layer (mm)	-50 – 50 %	+ 21 %	+ 21 %
CH_N2†	Manning's "n" value for the main channel	0.01 – 0.3	0.011	0.015
CH_N1†	Manning's "n" value for the tributary channels	0.01 – 30	0.508	0.556
SURLAG*	Surface runoff lag coefficient	0.5 – 24	10.12	7.70

Note: The ranges of parameters with superscripts (*, #, and †) are derived from Gitau and Chaubey (2010), Wu and Xu (2006), and Yen et al. (2014), respectively. The highlighted parameters are re-adjusted in the second calibration.

4.2.6 Evaluation of inundated area prediction uncertainty: spatial pattern analysis

Despite the fact that distributed hydrological models are used for a wide variety of applications, it is common to apply uniform parameter values at some point within spatial modeling units (Grayson and Blöschl, 2002). The implication of imposing uniform spatial parameters on simulated spatial results (e.g., inundated areas or inter-watershed response) is not easily measurable, as model performance is generally tested against aggregated hydrological variables. In this case, simulation results can be equally acceptable, regardless of the degree of spatial heterogeneity imposed on parameters or process representation. To illustrate this equifinality

problem with improved RWM, we prepared three sets (referred to as Set A, B, and C) of wetland parameters, imposing varying degree of spatial heterogeneity at the sub-watershed scale (Table 4.3). Note that the sub-watershed scale is the elementary modeling unit of RWM. SWAT delineates a sub-watershed as a drainage area of each stream segment, and wetland are aggregated and interact with stream segment within a sub-watershed. The first set, Set A (i.e., spatialized wetland parameters), was prepared using spatially explicit information from inundation maps, as in section 4.2.4.2. Two additional sets (Set B and C) were prepared by assuming uniform wetland parameters for the entire watershed, following typical approaches used in previous studies (Liu et al., 2008; Wu and Johnson, 2008; Babbar-Sebens et al., 2013; Comín et al., 2014; Records et al., 2014). Set B was determined by taking mean values of the sub-watershed scale wetland parameters (from Set A), without separating RWs and NRWs. Set C was adopted from Liu et al. (2008), as it described parameters for forested wetlands, the most dominant type of wetlands at the study site. Figure 4.7 illustrates the differences in the parameter values from Set A-C summarized by stream order and hierarchy.

Table 4.3. Wetland parameters and normal depth of RW estimated by three parameterizations

Parameters	Set A	Set B	Set C
Maximum area	NWI	NWI	NWI
Normal area	2007 inundation map	Maximum area \times 12 % ^[1]	Maximum area \times 30 % ^[1]
Maximum volume	Geoprocessing using NWI and DEM	Maximum area \times 0.6 m ^[2]	Maximum area \times 0.5 m ^[2]
Normal volume	Geoprocessing using 2007 inundation map and DEM	Normal area \times 0.2 m ^[3]	Normal area \times 0.1 m ^[3]
Normal depth of RW	Normal volume / normal area (0.02 – 0.8 m)	0.2 m ^[3]	0.1 m ^[3]

Note: The proportion ⁽¹⁾, maximum depth ⁽²⁾, and normal depth ⁽³⁾ were estimated by calculating the mean value of the proportions of normal areas to maximum areas, maximum volume/maximum area, and normal volume/normal area for all wetlands in Set A, respectively. Normal depth of RW in Set A was calculated by dividing normal volume by normal area for individual RWs. Presented parameter values were separately estimated for RWs and NRWs.

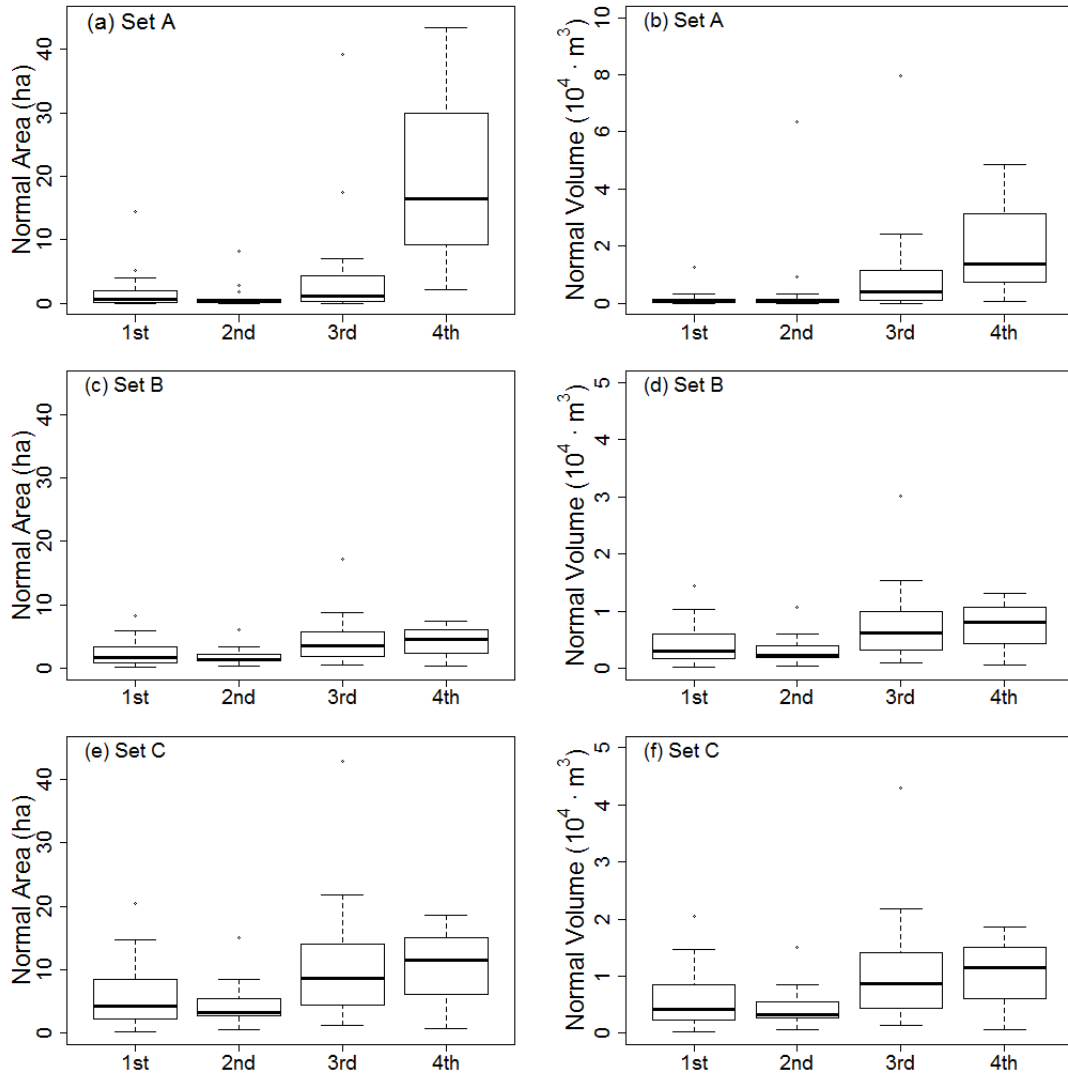


Figure 4.7. The normal volume and area of RWs by stream orders; (a & b) Set A, (c & d) Set B, and (e & f) Set C.

The simulated inundated areas within RWs were compared with inundation maps at the sub-watershed scale. Inundated extent (estimated as a weighted sum of inundation pixels, as discussed in section 4.2.4.2) within RWs from inundation maps were spatially aggregated at the sub-watershed scale, and this was served as the baseline for the comparison. We computed the Spearman's rank-order correlation coefficient (r_s) to statistically measure similarity between the simulated and observed

inundated areas. After ranking inundated areas (aggregated at the sub-watershed scale) from the largest to the smallest and calculating differences (d) in ranks between the observed and the simulated inundation, the correlation coefficient (r_s) was computed as:

$$r_s = 1 - \frac{6 \sum_{i=1}^n d^2}{n(n^2 - 1)} \quad (4.12)$$

where n is the number of sub-watersheds that included RWs ($n = 60$). As r_s is closer to 1, the simulated is more closely matched to the observed. In addition, a Mean Squared Error (MSE) was computed to quantify the difference between the observed and the predicted (Moriasi et al., 2007), as:

$$MSE = \frac{1}{n} \sum_{i=1}^n (P_i - Y_i)^2 \quad (4.13)$$

where P_i is predicted inundated area (ha) within RWs and Y_i observed from inundation maps. The spatial pattern analysis was performed with annual inundation maps delineated over the period of 2001-2008 under different weather conditions. The 2007 inundation map was excluded from the analysis as it was used to develop Set A (section 4.2.4.2) and the model calibration.

4.2.7 Evaluation of inter-annual variability of wetland water storage

We analyzed seasonal variations in the water stored in RWs by stream hierarchy. It was to investigate whether spatial wetland parameterization (Set A) better captured local wetland characteristics and inter-annual variability in wetland

function, compared to two other sets with uniform parameters (Sets B and C). We computed 8-year monthly averages and coefficient of variation (i.e., mean normalized by the standard deviation) of wetland water storage. The monthly means and coefficients of variations were categorized by stream order and compared to each other. In total, there were 60 RWs, aggregated at the sub-watershed scale. We analyzed 57 RWs, excluding those outliers with extremely high water storage values.

4.3 Results and Discussions

4.3.1 Model calibration and validation

Daily observations of streamflow at the outlet of the TCW were compared with simulated streamflow without the wetland modules (Flow_WO), and then those with the modules (Flow_W, Figure 4.8). Overall, both simulation outputs were in good agreement with corresponding observations of streamflow. The model performance statistics computed with daily simulation (Table 4.4) met evaluation criteria outlined by Moriasi et al. (2007) although NSE and RSR estimated during the calibration period was slightly below the “satisfactory” rank. However, it should be noted these criteria and accuracy ratings (Moriasi et al., 2007) were established based on monthly simulation and our study used a daily simulation period. Use of more relaxed criteria was recommended for daily simulation as model prediction naturally becomes less accurate at a finer time step (Moriasi et al. 2007). Indeed, these statistical performance measures, when computed using the monthly simulation

outputs (aggregated from the same daily simulation), were shown to exceed the “satisfactory” criteria (Table 4.4).

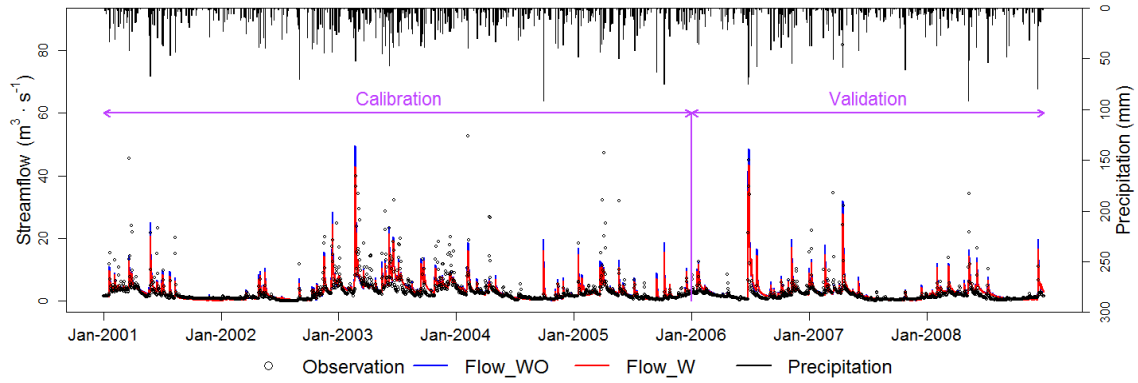


Figure 4.8. Observed and simulated daily streamflow without and with wetland modules

Note: “Flow_WO” and “Flow_W” represent simulated streamflow without and with wetland modules, respectively.

Table 4.4. Model performance measures for streamflow

	Period	NSE	RSR	P-bias
Daily simulation				
Flow_WO	Calibration	0.424	0.758	- 0.3
	Validation	0.534	0.682	23.5
Flow_W	Calibration	0.458	0.735	- 4.85
	Validation	0.550	0.670	17.4
Monthly simulation				
Flow_WO	Calibration	0.783***	0.461***	-0.2***
	Validation	0.577*	0.641*	23.5*
Flow_W	Calibration	0.801***	0.442***	-5.3***
	Validation	0.617*	0.609*	17.2*

Monthly model performances were rated based on the criteria of Moriasi et al. (2008) ; * Satisfactory ($0.5 < NSE \leq 0.65$, $0.6 < RSR \leq 0.7$, and $\pm 15 \leq P\text{-bias} < \pm 25$), ** Good ($0.65 < NSE \leq 0.75$, $0.5 < RSR \leq 0.6$, and $\pm 10 \leq P\text{-bias} < \pm 15$), and *** Very Good ($0.75 < NSE \leq 1.0$, $0.0 < RSR \leq 0.5$, $P\text{-bias} < \pm 10$).

While the overall modeled discharge pattern depicted seasonal variations and low flows well, it did not capture peak streamflow after large storm events. This is

due to the inherent limitation of SWAT and input climate data. The SCS-CN method used in SWAT has a limited ability to accurately predict storm effects because its surface runoff calculation does not consider the duration and intensity of precipitation (Kim and Lee, 2008; Neitsch et al. 2011; Qiu et al., 2012). This may explain why SWAT poorly predicted streamflow following multiple storm events. In addition, climate input data were acquired from two weather stations located either ~ 15 or ~ 35 km away from the study watershed. These datasets did not capture localized storm effects and instead provided inaccurate spatial distribution of rainfalls over the study area. Previous studies reported similar finding (Larose et al., 2009, Sexton et al., 2010, Yeo et al., 2014).

Overall, Flow_W was slightly lower than Flow_WO. This was expected because the wetland modules simulate wetland water storage, i.e., the portion of inflow received from uplands that is stored in wetlands and then released slowly over time to the stream. The wetland modules are expected to reduce streamflow after precipitation and during wet periods. The overall performance statistics were slightly improved with wetland modules (Table 4.4).

4.3.2 Effects of wetland parameterization on simulated inundated area

Streamflows that were simulated using with the three different wetland parameter sets were very similar to each other. This near 1:1 relationship (Figure 4.9) indicates equifinality. However, the spatial distribution of simulated inundated areas within RWs varied with different parameterizations (Figure 4.10–4.12). While all parameter sets predicted the distribution of inundated area reasonably with RWM (r_s

> 0.68), the spatial pattern of inundation derived from Set A showed the highest correlation with inundation maps ($r_s = 0.86$) with a much lower MSE value, compared to those from Sets B and C (Figure 10ab). Sets B and C considerably overestimated absolute inundated areas on upstream sub-watersheds (e.g., #1 – 4 and 8 in Fig. 3) by ~ 8 ha and underestimated those on downstream sub-watersheds (e.g., #53, 60, 66 and 69 in Fig. 3) by ~ 35 ha, compared to observed inundation, resulting in great MSE (Fig. 10b).

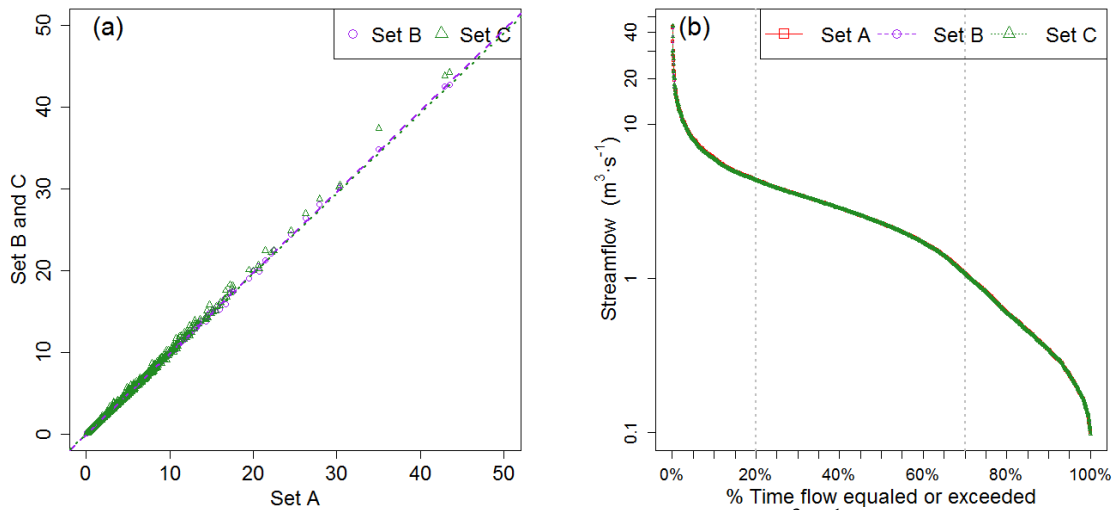


Figure 4.9. Comparison of simulated daily streamflow ($\text{m}^3 \cdot \text{s}^{-1}$) from three sets of wetland parameters

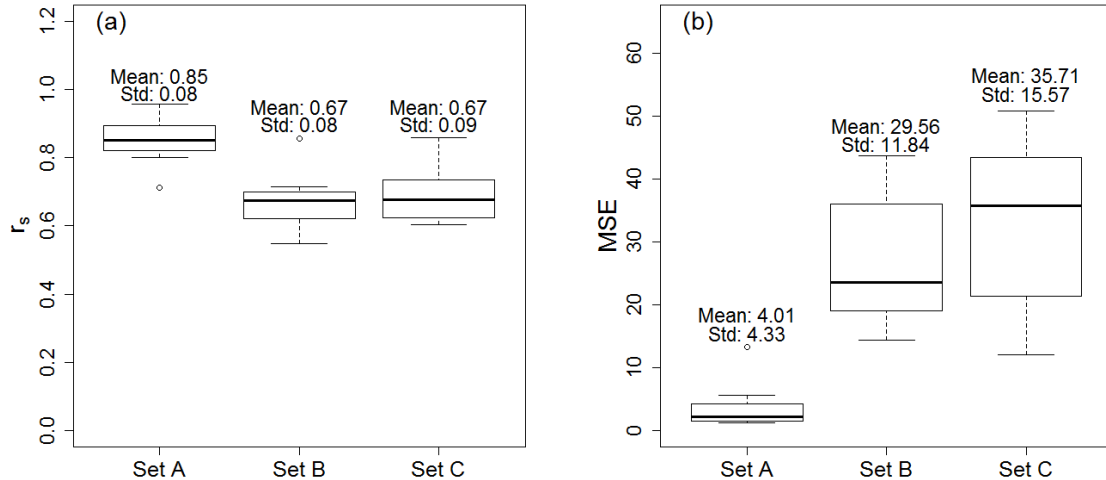


Figure 4.10. Statistical comparison of simulated and observed inundation within riparian wetlands: (a) Spearman's rank-order correlation coefficient (r_s) and (b) MSE value between inundation maps and simulated inundation with three parameterizations.

Note: All relationships (r_s) were significant with p -value < 0.01 . The comparison was made with 7 annual inundation maps developed during the simulation period (2001 – 2008). Std. stands for standard deviation.

Figure 4.11 illustrates how well simulated inundation patterns with different parameterization sets matched with inundation maps under different weather conditions (i.e., dry, normal, and wet). Weather conditions were determined according to monthly PDSI and long-term records of streamflow and precipitation. Regardless of weather conditions, inundation maps showed increasing inundation downstream, following the hierarchical structure of the stream network and associated floodplain. Inundation maps consistently showed most inundated area near the outlet where Tuckahoe Lake is located, and the sub-watershed located immediately downstream of the confluence of two main upstream channels. The inundation maps showed less inundation in upstream areas regardless of weather conditions (Figure 4.11). Simulated inundation from Set A replicated this spatial

pattern quite well for all sub-watersheds with varying degrees of inundation under different weather conditions (Figure 4.12), as indicated by the small MSE value. However, this spatial pattern was less pronounced within simulated results from Sets B and C. Set B resulted in underestimation of inundated area, particularly for those sub-watersheds that included larger inundation extent (i.e., downstream sub-watersheds), regardless of weather conditions. Spatial inundation prediction from Set B remained more uniform for most sub-watersheds, with predicted inundated areas under 10 ha (Figure 4.11 and 4.12). While Set C showed more variable estimates of inundated areas compared to Set B, resulting spatial patterns of inundation in upstream sub-watersheds did not follow a logical distribution.

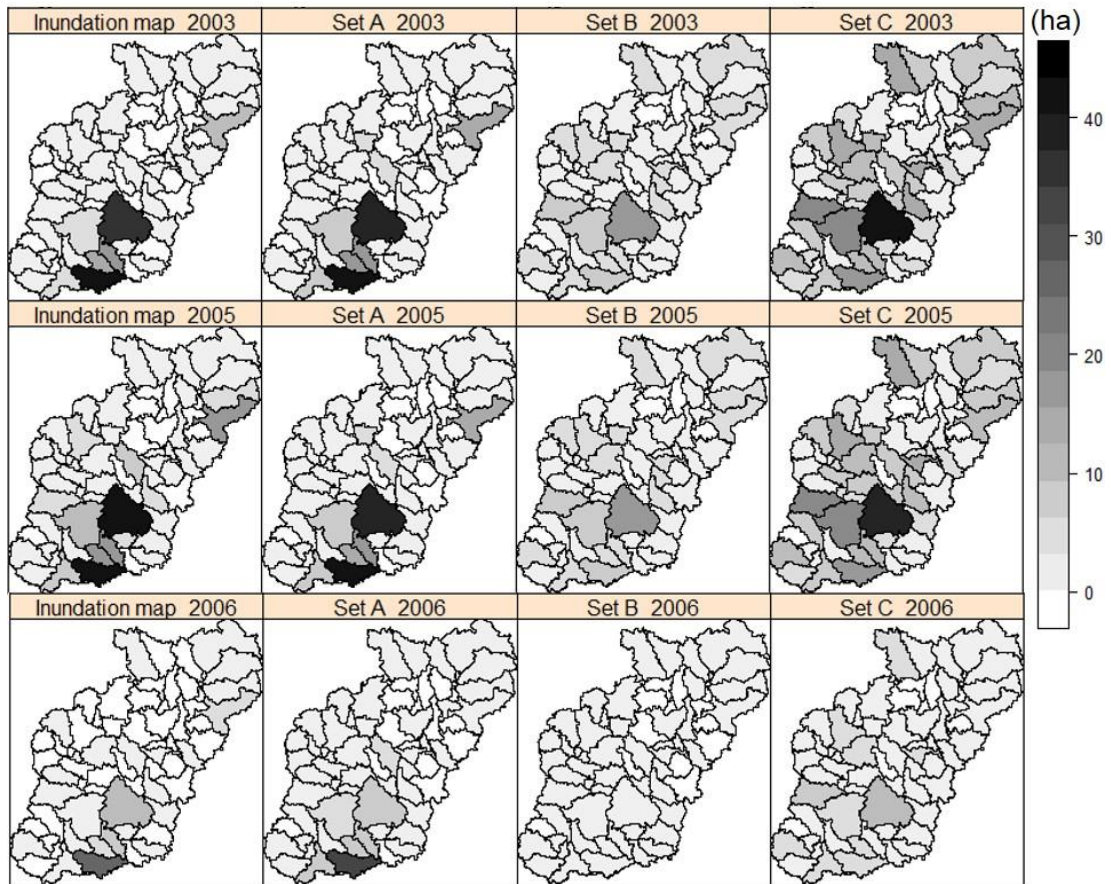


Figure 4.11. The spatial distribution of inundated areas (ha) within riparian wetlands derived from inundation maps and simulated inundation (A-C) under different weather conditions (Normal: 2003, Wet: 2005, and Dry: 2006).

We noticed the largest disagreement between simulated and referenced inundation patterns was shown in 2004 (Figure 4.12a). This could be resulted from mapping errors caused by the processing algorithm or image/data quality. Land cover maps derived from remotely sensed data have some degree of uncertainty. While overall accuracy of the inundation maps was quite high (> 93 %; Jin et al., 2017), the quality of each inundation map varies depending on image condition and training data samples used in the mapping algorithm. For example, the 2004 map showed more noticeable anomalies in SWF than other maps due to overfitting. This overfitting was

caused by insufficient training samples, which did not include varying degree of inundation in data processing for the mapping (Jin et al., 2017). This technical problem likely misrepresented inundated areas and resulted in the largest disagreement between simulated and ‘observed’ inundation patterns in 2004. The limitation of remotely sensed data products and associated mapping errors should be considered when developing the spatialized parameters or assessing the prediction uncertainty.

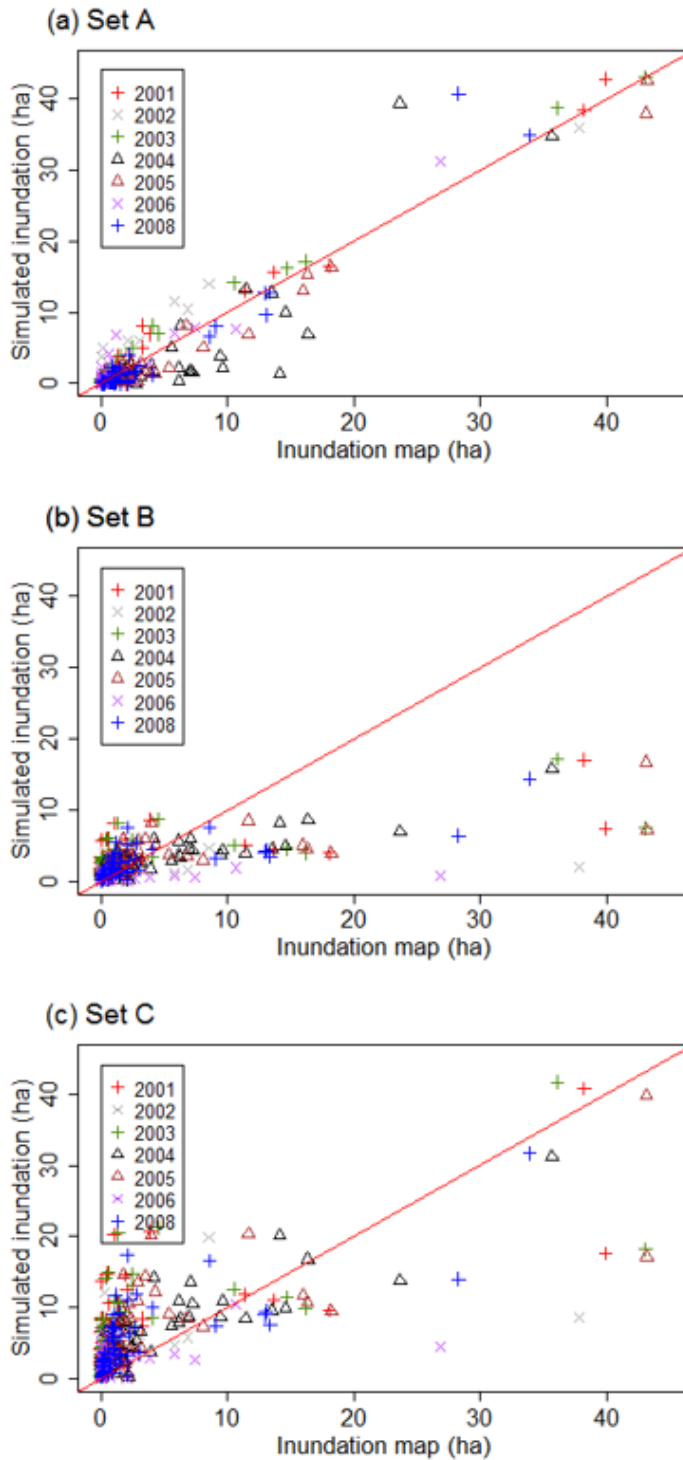


Figure 4.12. The relationship between inundation maps and simulated inundation areas within riparian wetlands from (a) Set A, (b) Set B, and (c) Set C, assessed at the sub-watershed scale under different weather conditions (×: Dry, +: Normal, and Δ: Wet condition).

4.3.3 Spatial parameterization to improve understanding on wetland function

Figure 4.13 shows 8-year monthly averages of water volume stored in 57 RWs with different parameterization sets, categorized by stream order. Overall, all simulation results, regardless of stream orders, showed that water stored gradually decreased from spring to summer and increased during winter season. It followed patterns exhibited in local field-based studies (Fisher et al., 2010; Denver et al., 2014). However, the amount of water stored in RWs, when analyzed by stream order, varied by different parameterizations. Set A exhibited much lower water storage in upstream RWs (1st and 2nd order streams), but higher in downstream RWs (4th order stream). Sets B and C predicted relatively less difference in stored volume between upstream and downstream RWs. The seasonal variation in water storage remained relatively constant within these two sets, as exhibited by the monthly coefficient of variation which remained constant throughout year, regardless of stream order.

We further analyzed two sub-watersheds (# 28 & 53 in Figure 4.3) including a similar coverage of NRWs in upland areas. It was to illustrate how different parameterizations represent hydrologic effects of RWs on upstream and downstream areas. Set A predicted 0.01 – 0.04 m³·s⁻¹ higher peak flow from an upstream sub-watershed outlet (i.e., #28 in Figure 4.3) after the two largest precipitation events (> 90 mm) occurred during the study period (results not shown). This is likely due to the fact that the water holding capacity in the upstream RW under Set A was simulated to be smaller than those from Set B and C. However, a lower peak flow with slower recession characteristics was shown from the downstream sub-watershed stream (i.e., #53 in Figure 4.3) with Set A (results not shown). With Set A, the downstream RW

showed increased wetland capacity to stabilize overall streamflow (e.g., less increase in water discharge during wet period and higher during dry period), in comparison to Set B and C. Highly variable water storage in downstream RW simulated with Set A suggest its greater ability to control flows under variable weather conditions, modified by interaction with streams. Hydroperiod of downstream RWs would be longer than that of upstream RWs, as the mean residence time of water flows should increase with larger water storage and wetland size given equal soil transmissivity. Although mean differences in sub-watershed scale hydrologic responses among different parameterizations may seem to be subtle, Set A demonstrated logical spatially contrasting, seasonally and inter-annually varying water dynamics of RWs.

The seasonal variation in water stored in RWs predicted by Set A also offers important insights to infer spatially varying wetland functions at the landscape scale. In this study site, the simulation results highlight the potentials of RWs in downstream areas. Downstream RWs were shown to be capable of controlling flows under different weather conditions, which likely indicates greater opportunity for water purification with larger water holding capacity and longer residence time of flows, compared to upstream areas. The representation of spatially-varying wetland hydrologic characteristics imposed by Set A helps to realize the value of downstream RWs and identify critical locations in need of wetland conservation/restoration

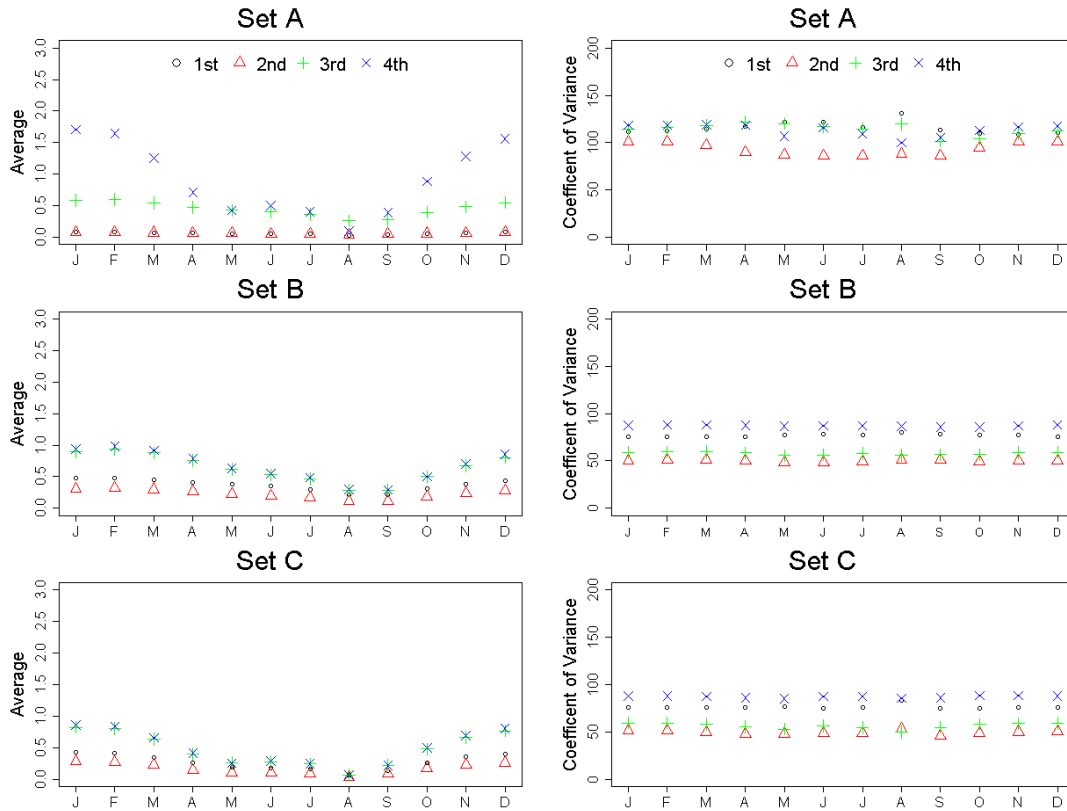


Figure 4.13. Seasonal variations in water volume stored in RWs by stream orders estimated using an 8-year monthly simulation.

4.4 Summary and conclusion

At the study site, significant efforts are being made to restore wetlands and the water quality benefits that they provide. Strategic targeting and prioritizing of areas for restoration require spatially explicit knowledge regarding wetland hydro-geochemical functions and their interaction with the surrounding landscape. Recent advances in integrated wetland and watershed modeling offer the opportunity to study cumulative impacts of wetlands and their spatial interactions with surrounding areas, with improved process representation. However, improved models still suffer from the equifinality problem and the prediction uncertainty associated with spatial pattern

of inundation and related wetland function has been rarely evaluated. It is still commonly accepted to parameterize wetlands with uniform values, regardless of the spatial locations and characteristics, but implication of imposing uniform parameters has not been fully appreciated.

Wetland inundation dynamics and changes in soil moisture (i.e., hydroperiod) are a key abiotic factor that controls wetland functioning, and hence a crucial simulation need. The large uncertainty in inundation spatial pattern can significantly decrease vital information content when inferring location-dependent wetland function to guide landscape scale decision making. Site specific information, such as reference inundation data, is needed to guide spatial parameterization for wetlands (e.g., wetland geometry and the area-volume relationship) and assess the model uncertainty. Recently developed inundation maps with LiDAR intensity and Landsat time series data provide crucial site information. These maps showed surface water fraction (SWF, or inundation percentage) at a 30-m resolution in early spring on an annual basis. We demonstrated how this new spatial information can be used to generate the landscape level wetland parameters, as required by (semi-) distributed hydrologic models such as SWAT. We then quantified how the spatialized wetland parameters better capture inundated area under varying weather conditions, compared to those uniform spatial wetland parameters. The comparison of three different parameter sets with RWM highlights the importance of spatial parameterization, hence the spatial information to improve the model prediction.

As the availability of LiDAR and Landsat data, as well as in-situ information increase, more accurate long-term inundation data should be used to develop wetland

parameters and evaluate the spatial prediction of inundation. In particular, the inundation maps that we used were produced during the leaf-off season (early spring), as dense plant canopies would obscure the ground surface from being observed by optical sensors (e.g., Landsat). The successful launch of the Landsat-8 and Sentinel-1/2 missions may help to overcome this data limitation, and may offer unprecedented opportunities to improve the spatial prediction of inundation through wetland modeling. The use of synthetic aperture radar (SAR) data (e.g., Sentinel-1) can improve the ability to map and monitor seasonal inundation of wetlands as longer wavelength microwave signals can penetrate the tree canopy and detect the underlying ground (Lang et al., 2008). With the launch of Landsat-8 and Sentinel-1/2, a continuous stream of satellite data is now freely available for monitoring land cover with a higher temporal coverage. The continuous inundation maps derived from the use of satellite optical and radar data will be extremely useful to better understand the spatial processes that control wetland functioning, aid spatial parameterization via data assimilation, and improve the capability of integrated wetland-watershed modeling for the decision making.

Chapter 5 Summary and conclusions

5.1 Summary and major findings

Agriculture is the single largest source of nutrient loads that degrade the CB. Therefore, mitigating nutrient loads from agriculture has been regarded as the most effective way to improve the overall health of the CB. Implementing both winter cover crops (WCCs) and wetland restoration and enhancement have been emphasized due to their effectiveness at reducing agricultural nutrient loads. However, little is known about their long-term, cumulative impacts at the watershed scale, which is crucial for ongoing conservation efforts to be successful. A watershed modeling approach has been widely used, because it can simulate agricultural runoff and nutrient loads from sources to receiving water bodies, as well as on-site effects of conservation practices on agricultural runoff and nutrient loads. When using a watershed modeling approach, accurate characterization of model parameters or structures associated with conservation practices and consideration of multiple stressors (e.g, climate change and human activities) are critical for obtaining reliable, actionable information. For effective implementation of the two conservation practices, it is crucial to understand nitrate uptake capacity of varying WCC implementation methods and their performances in different landscape settings. The spatial distribution of wetland inundation is key information to identify the location in need of wetland restoration and enhancement.

Chapter 2 demonstrated that WCCs are an effective conservation practice in reducing nitrate loads at the watershed scale, and their effectiveness differed by the

implementation methods. To accurately simulate WCC nitrate uptake efficiency at the watershed scale, landscape-level biomass observations derived from remotely sensed data and in-situ measurements were used to calibrate WCC biomass growth parameters. The calibrated results accurately depicted the typical growth pattern of three WCC species (e.g., wheat, barley, and rye) that was consistent with field observations. Early-planted WCCs (October 3rd) were more effective at reducing nitrate leaching than late-planted ones (November 1st) by ~ 50 % due to conducive conditions for WCC growth (e.g., warmer temperature). Rye exhibited better nitrate uptake efficiency than did barley or wheat by ~ 36 %, due to its rapid growth rate and winter-hardiness. Early-planted rye was shown to be the most effective WCC practice with the nitrate leaching reduction potential of 93.1 % in this region. Therefore, WCCs should be implemented on the Coastal Plain of the CBW to reduce agricultural nitrate loads, and planting timing and species of WCCs should be considered for enhanced WCC water quality benefits.

Chapter 3 focused on WCC nitrate uptake efficiency in different soil characteristics (i.e., well-drained vs. poorly-drained soils) and crop rotations (i.e., continuous corn vs. corn-soybean rotation) to suggest effective WCC implementation plans considering local characteristics via a paired watershed study. Simulation results exhibited that WCCs mainly absorbed nitrate in soils and groundwater, and residual nitrate was high in well-drained soils, due to their higher infiltration rate. Accordingly, WCCs were more effective at reducing nitrate in well-drained areas, compared to poorly-drained soils. It was because poorly-drained soils are characterized by low soil nitrate levels due to denitrification and drainage ditch

system. The WCCs exhibited a greater nitrate uptake efficiency in fields under corn-soybean rotation relative to continuous corn. This is because a faster mineralization of soybean residue resulted in a greater amount of soil nitrate being available to be absorbed by WCCs. Based on simulation results, it could be concluded that WCCs should be prioritized on the agricultural lands with high baseline soil nitrate (e.g., well-drained soils frequently used for soybean cultivation) for effective nitrate reduction.

Chapter 4 demonstrated that the use of remotely sensed data (i.e., inundation maps at a 30-m resolution) accurately predicted the spatial distribution of wetland inundation while decreasing model prediction uncertainty. This outcome was extremely important for understanding wetland quality benefits because wetland inundation can represent the interactions of wetlands with surrounding areas and pollutant loads. Accordingly, the pollutant removal function of wetlands can be inferred from inundation information. Model parameterized with inundation maps accurately replicated observed spatial pattern of wetland inundation with a varying degree of inundation in response to weather variability. However, simulations with a general, lumped parameterization approach used in previous literatures poorly represented wetland inundation while increasing prediction error. Thus, the simulation results using remotely sensed data provided accurate and practical information for wetland hydrology, which would contribute to understanding current watershed-scale wetland functioning and developing the wetland restoration and enhancement plan.

5.2 Policy-related contribution of this dissertation

It has been challenging for conservation managers to determine appropriate actions for specific locations and management goals (Pullin and Knight, 2003). Allocation of appropriate conservation practices to the specific areas, which can be pollutant source areas or areas that are most vulnerable to environmental and anthropogenic stressors (i.e., critical areas), is an effective way to achieve conservation goals, while taking into consideration the trade-offs between cost and efficacy (Pionke et al., 2000; Wilson et al., 2007). This dissertation can guide the effective implementation plan for WCC and wetland restoration and enhancement while maintaining the balance between environmental benefits and economical cost.

According to the Maryland Agricultural Cost Share (MACS) program, local farmers gain varying incentives when they plant WCCs on their croplands, and more incentives are offered for rye and early planting, compare to others (e.g., barely, wheat, and late planting) (MDA, 2015). Based on the results of this dissertation, the economically- and environmentally-efficient WCC implementation plans could be suggested as follows: 1) more robust WCC practices (e.g., rye and early planting) should be implemented in the areas characterized by a high level of remaining soil nitrate (e.g., well-drained agricultural areas used for frequent cultivation of soybean), and 2) less robust WCC practices (e.g., barley, wheat, and late planting) would be sufficient to achieve targeted water quality goals in the areas with less soil nitrate (e.g., poorly-drained agricultural areas used for frequent cultivation of corn). This implementation strategy could maximize WCC effects on reducing nitrate while minimizing cost for WCC installation.

Wetland restoration and enhancement are performed to bring degraded wetlands back to their original or enhanced conditions (Lewis, 1989). The important information is to know where those degraded wetlands are located within a watershed. On the Coastal Plain of the CBW, it is important to restore and enhance especially wetlands' water quality function (Steven et al., 2011). N transports and their exposure to anaerobic conditions are the most decisive factors for mitigating agricultural nitrate loads in this region (Denver et al., 2014). Denver et al. (2014) found that the wetlands adjacent to nutrient source areas (e.g., agricultural lands) effectively removed nitrate because nitrate from source areas was readily trapped by those wetlands in this region. However, those wetlands with aerobic substrates and groundwater systems rarely reduced nitrate (Denver et al., 2014). This dissertation showed spatially explicit wetland inundation strongly associated with the nutrient removal process. The simulated inundation information can help to identify the wetlands with limited hydrologic connections to water and nutrient transports. Accordingly, restoring and enhancing the hydrologic connectivity of those specific wetlands to critical areas or flow pathways can lead to increasing the potential of wetlands to intercept nutrient loads, eventually resulting in increased nutrient reduction by wetlands. Continuous monitoring and management should be carried out in order to maintain the functions of restored or enhanced wetlands (Gray et al., 1992).

The findings of this dissertation can also lead to effective nutrient reduction at the operational level (e.g., cropland or farm level). There is a gap in implementing conservation practices between regulatory and operational levels. Nutrient reduction

goals are set at the jurisdictional or watershed levels, but actual conservation activities occur at the operational level (Shirmohammadi et al., 2005). Depending on the scales, associated groups have different viewpoints and their interests can be in conflict with each other. For example, policy-makers may only focus on improving the overall health of ecosystems using conservation practices, but local farmers or people who actually implement conservation practices would have more concern about their economic gain/loss (Shirmohammadi et al., 2005). Thus, it is important to apply conservation policies and plans set at the regulatory level into the operational level.

Local farmers are required to register the WCC program to receive a subsidy for WCC implementation. It is possible to be aware of the characteristics (e.g., crop rotation and soil types) of croplands adopting WCCs before implementing WCCs. The wetlands that are especially adjacent to agricultural lands are commonly situated within local farmers' properties. Hence, the results of this dissertation can help to identify local farmers whose properties are identified as critical areas. If decision makers at the regulatory level allocate more economic incentives and technical support to the these local farmers, implementing conservation practices on critical areas would be achieved, resulting in effectively reducing nutrient loads at the operational level.

5.3 Scientific contribution of this dissertation

Processes-based (semi-) distributed watershed models, such as SWAT, have been widely used to examine the impacts of conservation practices on water and nutrient

budgets at the watershed scale (Gassaman et al., 2007). However, data for characterizing the physical processes that drive conservation practices benefits and validating model predictions of intra-watershed processes are limited. Model simulation using the limited data poses a major concern, as it increases model uncertainty while decreasing model reliability. Remotely sensed data can be used to eliminate temporal-spatial constraints in monitoring environmental and natural processes for ecological conservation and management (Palumbo et al., 2016). Remotely sensed data offer landscape- or regional-level information (e.g., WCC biomass and inundation patterns) that is not easily measurable at the field scale. However, few studies assess the effects of conservation practices on watershed processes using a watershed modeling approach supported by remotely sensed data. This dissertation demonstrates the usefulness of remotely sensed data to improve model parameters associated with conservation practices. In addition, remotely sensed data used for model validation help to quantitatively assess intra-watershed processes. The integration of remotely sensed data into a watershed modeling approach contributes to extending the capacity of a watershed model for addressing environmental problems.

5.4 Future research

Climate change is regarded as the potential greatest natural threat to coastal ecosystems (IPCC, 2007). Current water quality problems in the CB are expected to be worsen under climate variability and changes due to increased nutrient loadings (Najjar et al., 2010; Lee et al., 2015). Moreover, climate change is also expected to

profoundly affect the performance of conservation practices (Bosch et al., 2014). Accordingly, great uncertainty exists regarding whether current conservation practices would be effective for mitigating nitrate loads caused by climate change. For example, elevated CO₂ concentration can lead to reduced plant stomatal conductance and transpiration, increasing water and nitrate loads (Field et al., 1995). This uncertainty can further increase when considering that current activities in agricultural lands (known as the single greatest nutrient source) may be altered to adapt to climate change. For example, planting timing of summer crops can be shifted earlier than the current condition to reduce increased heat stress caused by climate change (Woznicki et al., 2015). Accordingly, a comprehensive understanding of natural and human responses to climate change impacts is crucial.

Numerous studies have been conducted to project future climate data using Global Circulation Models (GCMs) resulting in CO₂ emission scenarios (Mearns, 2001). A watershed modeling approach has been extensively applied to predict potential climate change impacts on various parameters of concerns, such as crop yield, water/nutrient cycles, and conservation/management practices, using projected climate data (Gassman et al., 2007). The simulation outputs provide plausible changes in overall watershed processes, and these projections play a key role in developing climate change adaptation strategies (Shrestha et al., 2012). Hence, further studies should consider climate change impacts on watershed processes to increase the resilience of the CB region to climate change.

This dissertation characterizes key physical processes of WCCs and wetlands within a watershed model using remotely sensed data. However, more

parameterization and validation are required to understand the model structure and assumptions under varying climate conditions. For example, WCC growth parameters inferred from remotely sensed data acquired at a single winter period cannot demonstrate the long-term variability of WCC nitrate uptake efficiency. The use of longer-term remotely sensed data along with field-based studies is critical to gaining more accurate model parameters, and to validating WCC growth during multiple winter periods. Wetland parameters were carefully prepared using remotely sensed data in order to meet model assumptions. However, the validation of intra-watershed processes is only available to the early spring season due to the limited availability of remotely sensed data. Continuous inundation maps derived from the long-term remotely sensed data are necessary for an enhanced understanding of wetland functioning to best support wetland protection and restoration. The availability of remotely sensed data is increasing. These long-term remotely sensed data, being highly accurate, offer the opportunity to further enhance model prediction of watershed processes and reduce model uncertainty.

Due to limitations of a SWAT extension (e.g., riparian wetland module), the cumulative impacts of wetlands on nitrate reduction have not been quantified at the watershed scale. Biochemical processes is also significantly oversimplified in watershed models because numerous elements interact one another under varying conditions (e.g., aerobic and anaerobic conditions). Accurate simulation of nutrient reduction process within a watershed model is still a great challenge and multiple groups have worked on improving wetland biochemical processes. In the future,

further research should be conducted for contemporary understanding of cumulative impacts of multiple wetlands on nutrient reduction on the Coastal Plain of the CBW.

5.5 Concluding remarks

Baseline annual N loads estimated on 2015 are required to decrease by 20 % in order to achieve N reduction goal of the CBW by 2025 (CBP, 2016). Although multiple sources account for N loads, agriculture is still the single largest nutrient source (CBP, 2016). WCCs were capable of reducing annual nitrate loads by ~ 50 % and wetlands were estimated to reduce incoming nitrate by ~ 25 % on the Coastal Plain of the CBW (USEPA, 2010c). Effective implementing two conservation (WCCs and wetland restoration and enhancement) based on this dissertation could collectively lead to reduction of agricultural nitrate loads by up to ~ 63 %. Therefore, two conservation practices should be implemented to successfully attain the target N reduction goal and eventually improve the health of the CB.

Bibliography

- Arnold, J. G., & Fohrer, N. (2005). SWAT2000: Current capabilities and research opportunities in applied watershed modelling. *Hydrological Processes*, 19(3), 563-572.
- Arnold, J. G., Kiniry, J. R., Srinivasan, R., Williams, J. R., Haney, E. B., & Neitsch, S.L., (2012). SWAT input/output file documentation version 2012. Texas Water Resources Institute Technical Report. Soil and Water Research Laboratory, Agricultural Research Service, Temple, TX.
- Ator, S. W., Denver, J. M., Krantz, D. E., Newell, W. L., & Martucci, S. K. (2005). A surficial hydrogeologic framework for the Mid-Atlantic coastal plain. U.S. Geological Survey, Denver, CO.
- Ator, S. W., & Denver, J. M. (2012). Estimating contributions of nitrate and herbicides from groundwater to headwater streams, Northern Atlantic Coastal Plain, United States. *Journal of the American Water Resources Association*, 48(6), 1075-1090.
- Ator, S. W., & Denver, J. M. (2015). Understanding nutrients in the Chesapeake Bay watershed and implications for management and restoration: the Eastern Shore. US Geological Survey, Reston, VA.
- Ator, S. W., Denver, J. M., Krantz, D. E., Newell, W. L., & Martucci, S. K. (2005). A surficial hydrogeologic framework for the Mid-Atlantic Coastal Plain. US Geological Survey, Reston, VA.

- Babbar-Sebens, M., Barr, R. C., Tedesco, L. P., & Anderson, M. (2013). Spatial identification and optimization of upland wetlands in agricultural watersheds. *Ecological Engineering*, 52, 130-142.
- Baggs, E. M., Watson, C. A., & Rees, R. M. (2000). The fate of nitrogen from incorporated cover crop and green manure residues. *Nutrient Cycling in Agroecosystems*, 56(2), 153-163.
- Beeson, P. C., Sadeghi, A. M., Lang, M. W., Tomer, M. D., & Daughtry, C. S. T. (2014). Sediment delivery estimates in water quality models altered by resolution and source of topographic Data. *Journal of Environmental Quality*, 43(1), 26-36.
- Beven, K. (2006). A manifesto for the equifinality thesis. *Journal of Hydrology*, 320(1), 18-36.
- Bergström, L. F., & Jokela, W. E. (2001). Ryegrass cover crop effects on nitrate leaching in spring barley fertilized with $^{15}\text{NH}_4^{15}\text{NO}_3$. *Journal of Environmental Quality*, 30(5), 1659-1667.
- Boesch, D. F., Brinsfield, R. B., & Magnien, R. E. (2001). Chesapeake Bay eutrophication: Scientific understanding, ecosystem restoration, and challenges for agriculture. *Journal of Environmental Quality*, 30(2), 303-320.
- Boithias, L., Srinivasan, R., Sauvage, S., Macary, F., & Sanchez-Perez, J. M. (2014). Daily nitrate losses: Implication on long-term river quality in an intensive agricultural catchment of southwestern France. *Journal of Environmental Quality*, 43(1), 46-54.
- Boryan, C., Yang, Z., & Di, L. (2012). Deriving 2011 cultivated land cover data sets using USDA National Agricultural Statistics Service historic Cropland Data

- Layers. IEEE International Geoscience and Remote Sensing Symposium, Munich, Germany.
- Bosch, N.S., Evans, M.A., Scavia, D. and Allan, J.D. (2014). Interacting effects of climate change and agricultural BMPs on nutrient runoff entering Lake Erie. *Journal of Great Lakes Research*, 40(3), 581-589.
- Bowden, W.B. (1987). The biogeochemistry of nitrogen in freshwater wetlands. *Biogeochemistry*, 4(3), 313-348.
- Bradley, C. (2002). Simulation of the annual water table dynamics of a floodplain wetland, Narborough Bog, UK. *Journal of Hydrology*, 261(1-4), 150-172.
- Brandi-Dohrn, F. M., Hess, M., Selker, J. S., Dick, R. P., Kauffman, S. M., & Hemphill, D. D. (1997). Nitrate leaching under a cereal rye cover crop. *Journal of Environmental Quality*, 26(1), 181-188.
- Brinsfield, R. B., & Staver, K. W. (1991). Use of cereal grain cover crops for reducing groundwater nitrate contamination in the Chesapeake Bay Region. *Cover crops for clean water. Soil Water Conserv. Sco., Ankeny, IA.*
- Camacho, R. (1990). Agricultural BMP nutrient reduction efficiencies: Chesapeake Bay watershed model BMPS: Interstate Commission on the Potomac River Basin.
- CBC (Chesapeake Bay Commission). (2004). Cost-effective strategies for the bay: smart investments for nutrient and sediment reduction, available at: <http://www.chesbay.us/Publications/cost%20effective.pdf> (last access: 19 October 2016)

CBP (Chesapeake Bay Program), 1983, The Chesapeake Bay Agreement of 1983, available at: http://www.chesapeakebay.net/content/publications/cbp_12512.pdf (last access: 19 October 2016)

CBP (Chesapeake Bay Program), 2000, The Chesapeake Bay Agreement of 1983, available at: http://www.chesapeakebay.net/channel_files/19193/chesapeake_2000.pdf (last access: 19 October 2016)

CBP (Chesapeake Bay Program), 2014, The Chesapeake Bay Agreement 2014, available at: <http://www.chesapeakebay.net/documents/ChesapeakeBayWatershedAgreementFINAL.pdf> (last access: 19 October 2016)

CBP (Chesapeake Bay Program), 2015, Addition of New Cover Crop Species with Nitrogen Reduction Efficiencies for Use in Phase 5.3.2 of the Chesapeake Bay Program Watershed Model, available at: http://www.chesapeakebay.net/channel_files/22023/cover_crop_report_with_species__nitrogen_reduction_efficiencies_draft_final_revised_10-09-2014.pdf. (last access: July 28 2015)

CBP (Chesapeake Bay Program), 2016, Reducing Nitrogen Pollution, available at: http://www.chesapeakebay.net/indicators/indicator/reducing_nitrogen_pollution (last access: 13 December 2016)

Cerco, C. F., & Noel, M. R. (2007). Can oyster restoration reverse cultural eutrophication in Chesapeake Bay? *Estuaries and Coasts*, 30(2), 331-343.

- Chaplot, V. (2005). Impact of DEM mesh size and soil map scale on SWAT runoff, sediment, and NO₃-N loads predictions. *Journal of Hydrology*, 312(1), 207-222.
- Chaubey, I., Cotter, A., Costello, T., & Soerens, T. (2005). Effect of DEM data resolution on SWAT output uncertainty. *Hydrological Processes*, 19(3), 621-628.
- Chen, F., Crow, W. T., Starks, P. J., & Moriasi, D. N. (2011). Improving hydrologic predictions of a catchment model via assimilation of surface soil moisture. *Advances in Water Resources*, 34(4), 526-536.
- Chiang, S. L. (1971). A runoff potential rating table for soils. *Journal of Hydrology*, 13, 54-62.
- Chu, T. W., Shirmohammadi, A., Montas, H., & Sadeghi, A. (2004). Evaluation of the SWAT model's sediment and nutrient components in the piedmont physiographic region of Maryland. *Transactions of the ASABE*, 47(5), 1523-1538.
- Clark, A. (2007). *Managing cover crops profitably* (3rd Ed.). Sustainable Agriculture Network, Beltsville, Maryland.
- Comin, F. A., Sorando, R., Darwiche-Criado, N., Garcia, M., & Masip, A. (2014). A protocol to prioritize wetland restoration and creation for water quality improvement in agricultural watersheds. *Ecological Engineering*, 66, 10-18.
- Cooper, A. B. (1990). Nitrate Depletion in the Riparian Zone and Stream Channel of a Small Headwater Catchment. *Hydrobiologia*, 202(1-2), 13-26.
- Dabney, S. M. (1998). Cover crop impacts on watershed hydrology. *Journal of Soil and Water Conservation*, 53(3), 207-213.

- Dabney, S. M., Delgado, J. A., & Reeves, D. W. (2001). Using winter cover crops to improve soil and water quality. *Communications in Soil Science and Plant Analysis*, 32(7-8), 1221-1250.
- Denman, K. L., Brasseur, G. P., Chidthaisong, A., Ciais, P., Cox, P. M., Dickinson, R. E., Hauglustaine, D. A., Heinze, C., Holland, E. A., Jacob, D. J. and Lohmann, U. (2007). Couplings between changes in the climate system and biogeochemistry. *Climate change 2007: The physical science basis*.
- Denver, J. M., Ator, S. W., Debrewer, L. M., Ferrari, M. J., Barbaro, J. R., Hancock, T. C., Brayton, M. J., & Nardi, M. R. (2004). Water quality in the Delmarva Peninsula, Delaware, Maryland, and Virginia, 1999-2001. US Geological Survey, Reston, Virginia.
- Denver, J. M., Tesoriero, A. J., & Barbaro, J. R. (2010). Trends and Transformation of Nutrients and Pesticides in a Coastal Plain Aquifer System, United States. *Journal of Environmental Quality*, 39(1), 154-167.
- Denver, J.M., Ator, S.W., Lang, M.W., Fisher, T.R., Gustafson, A.B., Fox, R., Clune, J.W. & McCarty, G.W. (2014). Nitrate fate and transport through current and former depressional wetlands in an agricultural landscape, Choptank Watershed, Maryland, United States. *Journal of Soil and Water Conservation*, 69(1), 1-16.
- Di Luzio, M., Srinivasan, R., & Arnold, J. G. (2004). A GIS-coupled hydrological model system for the watershed assessment of agricultural nonpoint and point sources of pollution. *Transactions in GIS*, 8(1), 113-136.

- Evenson, G. R., Golden, H. E., Lane, C. R., & D'Amico, E. (2015). Geographically isolated wetlands and watershed hydrology: A modified model analysis. *Journal of Hydrology*, 529, 240-256.
- Evenson, G. R., Golden, H. E., Lane, C. R., & D'Amico, E. (2016). An improved representation of geographically isolated wetlands in a watershed-scale hydrologic model. *Hydrological Processes*.
- Federal Leadership Committee for the Chesapeake Bay, 2010, Executive Order 13508: Strategy for Protecting and restoring the Chesapeake Bay Watershed, available at: <http://executiveorder.chesapeakebay.net/file.axd?file=2010%2f5%2fChesapeake+EO+Strategy%20.pdf> (last access: 19 October 2016)
- Feng, X. Q., Zhang, G. X., & Xu, Y. J. (2013). Simulation of hydrological processes in the Zhalong wetland within a river basin, Northeast China. *Hydrology and Earth System Sciences*, 17(7), 2797-2807.
- Feyereisen, G. W., Wilson, B. N., Sands, G. R., Strock, J. S., & Porter, P. M. (2006). Potential for a rye cover crop to reduce nitrate loss in southwestern Minnesota. *Agronomy Journal*, 98(6), 1416-1426.
- Field, C.B., Jackson, R.B. & Mooney, H.A. (1995). Stomatal responses to increased CO₂: implications from the plant to the global scale. *Plant, Cell & Environment*, 18(10), 1214-1225.
- Fisher, T., Jordan, T., Staver, K., Gustafson, A., Koskelo, A., Fox, R. J., Sutton, A. J., Kana, T., Beckert, K. A., Stone, J. P., McCarty, G., & Lang, M. (2010). The Choptank Basin in transition: intensifying agriculture, slow urbanization, and

- estuarine eutrophication. Coastal lagoons: systems of natural and anthropogenic change, CRC Press, Boca Raton, FL.
- Fonseca, A., Ames, D.P., Yang, P., Botelho, C., Boaventura, R. & Vilar, V. (2014). Watershed model parameter estimation and uncertainty in data-limited environments. *Environmental Modelling & Software*, 51, 84-93.
- Francis, G., Bartley, K., & Tabley, F. (1998). The effect of winter cover crop management on nitrate leaching losses and crop growth. *The Journal of Agricultural Science*, 131(03), 299-308.
- Fretwell, J.D., Williams, J.S., & Redman, P.J. (1996). National water summary on wetland resources. US Geological Survey.
- Ganasri, B.P. & Ramesh, H. (2015). Assessment of soil erosion by RUSLE model using remote sensing and GIS-A case study of Nethravathi Basin. *Geoscience Frontiers*.
- Gardner, R., & Davidson, N. (2011). The Ramsar Convention. In 'Wetlands—Integrating Multidisciplinary Concepts' (Ed. B. Le Page.). Springer, Dordrecht, Netherlands.
- Gassman, P. W., Reyes, M. R., Green, C. H., & Arnold, J. G. (2007). The soil and water assessment tool: historical development, applications, and future research directions. *Transactions of the ASABE*, 50(4), 1211-1250.
- Gillmore, J., Glendening, P., Ridge, T., Williams, A., Browner, C., & Bolling, B. (2000). Chesapeake 2000 Agreement. United States Environmental Protection Agency Chesapeake Bay Program, Annapolis, MD, USA.

- Gentry, L. E., Below, F. E., David, M. B., & Bergerou, J. A. (2001). Source of the soybean N credit in maize production. *Plant and Soil*, 236(2), 175-184.
- Gitau, M. W., & Chaubey, I. (2010). Regionalization of SWAT Model Parameters for Use in Ungauged Watersheds. *Water*, 2(4), 849-871.
- Glancey, J., Brown, B., Davis, M., Towle, L., Timmons, J., & Nelson, J. (2012): Comparison of Methods for Estimating Poultry Manure Nutrient Generation in the Chesapeake Bay Watershed, available at: <http://www.csgeast.org/2012annualmeeting/documents/Glancey.pdf> (last access: 25 September 2014).
- Grayson, R. B., Blöschl, G., Western, A. W., & McMahon, T. A. (2002). Advances in the use of observed spatial patterns of catchment hydrological response. *Advances in Water Resources*, 25(8), 1313-1334.
- Gray, R., Tuttle, R. and Wenberg, R.D. (1992). Wetland restoration, enhancement, or creation. *Engineering Field Handbook*, USDA-Natural Resources Conservation Service (NRCS).
- Hattermann, F., Krysanova, V., Habeck, A., & Bronstert, A. (2006). Integrating wetlands and riparian zones in river basin modelling. *Ecological Modelling*, 199(4), 379-392.
- Hillman, G. R. (1998). Flood wave attenuation by a wetland following a beaver dam failure on a second order boreal stream. *Wetlands*, 18(1), 21-34.
- Hively, W. D., Lang, M., McCarty, G. W., Keppler, J., Sadeghi, A., & McConnell, L. L. (2009). Using satellite remote sensing to estimate winter cover crop nutrient uptake efficiency. *Journal of Soil and Water Conservation*, 64(5), 303-313.

- Huang, C., Peng, Y., Lang, M., Yeo, I.-Y., & McCarty, G. (2014). Wetland inundation mapping and change monitoring using Landsat and airborne LiDAR data. *Remote Sensing of Environment*, 141, 231-242.
- Hunter, R.G. & Faulkner, S.P. (2001). Denitrification potentials in restored and natural bottomland hardwood wetlands. *Soil Science Society of America Journal*, 65(6), 1865-1872.
- IPCC (Intergovernmental Panel on Climate Change). (2007). Summary for policymakers. In: Solomon, S., Qin, D., Manning, M., Chen, Z., Marquis, M., Averyt, K.B., Tignor, M., Miller, H.L. (Eds.), *Climate Change 2007: The Physical Science Basis. Contribution of Working Group I to the Fourth Assessment Report of the Intergovernmental Panel on Climate Change*. Cambridge University Press, Cambridge, United Kingdom and New York, NY, USA
- Islam, N., Wallender, W. W., Mitchell, J., Wicks, S., & Howitt, R. E. (2006). A comprehensive experimental study with mathematical modeling to investigate the affects of cropping practices on water balance variables. *Agricultural Water Management*, 82(1-2), 129-147.
- Jha, M. K., Gassman, P. W., & Arnold, J. G. (2007). Water quality modeling for the Raccoon River watershed using SWAT. *Transactions of the Asabe*, 50(2), 479-493.
- Jin, H., Huang, C., Lang, M. W., Yeo, I. Y., & Stehman, S. V., (2017). Monitoring of wetland inundation dynamics using Landsat time-series imagery from 1985 to 2011. *Remote Sensing of Environment*, 190, 26-41.

- Jordan, T. E., Correll, D. L., & Weller, D. E. (1997). Effects of agriculture on discharges of nutrients from coastal plain watersheds of Chesapeake Bay. *Journal of Environmental Quality*, 26(3), 836-848.
- Julich, S., Breuer, L., & Frede, H.-G. (2012). Integrating heterogeneous landscape characteristics into watershed scale modelling. *Advances in Geosciences*, 31, 31-38.
- Kaboneka, S., Sabbe, W. E., & Mauromoustakos, A. (1997). Carbon decomposition kinetics and nitrogen mineralization from corn, soybean, and wheat residues. *Communications in Soil Science & Plant Analysis*, 28(15-16), 1359-1373.
- Kang, M. S., Park, S. W., Lee, J. J., & Yoo, K. H. (2006). Applying SWAT for TMDL programs to a small watershed containing rice paddy fields. *Agricultural Water Management*, 79(1), 72-92.
- Kaspar, T. C., Jaynes, D. B., Parkin, T. B., & Moorman, T. B. (2007). Rye cover crop and gammagrass strip effects on NO₃ concentration and load in tile drainage. *Journal of Environmental Quality*, 36(5), 1503-1511.
- Kaspar, T., Jaynes, D., Parkin, T., Moorman, T., & Singer, J. (2012). Effectiveness of oat and rye cover crops in reducing nitrate losses in drainage water. *Agricultural Water Management*, 110, 25-33.
- Kazezyilmaz-Alhan, C. M., Medina, M. A., & Richardson, C. J. (2007). A wetland hydrology and water quality model incorporating surface water/groundwater interactions. *Water Resources Research*, 43(4).
- Kemp, W. M., Boynton, W. R., Adolf, J. E., Boesch, D. F., Boicourt, W. C., Brush, G., Cornwell, J.C., Fisher, T.R., Glibert, P.M., Hagy, J.D. & Harding, L.W.

- (2005). Eutrophication of Chesapeake Bay: historical trends and ecological interactions. *Marine Ecology Progress Series*, 303, 1-29.
- Kettlewell, C. I., Bouchard, V., Porej, D., Micacchion, M., Mack, J. J., White, D., & Fay, L. (2008). An assessment of wetland impacts and compensatory mitigation in the Cuyahoga River Watershed, Ohio, USA. *Wetlands*, 28(1), 57-67.
- Kim, N. W., & Lee, J. (2008). Temporally weighted average curve number method for daily runoff simulation. *Hydrological Processes*, 22(25), 4936-4948.
- Kimball, B.A. and Idso, S.B. (1983). Increasing atmospheric CO₂: effects on crop yield, water use and climate. *Agricultural Water Management*, 7(1), 55-72.
- Klocke, N. L., Watts, D. G., Schneekloth, J. P., Davison, D. R., Todd, R. W., & Parkhurst, A. M. (1999). Nitrate leaching in irrigated corn and soybean in a semi-arid climate. *Transactions of the ASAE*, 42(6), 1621-1630.
- Lakshmi, V., 2013. Remote sensing of soil moisture, *ISRN Soil Sci.* 2013, 33.
- Lam, Q., Schmalz, B., & Fohrer, N. (2009). Ecohydrological modelling of water discharge and nitrate loads in a mesoscale lowland catchment, Germany. *Advances in Geosciences*, 21(21), 49-55.
- Lane, C. R., & D'Amico, E. (2010). Calculating the Ecosystem Service of Water Storage in Isolated Wetlands using LiDAR in North Central Florida, USA. *Wetlands*, 30(5), 967-977.
- Lang, M. W., & McCarty, G. W. (2009). LiDAR intensity for improved detection of inundation below the forest canopy. *Wetlands*, 29(4), 1166-1178.

- Lang, M., McDonough, O., McCarty, G., Oesterling, R., & Wilen, B. (2012). Enhanced detection of wetland-stream connectivity using LiDAR. *Wetlands*, 32(3), 461-473.
- Lang, M., McCarty, G., Oesterling, R., & Yeo, I.-Y. (2013). Topographic metrics for improved mapping of forested wetlands. *Wetlands*, 33(1), 141-155.
- Lang, M., McCarty, G. W., Ducey, T. F., Hunt, P. G., Miller, J. O., Rabenhorst, M., Baldwin, A., Fenstermacher, D., Yepsen, M., McFarland, E., Sharifi, A., Church, C., Devner, J., Ator, S., Mitchell, J., Whigham, D., & Walbridge, M. R. (2016). Effects and effectiveness of USDA wetland conservation practices in the Mid-Atlantic region: A report on the conservation effects assessment project Mid-Atlantic regional wetland assessment 2008 - 2015. Government Publication/Report. APP:1/14/2016.
- Larose, M., Heathman, G., Norton, L., & Engel, B. (2007). Hydrologic and atrazine simulation of the Cedar Creek watershed using the SWAT model. *Journal of Environmental Quality*, 36(2), 521-531.
- Lee, E. R., Mostaghimi, S., & Wynn, T. M. (2002). A MODEL TO ENHANCE WETLAND DESIGN AND OPTIMIZE NONPOINT SOURCE POLLUTION CONTROL¹, *Journal of the American Water Resources Association*, 38(1), 17-32.
- Lee, K. Y., Fisher, T. R., Jordan, T. E., Correll, D. L., & Weller, D. E. (2000). Modeling the hydrochemistry of the Choptank River Basin using GWLF and Arc/Info: 1. Model calibration and validation. *Biogeochemistry*, 49(2), 143-173.

- Lee, S., Yeo, I.Y., Sadeghi, A.M., McCarty, G.W. & Hively, W.D. (2015). Prediction of climate change impacts on agricultural watersheds and the performance of winter cover crops: Case study of the upper region of the Choptank River Watershed, Proceedings of the ASABE 1st Climate Change Symposium: Adaptation and Mitigation, Chicago, IL.
- Lee, S., Yeo, I.-Y., Sadeghi, A. M., McCarty, G. W., Hively, W. D., & Lang, M. W. (2016). Impacts of watershed characteristics and crop rotations on winter cover crop nitrate-nitrogen uptake capacity within agricultural watersheds in the Chesapeake Bay region. *PLoS One*, 11(6), e0157637.
- Lewis, R.R. (1990). Wetlands restoration/creation/enhancement terminology: suggestions for standardization. *Wetland creation and restoration: the status of the science*. Island Press, Washington, DC.
- Liu, Y. B., Yang, W. H., & Wang, X. X. (2008). Development of a SWAT extension module to simulate riparian wetland hydrologic processes at a watershed scale. *Hydrological Processes*, 22(16), 2901-2915. doi:Doi 10.1002/Hyp.6874
- Loumagne, C., Normand, M., Riffard, M., Weisse, A., Quesney, A., Hegarat-Masclé, S. L., & Alem, F. (2001). Integration of remote sensing data into hydrological models for reservoir management. *Hydrological sciences journal*, 46(1), 89-102.
- Malhi, S. S., Johnston, A. M., Schoenau, J. J., Wang, Z. H., & Vera, C. L. (2006). Seasonal biomass accumulation and nutrient uptake of wheat, barley and oat on a Black Chernozem soil in Saskatchewan. *Canadian Journal of Plant Science*, 86(4), 1005-1014.

- Martinez-Martinez, E., Nejadhashemi, A. P., Woznicki, S. A., & Love, B. J. (2014). Modeling the hydrological significance of wetland restoration scenarios. *Journal of Environmental Management*, 133, 121-134.
- Martinez-Martinez, E., Nejadhashemi, A. P., Woznicki, S. A., Adhikari, U., & Giri, S. (2015). Assessing the significance of wetland restoration scenarios on sediment mitigation plan. *Ecological Engineering*, 77, 103-113.
- Maryland General Assembly. (2007). Chesapeake Bay Restoration and the Tributary Strategy: An Analysis of Maryland's Efforts to Meet the Nutrient and Sediment Reduction Goals of the Chesapeake 2000 Agreement. Office of Policy Analysis, Department of Legislative Services, Maryland General Assembly, Annapolis, MD.
- McCarty, G. W., McConnell, L. L., Hapernan, C. J., Sadeghi, A., Graff, C., Hively, W. D., Lang, M.W., Fisher, T.R., Jordan, T., Rice, C.P. & Codling, E.E. (2008). Water quality and conservation practice effects in the Choptank River watershed. *Journal of Soil and Water Conservation*, 63(6), 461-474.
- McCracken, D. V., Smith, M. S., Grove, J. H., Blevins, R. L., & MacKown, C. T. (1994). Nitrate leaching as influenced by cover cropping and nitrogen source. *Soil Science Society of America Journal*, 58(5), 1476-1483.
- McDonough, O. T., Lang, M. W., Hosen, J. D., & Palmer, M. A. (2015). Surface hydrologic connectivity between Delmarva Bay wetlands and nearby streams along a gradient of agricultural alteration. *Wetlands*, 35(1), 41-53.

- McLaughlin, D. L., Kaplan, D. A., & Cohen, M. J. (2014). A significant nexus: geographically isolated wetlands influence landscape hydrology. *Water Resources Research*, 50(9), 7153-7166.
- MDA (Maryland Department of Agriculture), 2015a, Maryland's 2014–2015 Cover Crop Sign-Up, available at: http://mda.maryland.gov/resource_conservation/counties/MDACoverCrop.pdf (last access: 1 April 2015)
- MDA (Maryland Department of Agriculture), 2015b, Maryland Agricultural Water Quality Cost-Share (MACS) program annual report 2015, available at: http://mda.maryland.gov/resource_conservation/counties/MAC SAR2015FINAL.pdf (last access: 18 October 2016)
- Meals, D. W., Dressing, S. A., & Davenport, T. E. (2010). Lag Time in Water Quality Response to Best Management Practices: A Review. *Journal of Environmental Quality*, 39(1), 85-96.
- Mearns, L. O., M. Hulme, T. R. Carter, R. Leemans, M. Lal, P. Whetton, Hay, L., Jones, R.N., Kittel, T., Smith, J. & Wilby, R. (2001). Climate scenario development. *Advances in Geocology*, 739-768.
- Meng, H., Sexton, A. M., Maddox, M. C., Sood, A., Brown, C. W., Ferraro, R. R., & Murtugudde, R. (2010). Modeling Rappahannock River Basin Using Swat - Pilot for Chesapeake Bay Watershed. *Applied Engineering in Agriculture*, 26(5), 795-805.

- Moriasi, D. N., Arnold, J. G., Van Liew, M. W., Bingner, R. L., Harmel, R. D., & Veith, T. L. (2007). Model evaluation guidelines for systematic quantification of accuracy in watershed simulations. *Transactions of the Asabe*, 50(3), 885-900.
- Najjar, R.G., Pyke, C.R., Adams, M.B., Breitburg, D., Hershner, C., Kemp, M., Howarth, R., Mulholland, M.R., Paolisso, M., Secor, D. and Sellner, K. (2010). Potential climate-change impacts on the Chesapeake Bay. *Estuarine, Coastal and Shelf Science*, 86(1), 1-20.
- Neitsch, S. L., Arnold, J. G., Kiniry, J. R., & Williams, J. R. (2011). Soil and water assessment tool theoretical documentation version 2009, Texas Water Resources Institute. College Station, TX.
- Nielsen, E. M., Prince, S. D., & Koeln, G. T. (2008). Wetland change mapping for the US mid-Atlantic region using an outlier detection technique. *Remote Sensing of Environment*, 112(11), 4061-4074.
- Niraula, R., Kalin, L., Srivastava, P., & Anderson, C. J. (2013). Identifying critical source areas of nonpoint source pollution with SWAT and GWLF. *Ecological Modelling*, 268, 123-133.
- Nygaard, B., & Ejrnæs, R. (2009). The impact of hydrology and nutrients on species composition and richness: evidence from a microcosm experiment. *Wetlands*, 29(1), 187-195.
- Padmanabhan, G., & Bengtson, M. L. (2001). Assessing the influence of wetlands on flooding. Paper presented at the Wetlands Engineering & River Restoration 2001.

- Palumbo, I., Rose, R. A., Headley, R. M., Nackoney, J., Vodacek, A., & Wegmann, M. (2016). Building capacity in remote sensing for conservation: present and future challenges. *Remote Sensing in Ecology and Conservation*.
- Parry, M.L., Rosenzweig, C., Iglesias, A., Livermore, M. and Fischer, G. (2004). Effects of climate change on global food production under SRES emissions and socio-economic scenarios. *Global Environmental Change*. 14(1), 53-67.
- Phillips, S. W., Focazio, M. J., & Bachman, L. J. (1999). Discharge, nitrate load, and residence time of ground water in the Chesapeake Bay watershed. *US Geological Survey*.
- Pionke, H. B., Gburek, W. J., & Sharpley, A. N. (2000). Critical source area controls on water quality in an agricultural watershed located in the Chesapeake Basin. *Ecological Engineering*, 14(4), 325-335.
- Prabhakara, K., Hively, W. D., & McCarty, G. W. (2015). Evaluating the relationship between biomass, percent groundcover and remote sensing indices across six winter cover crop fields in Maryland, United States. *International Journal of Applied Earth Observation and Geoinformation*, 39, 88-102.
- Primrose, N. L., Millard, C. J., McCoy, J. L., Dobson, M. G., Sturm, P. E., Bowen, S. E., & Windschitl, R. J. (1997). German Branch Targeted Watershed Project. Biotic and Water Quality Monitoring Evaluation Report 1990 through 1995. Maryland Department of Natural Resources, Annapolis, MD.
- Pullin, A.S., & Knight, T.M. (2003). Support for decision making in conservation practice: an evidence-based approach. *Journal for Nature Conservation*, 11, 83–90.

- Qiu, L.-j., Zheng, F.-l., & Yin, R.-s. (2012). SWAT-based runoff and sediment simulation in a small watershed, the loessial hilly-gullied region of China: capabilities and challenges. *International Journal of Sediment Research*, 27(2), 226-234.
- Ranalli, A. J., & Macalady, D. L. (2010). The importance of the riparian zone and in-stream processes in nitrate attenuation in undisturbed and agricultural watersheds—a review of the scientific literature. *Journal of Hydrology*, 389(3), 406-415.
- Reckhow, K. H., Norris, P. E., Budell, R. J., Di Toro, D. M., Galloway, J. N., Greening, H., Sharpley, A. N., Shirmhhamadi, A., & Stacey, P. E. (2011). Achieving nutrient and sediment reduction goals in the Chesapeake Bay: An evaluation of program strategies and implementation. National Academies Press, Washington, D.C.
- Records, R. M., Arabi, M., Fassnacht, S. R., Duffy, W. G., Ahmadi, M., & Hegewisch, K. C. (2014). Climate change and wetland loss impacts on a western river's water quality. *Hydrology and Earth System Sciences*, 18(11), 4509-4527.
- Restrepo, J. I., Montoya, A. M., & Obeysekera, J. (1998). A wetland simulation module for the MODFLOW ground water model. *Ground Water*, 36(5), 764-770.
- Rinnofner, T., Friedel, J., De Kruijff, R., Pietsch, G., & Freyer, B. (2008). Effect of catch crops on N dynamics and following crops in organic farming. *Agronomy for sustainable development*, 28(4), 551-558.

- Ritter, W., Scarborough, R., & Chirnside, A. (1998). Winter cover crops as a best management practice for reducing nitrogen leaching. *Journal of Contaminant Hydrology*, 34(1), 1-15.
- Runkel, R. L., Crawford, C. G., & Cohn, T. A. (2004). Load estimator (LOADEST) a FORTRAN program for estimating constituent loads in streams and rivers. US Geological Survey, Reston, Virginia.
- Sadeghi, A., Yoon, K., Graff, C., McCarty, G., McConnell, L., Shirmohammadi, A., Hively, W. D., & Sefton, K. (2007). Assessing the performance of SWAT and AnnAGNPS Models in a Coastal Plain Watershed, Choptank River, Maryland, Proceedings of the 2007 ASABE Annual International Meeting, St. Joseph, MI.
- Saleh, A., & Du, B. (2004). Evaluation of SWAT and HSPF within BASINS program for the Upper North Bosque River watershed in Central Texas. *Transactions of the ASAE*, 47(4), 1039-1049.
- Santhi, C., Srinivasan, R., Arnold, J.G. & Williams, J.R. (2006). A modeling approach to evaluate the impacts of water quality management plans implemented in a watershed in Texas. *Environmental Modelling & Software*, 21(8), 1141-1157.
- Seibert, J., & McDonnell, J. (2013). Gauging the ungauged basin: relative value of soft and hard data. *Journal of Hydrologic Engineering*, 20(1), A4014004.
- Seibert, J., & McDonnell, J. J. (2002). On the dialog between experimentalist and modeler in catchment hydrology: Use of soft data for multicriteria model calibration. *Water Resources Research*, 38(11).

- Seo, M., Yen, H., Kim, M. K., & Jeong, J. (2014). Transferability of SWAT Models between SWAT2009 and SWAT2012. *Journal of Environmental Quality*, 43(3), 869-880.
- Sexton, A. M., Sadeghi, A. M., Zhang, X., Srinivasan, R., & Shirmohammadi, A. (2010). Using Nexrad and Rain Gauge Precipitation Data for Hydrologic Calibration of Swat in a Northeastern Watershed. *Transactions of the ASABE*, 53(5), 1501-1510.
- Sharifi, A., Lang, M. W., McCarty, G. W., Sadeghi, A. M., Lee, S., Yen, H., Rabenhorst, M.C., Jeong, J. & Yeo, I.Y. (2016). Improving model prediction reliability through enhanced representation of wetland soil processes and constrained model auto calibration—A paired watershed study. *Journal of Hydrology*.
- Shipley, P. R., Meisinger, J. J., & Decker, A. M. (1992). Conserving Residual Corn Fertilizer Nitrogen with Winter Cover Crops. *Agronomy Journal*, 84(5), 869-876.
- Shirmohammadi, A., Djodjic, F. & Bergström, L. (2005). Scaling issues in sustainable management of nutrient losses. *Soil Use and Management*, 21(s1), 160-166.
- Shirmohammadi, A., Chaubey, I., Harmel, R.D., Bosch, D.D., Muñoz-Carpena, R., Dharmasri, C., Sexton, A., Arabi, M., Wolfe, M.L., Frankenberger, J. & Graff, C. (2006). Uncertainty in TMDL models. *Transactions of the ASABE*, 49(4), 1033-1049.

- Shrestha, R.R., Dibike, Y.B. & Prowse, T.D. (2012). Modelling of climate-induced hydrologic changes in the Lake Winnipeg watershed. *Journal of Great Lakes Research*, 38, 83-94.
- Singh, A., Imtiyaz, M., Isaac, R. K., & Denis, D. M. (2014). Assessing the performance and uncertainty analysis of the SWAT and RBNN models for simulation of sediment yield in the Nagwa watershed, India. *Hydrological Sciences Journal-Journal Des Sciences Hydrologiques*, 59(2), 351-364.
- Smith, S., & Sharpley, A. (1990). Soil nitrogen mineralization in the presence of surface and incorporated crop residues. *Agronomy Journal*, 82(1), 112-116.
- Smith, V. H. (2003). Eutrophication of freshwater and coastal marine ecosystems a global problem. *Environmental Science and Pollution Research*, 10(2), 126-139.
- Smith, V. H., Joye, S. B., & Howarth, R. W. (2006). Eutrophication of freshwater and marine ecosystems. *Limnology and Oceanography*, 51(1, part2), 351-355.
- Staver, K., & Brinsfield, R. (1989). Effect on best management practices on nitrogen transport into Chesapeake Bay. Pan-american Regional Conference on the International Commission on Irrigation and Drainage, Ottawa, Canada.
- Staver, K. W., & Brinsfield, R. B. (2000). Evaluating changes in subsurface nitrogen discharge from an agricultural watershed into Chesapeake Bay after implementation of a groundwater protection strategy. Final report to Maryland Department of Natural Resources, Section, 319.-Need to be updated
- Steven, D. D., & Lowrance, R. (2011). Agricultural conservation practices and wetland ecosystem services in the wetland-rich Piedmont-Coastal Plain region. *Ecological Applications*, 21(sp1).

- Stevenson, F. J., & Cole, M. A. (1999). Cycles of soils: carbon, nitrogen, phosphorus, sulfur, micronutrients: John Wiley & Sons.
- Tiner, R. W., & Burke, D. G. (1995). Wetlands of Maryland.
- Tiner, R. W. (1997). NWI maps: what they tell us. National Wetlands Newsletter, 19(2), 7-12.
- Tiner, R. W. (2005). Assessing cumulative loss of wetland functions in the Nanticoke River watershed using enhanced National Wetlands Inventory data. Wetlands, 25(2), 405-419.
- Ullrich, A., & Volk, M. (2010). Influence of different nitrate-N monitoring strategies on load estimation as a base for model calibration and evaluation. Environmental Monitoring and Assessment, 171(1-4), 513-527.
- UNEP (United Nations Environment Programme), 2011, Taking Steps toward Marine and Coastal Ecosystem-Based Management - An Introductory Guide, available at: http://www.unep.org/pdf/EBM_Manual_r15_Final.pdf (last access: 19 October 2016)
- USDA-ARS (Agricultural Research Service), 2012, Soil & Water Research Laboratory: SWAT changes in Revision 481 and Revision 535, available at: http://swat.tamu.edu/media/51071/swat_changes_481_535.pdf (last access: 25 September 2013).
- USEPA (US Environmental Protection Agency), 2010a, Chesapeake Bay total Maximum Daily Load (TMDL) Section 6 Chesapeake Bay TMDL Development, available at: [163](https://www.epa.gov/sites/production/files/2014-</p></div><div data-bbox=)

- 12/documents/cbay_final_tmdl_section_6_final_0.pdf (last access: 19 October 2016)
- USEPA (US Environmental Protection Agency), 2010b, Chesapeake Bay total Maximum Daily Load (TMDL) Section 8 Watershed Implementation Plan Evaluation and Resultant Allocations, available at: https://www.epa.gov/sites/production/files/2014-12/documents/cbay_final_tmdl_section_8_final_0.pdf (last access: 19 October 2016)
- USEPA (US Environmental Protection Agency), 2010c, Chesapeake Bay Phase 5.3 Community Watershed Model. EPA 903S10002 - CBP/TRS-303-10. U.S. Environmental Protection Agency, Chesapeake Bay Program Office, Annapolis MD
- USEPA (U.S. Environmental Protection Agency), 2015, Connectivity of Streams and Wetlands to Downstream Waters: A Review and Synthesis of the Scientific Evidence. Office of Research and Development, USEPA, Washington, D.C.
- Vaché, K. B., & McDonnell, J. J., (2006). A process-based rejectionist framework for evaluating catchment runoff model structure. *Water Resource Research*. 42(2).
- Van Liew, M. W., Veith, T. L., Bosch, D. D., & Arnold, J. G. (2007). Suitability of SWAT for the conservation effects assessment project: Comparison on USDA Agricultural Research Service watersheds. *Journal of Hydrologic Engineering*, 12(2), 173-189.
- VDCR (Virginia Department of Conservation & Recreation), 2016, Program Year 2017 Virginia Agricultural Cost-Share (VACS) BMP Manual, available at:

- <http://dswcapps.dcr.virginia.gov/htdocs/agbmpman/csmanual.pdf> (last access: 19 October 2016)
- Vining, K. C., (2002). Simulation of streamflow and wetland storage, Starkweather Coulee subbasin, North Dakota, water years 1981-98. US Geological Survey (in cooperation with the North Dakota State Water Commission), Bismarck, ND.
- Wang, X., Yang, W., & Melesse, A. M. (2008). Using hydrologic equivalent wetland concept within swat to estimate streamflow in watersheds with numerous wetlands. *Transactions of the ASABE*, 51(1), 55-72.
- Wang, X. X., Shang, S. Y., Qu, Z. Y., Liu, T. X., Melesse, A. M., & Yang, W. H. (2010). Simulated wetland conservation-restoration effects on water quantity and quality at watershed scale. *Journal of Environmental Management*, 91(7), 1511-1525.
- Weed, D. A. J., & Kanwar, R. S. (1996). Water quality - Nitrate and water present in and flowing from root-zone soil. *Journal of Environmental Quality*, 25(4), 709-719.
- Wilson, K.A., Underwood, E.C., Morrison, S.A., Klausmeyer, K.R., Murdoch, W.W., Reyers, B., Wardell-Johnson, G., Marquet, P.A., Rundel, P.W., McBride, M.F. and Pressey, R.L. (2007). Conserving biodiversity efficiently: what to do, where, and when. *PLoS Biol*, 5(9), e223.
- Winchell, M., Srinivasan, R., Di Luzio, M., & Arnold, J. (2011). ArcSWAT interface for SWAT2009 User's guide. Texas Agricultural Experiment Station and U.S. Department of Agriculture, Temple, TX.

- Woznicki, S.A., Nejadhashemi, A.P. and Parsinejad, M. (2015). Climate change and irrigation demand: Uncertainty and adaptation. *Journal of Hydrology: Regional Studies*, 3, 247-264.
- Wu, K., & Xu, Y. J. (2006). EVALUATION OF THE APPLICABILITY OF THE SWAT MODEL FOR COASTAL WATERSHEDS IN SOUTHEASTERN LOUISIANA¹. *Journal of the American Water Resources Association*, 42(5), 1247.
- Wu, K. S., & Johnston, C. A. (2008). Hydrologic comparison between a forested and a wetland/lake dominated watershed using SWAT. *Hydrological Processes*, 22(10), 1431-1442.
- Yang, W. H., Wang, X. X., Liu, Y. B., Gabor, S., Boychuk, L., & Badiou, P. (2010). Simulated environmental effects of wetland restoration scenarios in a typical Canadian prairie watershed. *Wetlands Ecology and Management*, 18(3), 269-279.
- Yang, P., Ames, D.P., Fonseca, A., Anderson, D., Shrestha, R., Glenn, N.F. & Cao, Y. (2014). What is the effect of LiDAR-derived DEM resolution on large-scale watershed model results?. *Environmental Modelling & Software*, 58, 48-57.
- Yen, H., Jeong, J., Feng, Q., & Deb, D. (2015). Assessment of input uncertainty in SWAT using latent variables. *Water Resources Management*, 29(4), 1137-1153.
- Yeo, I.-Y., Lee, S., Sadeghi, A. M., Beeson, P. C., Hively, W. D., McCarty, G. W., & Lang, M. W. (2014). Assessing winter cover crop nutrient uptake efficiency using a water quality simulation model. *Hydrology and Earth System Sciences*, 18(12), 5239-5253.

- Zhang, L., Yao, X., Tang, C., Xu, H., Jiang, X., & Zhang, Y. (2016). Influence of long-term inundation and nutrient addition on denitrification in sandy wetland sediments from Poyang Lake, a large shallow subtropical lake in China. *Environmental Pollution*.
- Zhang, X., Hörmann, G., Gao, J., & Fohrer, N. (2011). Structural uncertainty assessment in a discharge simulation model. *Hydrological sciences journal*, 56(5), 854-869.
- Zhang, X., Srinivasan, R., & Van Liew, M. (2008). Multi-Site Calibration of the Swat Model for Hydrologic Modeling. *Transactions of the ASABE*, 51(6), 2039-2049.